Propagation Models for Dimensioning and Estimation of Performance and Availability of New Satellite Communication Systems

Doktor Ingeniør Dissertation

Lars Erling Bråten

Department of Telecommunications
Norwegian University of Science and Technology
N-7491, Trondheim, Norway

April 2001

Foreword

I started my PhD studies in 1998 with the loose working title *Radio channel modeling for satellite communication*. The work focused on atmospheric propagation effects between 20 and 60 GHz and mobile propagation effects of terrain at 1.5 GHz. Both of these fields are important and research has been ongoing for decades. I was lucky to be able to work on L-band propagation data measured by Inmarsat and on Ka-band data from the NASA propagation campaign with the Advanced Communications Technology Satellite (ACTS). In addition, a part of my previous work at Telenor R&D involved measuring the 50 GHz beacon from the Italsat F1 satellite. I tried to focus on methods and models of system performance, quality of service and availability, building upon the previous results in the field. The approach in most of the work was to analyze measurements and develop models useful for engineers working on system design.

Contents

Abstract

A rapid growth of new satellite systems utilizing the Ka-band (27 - 40 GHz) and even higher frequencies is expected in the coming years. The services offered will include broadband communication, interactive broadcasting, multimedia applications, interconnection of local area networks and Internet connectivity. Many of the new systems will use technologies as multiple spot-beams, onboard processing, and switching of packets between beams and inter satellite links. Because of congestion in the lower bands, such as C (4 - 8 GHz) and Ku-band (12 - 18 GHz), numerous of these services will use Ka-band. One additional advantage to the spectrum availability at Ka-band is the potential of smaller terminals compared to those used in lower frequency bands.

Several mobile satellite systems have recently started operation and more are planned or scheduled for implementation within a few years to provide personal and data communication at L-band (1 - 2 GHz) and S-band (2 - 4 GHz) frequencies. The systems will utilize different orbit types, for example low, medium or geostationary earth orbits, to provide voice and data services to mobile users.

Understanding of the propagation aspects is important for successful design of a satellite system obtaining the targeted service quality and availability. For systems operating above about 10 GHz, attenuation caused by hydrometeor effects is the dominant propagation impairment on line-of-sight (LOS) links. For mobile communications systems operating at lower frequencies, the impairments resulting from multipath propagation, shadowing and blockage from obstacles on the ground severely affect the radio signals. Estimation of dynamic propagation impairments is essential for the design of reliable and spectrum efficient communication systems. The systems can adapt the transmission methodology that maximizes the throughput of information and optimizes the delivery time. The design of such mitigation techniques will depend on the dynamics and how often the events occur.

The research conducted in this study on mobile propagation effects of terrain at L-band has led to an improved three-state channel model for land mobile satellite systems. The time spent in each of the states is quite realistic, facilitating better simulation of the performance of communication systems. A new methodology was developed to perform large area coverage estimation by calculating satellite visibility for low earth orbit and geostationary constellations based on digital terrain maps. The procedure takes into account large terrain obstacles and produces a gross overview of the potential area covered with one or several satellites. A photogrammetric technique to assess performance of non-geostationary orbit (NGSO) systems in mid- and high latitude urban areas was used to estimate channel fading and diversity improvement. Some measurements of the maximum obtainable call duration for the Iridium system are included as well.

The studies on atmospheric propagation effects between 20 and 60 GHz included analyses of fade and inter-fade duration statistics, which are important when evaluating fade mitigation techniques and estimating system outages. Fade duration measurements were analyzed and an effort made to find a common statistical fade duration model. Based on this work, a new prediction method for fade durations on satellite-earth paths was developed. The ability to forecast rain attenuation was investigated with the aid of statistical prediction methods and terrestrial measurements on a 60 GHz link. Finally, beacon measurements at 50 GHz from Italsat F1 were used to test and compare available scintillation prediction models.

The work has improved the ability to estimate and simulate propagation effects on mobile and fixed satellite system performance.

1. Introduction

Several new satellite systems are about to be placed in service for broadband and personal communication needs. These systems utilize satellites in geostationary, medium and/or low earth orbits to provide interactive broadband multimedia services and Internet connectivity. The traditional broadcast, telecommunication and data networks are emerging into networks integrating the different services. The satellite systems may provide global coverage - virtually every spot on the earth can be reached.

The increasing interest for systems operating at very high frequency, for example Ka-band, is driven by the crowding in the lower part of the spectrum and growing demand for higher bandwidth services. Most of the new systems propose to employ advanced technologies as multiple narrow spot beam antennas, and on-board processing with de- and remodulation. The networks are often based on transmission of packets, with routing of the traffic between spot beams and inter satellite links. Examples of proposed Ka-band systems planning to offer global service are the two geostationary (GEO) systems Astrolink and Cyberstar, and the low earth orbit (LEO) system Teledesic. Astrolink and Cyberstar were designed with 9 and 3 satellites respectively, while the original Teledesic design originally planned to use 840 satellites. All of the systems use narrow spot-beams, inter satellite links and have on-board digital processors [1]. The systems have to overcome the significant attenuation due to hydrometeors that can occur in this frequency band [2]. Refractive effects such as signal scintillation, caused by atmospheric turbulence, and gaseous absorption are also propagation impairments that can be encountered [3].

Mobile satellite systems providing services like voice, data and multimedia typically operate at lower frequencies in the L- and S-band. Table 1 summarizes selected properties of four mobile satellite systems. The Iridium and Globalstar satellite constellations utilize low earth orbits, while the planned ICO-Global system use a medium earth orbit (MEO) to provide personal satellite communication to handheld terminals. Inmarsat uses a fleet of geostationary orbiting satellites to provide voice and data capabilities to nomadic and mobile users.

The limited satellite and terminal power often results in mobile systems with low to medium fade margin, a marked contrast compared to that for terrestrial wireless communication systems. The user environment, separated into clear line-of-sight, shadowed by vegetation or blocked by solid obstacles, has a major impact on the service quality and availability obtainable in land mobile satellite systems (LMSS).

	Satellite system			
Parameter	Iridium	Globalstar	ICO-Global	Inmarsat-3
Orbital type	LEO	LEO	MEO	GEO
Orbital altitude (km)	780	1414	10355	36000
No. of active satellites	66	48	10	3
# spot beams per satellite	48	16	163	7 + 1
User link freq. band	L	L/S	L/S	L
Nominal link margin (dB)	16.5	3-6*	10	~5
On-board processing	De- and re-modulation Packet routing	No	Routing	Routing, bandwidth and power adjustment
Inter satellite links	Yes	No		No
Satellite diversity	No	Yes		No

*: For a small number of channels this can be raised to 11 dB

Table 1. Some existing and proposed global mobile satellite systems [1]

The introduction of LEO and MEO constellations gives satellites moving relatively to the users, resulting in for example more complex antenna tracking and traffic routing compared to GEO systems. The major propagation impairment at L- and S-band for mobile users are shadowing by vegetation and blockage by buildings and terrain.

In developing or evaluating new satellite systems the service quality and economy are of special importance. The system economy is closely linked to effective utilization of satellite capacity, because both power and bandwidth resources are limited. Realistic radio channel models are needed to design systems obtaining the targeted service availability and quality. Optimization with respect to system capacity, and ensuring and sound economic basis for the services, also depends on good models for the radio channel and an understanding of its possibilities and limitations. A combination of uplink power control, adaptive forward error control and variable transfer rate can be used to mitigate attenuation and/or fading, and to maintain service availability during less favorable propagation conditions. Traditional propagation quantities used when designing fixed satellite systems are for example annual average statistics of attenuation due to rain, and the percentage of time a fade level is exceeded for mobile systems. The mitigation methods require specialized information on impairment dynamics, such as statistics of the impairment duration and the time between them [4].

The works done are reported in the form of published papers reproduced as part of this thesis. The thesis itself contains a summary of the work and a short description of each paper. Statements from co-authors of the papers regarding the individual contributions were given to the committee evaluating the thesis. The work was focused toward the two areas illustrated in Fig. 1, atmospheric propagation effects at frequencies between 20 and 60 GHz, and mobile propagation effects of terrain at L-band.

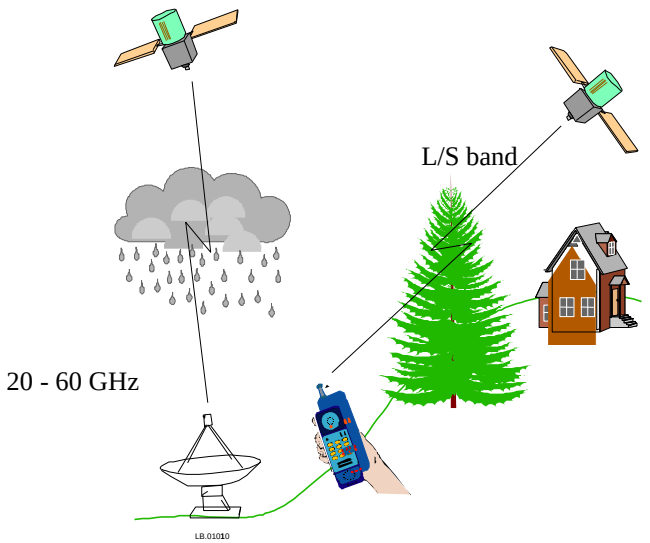

Figure 1. Some terrain and atmospheric propagation effects on satellite-earth links covered in the thesis

1.1. Terrain effects for land mobile satellite systems

There is a wide range of channel models for LMSS described in the literature. The two main approaches are statistical modeling utilizing one or more environmental states [5], and deterministic modeling such as ray tracing [6] or geometrical theory of diffraction [7]. It is also possible to combine the two techniques to describe urban areas for instance using statistical environment description (building height, width, placement) and using deterministic approaches to calculate signal strength, given the environmental description [8]. An alternative method of accessing the performance limitation due to terrain effects is by statistically analyzing fisheye photographs of the area of interest [9].

The work on terrain propagation effects on mobile systems focused on three aspects: satellite visibility studies based on large-scale digital elevation maps, a photogrammetric study in urban areas to estimate the effects of built-up terrain, and finally the development of a new three-state statistical channel model for LMSS based on L-band measurements. Limited measurements of call-dropping in the Iridium systems are included as well.

1.2. Atmospheric propagation effects

The influence of the atmosphere and precipitation on the propagation conditions typically increases with frequency, and rain attenuation in particular can limit the system availability for frequencies above about 10 GHz [2]. The troposheric clear-air and precipitation effects are often dealt with separately. Clear-air effects are present over the whole frequency range of interest. Refractive variations due to atmospheric turbulence cause multipath propagation, influencing the system performance for small percentages of time. Available scintillation prediction methods were compared to beacon measurement results at 49.5 GHz obtained during a measurement campaign at Kjeller, Norway.

Work has been done over many years to measure, characterize and predict the cumulative statistics of attenuation. The time dynamic behavior of attenuation, and the statistics of the individual events comprising the cumulative distribution, has been studied to a lesser extent. The fade dynamics are concerned with the number of attenuation events and the duration of such events, as well as statistical description of the attenuation as a stochastic process. Fade duration measurements at 20 and 27 GHz from several sites receiving beacons from NASA's Advanced Communications Technology Satellite (ACTS) were analyzed and an effort made to find a common statistical fade duration model. Based on this common model, a new prediction method for fade durations on satellite-earth paths was developed. The connection between system availability, attenuation statistics and fade and inter-fade duration distributions were explored.

Prior estimates of foreseen propagation impairments can be used by the service provider to optimize system performance. Forecasting of attenuation is another topic closely connected to fade dynamics. Terrestrial measurements of rain attenuation on a 60 GHz link were used to investigate the ability to forecast rain attenuation.

2. Terrain effects for land mobile satellite systems

Land mobile satellite systems provide communication services in a variety of propagation environments. Service availability and quality are the most important characteristics when evaluating user satisfaction with mobile satellite systems.

Three approaches were used to characterize the propagation environment and its influence on coverage and system performance. The first employed a global digital elevation map to access the limitations in satellite visibility due to large-scale terrain features. Satellite visibility for a NGSO constellation is defined as the percentage of the spherical sky visible to the user. This information was used to calculate visibility reduction for an Iridium-like NGSO constellation in Northern Europe. In the second part of the study, a large number of fisheye photographs were taken in urban environments in Canada and Norway to access the performance of a Globalstar-like system in built-up areas with vegetation. Finally, land mobile L-band measurements were analyzed and a new three-state statistical channel model was developed. In the last Section, limited test results of the real Iridium system with respect to dropped calls are reported.

2.1. Satellite visibility - Paper 1

The availability of a mobile system is, to a first degree of approximation, linked to optical visibility of the serving satellites. Thus, an approach linked to determining optical visibility is considered appropriate when an overview of the potential system availability is considered. Practical implementation losses, as for example traffic routing strategies, are not included, and the visibility is considered as an optimistic upper bound on link connectivity.

The methodology, described in the paper entitled *Satellite Visibility in Northern Europe based on Digital Maps*, tries to bridge the gap between detailed deterministic models and combined deterministic-statistical models, as in for example [8], and the approaches taking only the satellite orbits into account, as in for example [10]. This is done by calculating the reduction of satellite visibility imposed by terrain elevation and thereby estimating the potential coverage in large areas by estimating the average number of visible satellites. The average number of visible satellites is considered as an important parameter when the objective is to compare the potential of a satellite constellation in the area of interest without involving lengthy simulations.

The paper presents the results of calculations of satellite visibility and system availability based on large-scale digital elevation maps for an Iridium-like system. New models for satellite visibility were derived for both non-geostationary orbiting satellite constellations and geostationary satellites. Regression models for satellite visibility and average number of visible satellites based on surface roughness variables were developed and tested. The variable selection used in the regression analysis followed the approach developed in [11]. Cumulative distributions were calculated for the percentage of time Iridium-like satellites were visible, taking large terrain obstacles into account, and the relation between satellite visibility and system availability was discussed. Small-scale terrain features, for example trees and houses, were not included in the digital map used and therefore not accounted for in this study. A supplementary methodology incorporating the effect of vegetation and buildings on the propagation channel, useful in for example urban areas, is described in the next Section.

2.2. System performance estimation based on fisheye photographs – Paper 2

Reliable communication using fixed- and mobile-satellite systems depends on local characteristics of the environment because operation is limited by the state of the propagation

path, i.e., whether it is clear, shadowed by vegetation, or blocked by buildings and other obstacles. A photograph study of urban environments in Ottawa, Canada, and Lillestrøm, Norway, was performed in cooperation with the Communications Research Centre Canada, to estimate fading, diversity gain and finally system performance. The objective of this work was to establish a methodology for estimating link availability for NGSO satellite telecommunication systems as a function of the local environment.

In Paper 2, entitled *Prediction of Coverage for a LEO System in Mid- and High-Latitude Urban Areas Using a Photogrammetric Technique*, the cumulative fade distributions are estimated based on hemispherical pictures for a Globalstar-like LEO satellite constellation in Ottawa, Lillestrøm and Oslo. The pictures were sorted into three states, vegetation, solid obstacles as terrain and building, and clear sky. The simulated satellite look-angles were combined with the digital pictures to determine the path state for each satellite (shadowed, blocked or clear line-of-sight). Cumulative distributions of narrowband fading were developed for the case when the receiver utilizes one (best or highest) satellite, and up to three-fold diversity with either switching or coherent combining of the received signals. The technique provides an important tool to predict path-diversity gain for specific satellite configurations.

2.3. Statistical multistate land mobile satellite channel models - Papers 3 and 4

The area of interest in this study was statistical modeling of land mobile satellite radio channels at L-band by using semi-Markov state models. The interest in statistical modeling is caused by the desire to estimate the obtainable service performance in an area or over time. Statistical modeling, as opposed to deterministic modeling, does not estimate the received radio signal from exact geometrical description of the terrain but models the variations in an area composed of a number of different obstacles.

Statistical channel models are often divided into two types: one representing non-homogenous large-areas (for example mixture of open areas, trees etc.) and another representing homogeneous small-areas. Large-area models are often realized by switching between the small-area models representing the different states in the large-area model [5]. The switching process may be assumed to follow a Markov process, but other realizations, such as re-alternating or semi-Markov schemes are also possible. An empirical statistical approach based on L-band measurements was used to improve the state duration statistics in simulation models for LMSS.

The third paper, entitled *Modelling of Mobile Satellite Channels Based on Measurements at 13^o and 29^o elevation angle*, presents results from land mobile propagation measurements conducted by Inmarsat at 13^o and 29^o elevation angles in the UK. A number of simultaneous recordings were made at L-band, using both directive and omni-directional antennas. The measurements took place in the suburbs of London in a variety of propagation environments ranging from open to shadowed areas. Also, the paper presents a new analogue fading channel model for use in simulation of low margin narrow-band systems. The channel model has two states, one representing an open area and the other representing a shadowed area. The model parameters were fitted to the recorded measurements. The interest was on models for the open and lightly shadowed states, though some deep fade analyses have been included.

In Paper 4, entitled *An Improved Three-State Semi-Markov Model Optimised for Land Mobile Satellite Communication*, the re-alternating two-state model was extended to a new three-state semi-Markov model for the land mobile satellite channel. The three states represent open areas, shadowing and blockage of the signal. The duration spent in each state was drawn from ITU-R

recommended probability distributions with modified parameters. This is an improvement over the more common Markov model where the duration in each state is forced to follow an exponential distribution. The model enables more accurate prediction and simulation of system performance and availability. The model was applied to measurements conducted by Inmarsat at L-band in the UK. The work resulted in a proposed revision [12] of ITU-R Recommendation 681-4 [13].

2.4. Measurements of dropped calls for Iridium

The Iridium service quality was tested with respect to maximum obtainable call duration in two different terrain scenarios, LOS and partly blocked by a building.

Calls dropping by the Iridium system in LOS conditions due to system errors have been measured at Kjeller, Norway. The measurement site is a plastic roof laboratory without obstacles blocking the view to the satellites. The telephone (Motorola 9500) was placed on a table, calls made were terminated manually after 10 minutes. The measurements where performed 16-17 February 1999 with blue-sky conditions. All the dropped calls are due to system errors as no terrain, building or human obstacles are blocking or shadowing the propagation path. From the call duration statistics for the LOS case, shown in Fig. 2, we find a 16 % probability of dropping a call with duration of 3 minutes, while a 6-minute call has 20 % probability of dropping. The maximum call duration tested in the experiments was 10 minutes, although a call with about one-hour duration was successfully retained during a cross-country skiing tour in the forest area Lillomarka outside Oslo. The perceived subjective quality was not investigated; however, results based on a few calls indicate difficulties understanding speech in periods. This may be caused by events like buffer overflow or handoff problems.

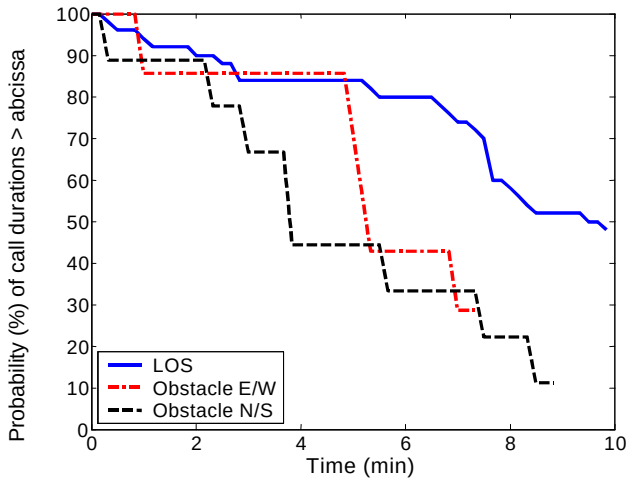

Figure 2. Cumulative distribution of maximum obtained call duration for Iridium

Maximum obtainable call duration was also measured with a large obstacle present, effectively blocking part of the sky. The measurement location was in General Laakes vei, Strømmen, where a curved building was used as a shield, see Fig. 3a. The terrain opposite the building is mainly below the local horizon, and a simple scenario dividing the sky in two was obtained. Two different outdoor locations near the concrete wall were used when making the calls, see Fig 3b.

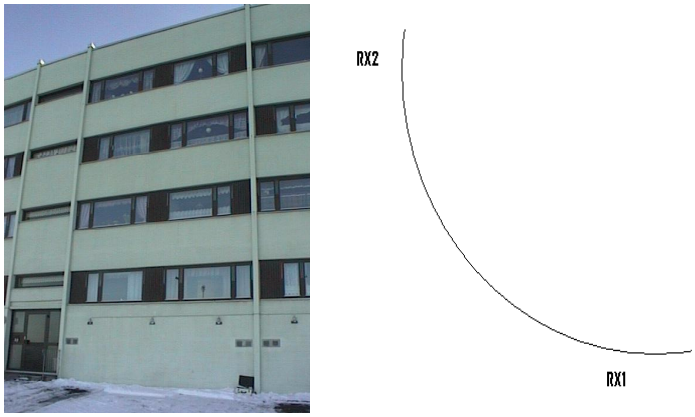

a) b)

Figure 3. a) Measurement site in General Laakes vei, Strømmen. b) Curved block serving as a radio shield in North/South and East/West direction

The first position is with the obstacle oriented East/West, the second with the building in the North/South direction. The maximum call duration obtained at the two sites with obstacles was 7.5 and 9 minutes for the East/West and North/South obstacle direction respectively. The cumulative distributions of call duration have relative large variations when an obstacle is present, as seen in Fig. 2. The East/West oriented obstacle gives a sharp transition in the range five to seven minutes while a smoother transition is obtained for the North/South position. The maximum passing time for one satellite in the polar orbit is about 14 minutes, implying maximum call duration without satellite handoff of about seven minutes in the first case. As none of the calls extended beyond this, we conclude that the system had problems when rapid inter satellite handoffs were required.

3. Atmospheric propagation effects

Propagation impairments produced by the troposphere are a limiting factor for communication at centimeter and millimeter wavelengths. Rain attenuation is the dominant propagation impairment at frequencies exceeding about 10 GHz, but hydrometeors such as snow and clouds, and also variability in refraction, affect the signal and limit the system availability [2].

Tropospheric refractive effects, such as scintillation and ray bending, are important for low margin systems. The atmosphere is characterized by its radio refractive index depending on meteorological conditions and varying in both time and space. Atmospheric turbulence causes rapid variations in radio refractivity along the path, resulting in angle-of-arrival, amplitude and phase variations of a received radio signal [3].

For communication systems designed to operate up to a given attenuation level, fade and inter-fade duration statistics indicate the number and duration of outages, while the cumulative attenuation statistics may be used to estimate the total time a system is available. Propagation impairment compensation techniques, such as adaptive modulation and coding, require specific information on the fading dynamics [4].

3.1. Tropospheric scintillation - Paper 5

There have been several experimental campaigns in the past to investigate the fast scintillation in received power caused by multipath propagation in the atmosphere, although the number of experiments at millimeter wavelengths is limited.

In Paper 5, entitled *Comparison of Predicted Scintillation with Data Measured from the 50 GHz Italsat Beacon in Norway*, measured signal scintillation in the horizontally polarized 49.5 GHz beacon from the Italsat F1 satellite was analyzed. Four months of scintillation data were sorted into "rainy" and "non-rainy" conditions and long-term probability density functions were extracted on a monthly basis. The empirical monthly cumulative density functions of scintillation levels were compared to ITU-R predictions [14], and the diurnal fluctuation in variance was described. A seasonal modification of the frequency exponent in the ITU-R prediction method improved the results, suggesting that this parameter might depend on frequency as well as site-specific characteristics. A modified prediction method was also compared with the measured cumulative distributions [3]. This alterative method gave excellent predictions for the two warm summer months; however, it underestimated the scintillation intensity during spring.

3.2. Fade and inter-fade duration on satellite-earth paths - Papers 6, 7, and 8

Fade and inter-fade duration statistics are important for evaluating fade mitigation techniques required to obtain a given telecommunication system availability. The most common way to present fade duration statistics is the cumulative conditional probability of a fade event lasting longer than a specified time given that the attenuation exceeds a threshold level. This measure gives an indication of the number of communication outages that last for a period equal to or exceeding a given duration.

Paper 6, entitled *Fade Duration at Ka-band on a Satellite-Earth Link in Vancouver: Modeling and Comparison with Measurements*, deals with 5-years of fade duration ACTS beacon data at 20.2 and 27.5 GHz measured in Vancouver, Canada. Several candidate fade duration models

were compared with the empirical fade duration distributions and the best model (Weibull) for this set of data was identified.

In Paper 7, entitled *Fade and Inter-fade Duration at Ka-Band on Satellite-Earth Links: Modeling and System Implications*, the work was extended to include three additional sites in North America. The overall best model for fade duration was identified as a triple-exponential model, which reduced to a double-exponential model if the fast varying scintillation was removed from the data. The connection between fade- and inter-fade duration with system availability was explored, and an algorithm derived to estimate availability according to the definition of available and unavailable time given in ITU-T Recommendation G.821 [15], based on a 10 second criterion. The difference between the annual system availability distribution and the annual rain attenuation distribution was found to be small.

A new fade duration prediction model for satellite-earth links, based on the triple-exponential distribution, was developed in Paper 8, *Fade Durations on Earth-Space Links: Dependence on path and climatic parameters*. The prediction method is based on measured fade durations from the five ACTS measurement sites Vancouver, Ottawa, Reston, Norman and Tampa. Both the shape of the distribution, and the average annual number of fades are predicted from local climatic and path specific parameters. The new prediction method performed well compared to previously reported fade duration models for the considered data sets.

3.3. Forecasting of rain attenuation - Paper 9

Communication systems where propagation effects due to precipitation have an effect on the signal transmission could adapt the transmission methodology that maximizes the throughput of information and optimizes the delivery time. The required forecast horizon for systems employing adaptive modulation and coding is typically in the order of a few seconds. An example requiring longer forecasts is a broadband cellular system delivering information on demand. Prior knowledge of the foreseen propagation impairments can be used by the service provider to optimize system performance in terms of, for example, minimizing the number of interruptions.

This paper, entitled *Prediction of Time Dynamic Rain Attenuation at Millimetre Wavelengths*, presents forecasting and modeling of rain attenuation based on measurements of a 60 GHz terrestrial link at Kjeller, Norway. Parameters for a dynamic rain attenuation model were extracted from measurements. Linear auto-regressive moving average and dynamic Bayesian methods for rain attenuation prediction were compared over a time span ranging from 10 to 100 seconds. The most suitable prediction method based on the prediction standard deviation was a logarithmic auto-regressive estimator of first order.

Although the results were based on terrestrial measurements, we would expect similar results on slant paths. The length of the path experiencing rain would probably be larger, resulting in a more slowly varying evolvement of the attenuation time series.

4. Conclusions

The work presented in the thesis covers models of the satellite-earth radio channel for mobile and fixed satellite systems. The focus is on propagation effects of terrain on land mobile satellite systems, and atmospheric propagation effects at 20 to 60 GHz with emphasis on signal scintillation and rain fade dynamics.

4.1. Terrain effects for land mobile satellite systems

The research on mobile propagation effects of terrain lead to the development of a new methodology to perform large area coverage estimation by calculating reduction in satellite visibility for low earth orbit and geostationary constellations based on digital terrain maps. The procedure takes into account large terrain obstacles and produces a gross overview of the potential area covered with one or several satellites. A photograph-based technique to access performance of non-geostationary orbit systems in built-up terrain were used to estimate channel fading and diversity improvement in mid- and high latitude urban areas. The method takes into account both shadowing by vegetation and blockage by buildings and terrain.

The work based on the L-band measurements provided by Inmarsat resulted in an improved three-state channel model for land mobile satellite systems. The duration of time spent in each of the states is more realistic than previously, facilitating better simulation of the performance of communication systems. Telenor R&D has proposed to include the results of the latter study in ITU-R Recommendation 681-4.

4.2. Atmospheric propagation effects

The studies of atmospheric propagation effects between 20 and 60 GHz focused on measuring and modeling of tropospheric scintillation at 49.5 GHz, modeling of rain fade duration statistics at 20 and 27 GHz, and finally forecasting of rain attenuation at 60 GHz.

The tropospheric scintillation measured at Kjeller indicated that a seasonal modification of the frequency exponent in the ITU-R prediction method would improved the results, suggesting that this parameter depend on frequency as well as site-specific characteristics. A modified prediction method was also compared with the measured cumulative distributions, giving excellent predictions for the two warm summer months; but underestimating the scintillation intensity during spring. The analysis of diurnal variation confirmed previous findings of peaks during early morning and around noon.

Fade and inter-fade duration statistics are important when evaluating fade mitigation techniques and estimating system outages. Analyses of measured fade duration from ACTS satellite beacons at several sites in North America resulted in the identification of a common triple-exponential fade duration model. Fade duration statistics derived from radiometer data indicated that the model reduces to a double-exponential model when tropospheric scintillation is removed. A new general prediction method for fade durations on satellite-earth links was developed based on the triple-exponential model. System availability, as defined in ITU-T Recommendation G.821, was compared to the distribution of annual rain attenuation with an attenuation margin threshold. The difference between the two methods was found to be small, and a good estimate of availability can in many cases be derived from annual attenuation statistics alone.

The ability to forecast rain attenuation was investigated with the aid of statistical prediction methods and terrestrial measurements on a 60 GHz link. It was found that the most suitable predictor was a logarithmic auto-regressive estimator of first order. The value of the autocorrelation function of the rain attenuation remained high for several minutes, however, it was difficult to accurately predict attenuation with a time horizon exceeding about one minute.

4.3. Major achievements and future work

The work has improved the ability to estimate and simulate propagation effects on mobile and fixed satellite system performance. The major achievements include the development of a semi-Markov state model for the land mobile satellite channel at L-band, as well as the new large-scale coverage estimation method for land mobile satellite systems based on digital elevation maps. Important are also the identification and validation of the cascaded-exponential fade duration model, and the development of a path and climatic dependent prediction model for fade durations at Ka-band. Furthermore, the connection between system availability and fade and inter-fade durations was explored.

Suggested future work is to:

validate and refine the fade duration prediction model with independent measurements
include channel models for higher frequencies than L-band, for example the roadside tree-shadowing model, in the coverage estimation method based on fisheye photographs. Compare the estimates with land-mobile measurements
simplify the fisheye methodology to enable estimation of fade depth distributions from a statistical description of the environment, extracted from the photographs

5. Acknowledgements

I would like to thank my wife Vibeke for encouraging me during this demanding project and for coming with me to Canada for one year. I appreciated that my son Fredrik started sleeping through the night when he was only five weeks old.

As seen from the papers, most of this work was a result of collaborative effort. This has been very inspiring for me, as my co-authors provided many good suggestions. In particular I am grateful to my supervisor at Telenor Research and Development, Terje Tjelta, who supported my research over several years and gave good advice on the direction of the work. My main supervisor at the Norwegian University of Science and Technology, Gunnar Stette, also gave very good advice during these years.

As part of the studies I spent one year at the Communications Research Centre Canada in Ottawa, where I had a very good collaboration with César Amaya. I would also like to thank David Rogers and Roderic Olsen at CRC; they always took time to discuss problems, review manuscripts and gave help and advice during our stay. As already said, the contributions from the other co-authors, especially Walther Åsen, are very much acknowledged as well.

Telenor Research and Development, Norway, financed this study, thereby enabling me to do interesting research for 3 years. I gratefully acknowledge their support and also the discussions with good colleagues at Telenor, especially Magne Pettersen.

Finally, I would like to thank the Center for Technology at Kjeller, UNIK, for their hospitality during my stay there.

6. References

[1] J. V. Evans, "Market forces and future drivers," *space communications*, vol. 16, no. 2, 3, pp. 85-96, 2000.

[2] A. Dissanayake, J. Allnutt and F. Haidara, "A Prediction Model that Combines Rain Attenuation and Other Propagation Impairments Along Earth-Satellite Paths," *IEEE Trans. Ant. Propagat.*, vol. 45, no. 10, pp. 1546-1558, Oct. 1997.

[3] M. M. J. L. van de Kamp, J. K. Tervonen, E. T. Salonen and J. P. V. Poiares Baptista, "Improved Models for Long-Term Prediction of Tropospheric Scintillation on Slant Paths," *IEEE Trans. Antennas Propagat.*, vol. 47, no. 2, pp. 249-260, Feb. 1999.

[4] D. Rogers, L. J. Ippolito and F. Davarian, "System Requirements for Ka-Band Earth-Satellite Propagation Data," *Proc. IEEE.*, vol. 85, no. 6, pp. 810-820, June 1997.

[5] F. P. Fontan, J. P. Gonzalez, M. J. S. Ferreiro, M. A. V. Castro, S. Buonomo and J. P. Baptista, "Complex Envelope Three-State Markov Model Based Simulator for the Narrow-Band LMS Channel", *Int. J. of Satellite Comm.*, vol. 15, issue 1, pp. 1-15, Jan. 1997.

[6] M. Dottling, A. Jahn, J. Kunisch, S. Buonomo, "A versatile propagation channel simulator for land mobile satellite applications," *Proc. IEEE Vehicular Technology Conference VTC 98*, vol. 1, pp. 213-217, 18-21 May 1998.

[7] P. A. Tirkas, C. M. Wangsvick, C. A. Balanis, "Propagation model for building blockage in satellite mobile communication systems," *IEEE Trans. Ant. Propagat.*, vol. 46, no. 7, pp. 991-997, July 1998.

[8] S. R. Saunders and B. G. Evans, "A physical-statistical model for land mobile satellite propagation in built-up areas," *Proc. IEE Tenth International Conference on Antennas and Propagation (ICAP'97)*, vol. 2, pp. 44-47, 14-17 April 1997.

[9] R. Akturan and W. Vogel, "Path Diversity for LEO Satellite-PCS in the Urban Environment," *IEEE Trans. Ant. Propagat.*, vol. 45, no. 7, pp. 1107-116, July 1997.

[10] W. Krewel and G. Maral, "Single and multiple satellite visibility statistics of first-generation non-geo constellations for personal communications," *Int. Journal of satellite communications*, vol. 16, issue 2, pp. 105-125, March/April 1998.

[11] T. Tjelta, R. L. Olsen and L. Martin, "Systematic Development of New Multivariable Techniques for Predicting the Distribution of Multipath Fading on Terrestrial Links," *IEEE Trans. Antennas Propagat.*, vol. 38, no. 10, pp. 1650-1665, Oct. 1990.

[12] ITU-R Contribution 3M/16-E, "Proposed revision to Recommendation ITU-R P.681-4 - Propagation data required for the design of earth-space land mobile telecommunication systems," International Telecommunication Union, Geneva, Switzerland, 2001.

[13] ITU-R Recommendation P.681-4, "Propagation data required for the design of earth-space land mobile telecommunication systems," International Telecommunication Union, Geneva, Switzerland, 1999.

[14] ITU-R Recommendation P.618-6, "Propagation data and prediction models required for the design of earth-space telecommunication systems," International Telecommunication Union, Geneva, Switzerland, 1999.

[15] ITU-T Recommendation G.821, "Error performance of an international digital connection operating at a bit rate below the primary rate and forming part of an integrated services digital network," International Telecommunication Union, Geneva, Switzerland, 1996.

7. Papers reproduced as part of the thesis

1. L. E. Bråten, "Satellite Visibility in Northern Europe based on Digital Maps," *International Journal on Satellite Communications*, vol. 18, issue 1, pp. 47-62, Jan./Feb. 2000.
2. L. E. Bråten, C. Amaya and D. V. Rogers, "Prediction of Coverage for a LEO System in Mid- and High-Latitude Urban Areas Using a Photogrammetric Technique," *Proc. IEEE Vehicular Technology Conference (VTC'2001)*, Rhodes Island, Greece, 6-9 May 2001.
3. L. E. Bråten, N. Kawai, Y. Louahdi and T. Tjelta, "Modelling of Mobile Satellite Channels Based on Measurements at 13^{o} and 29^{o} elevation angle," *Proc. Tenth International Conference on Antennas and Propagation (ICAP'97)*, Edinburgh, UK, 14-17 April 1997.
4. L. E. Bråten and T. Tjelta, "An Improved Three-State Semi-Markov Model Optimised for Land Mobile Satellite Communication," *Proc. AP2000 Millennium Conference on Antennas & Propagation*, Davos, Switzerland, April 9-14 2000.
5. L. E. Bråten, "Comparison of Predicted Scintillation with Data Measured from the 50 GHz Italsat Beacon in Norway," *Proc. 6th Ka-band Utilization Conference*, Cleveland, USA, May 31-June 2 2000.
6. L. E. Bråten and C. Amaya, "Fade Duration at Ka-band on a Satellite-Earth Link in Vancouver: Modeling and Comparison with Measurements," *Proc. IX Simpósio Brasileiro de Microondas e Optoeletrônica (SBMO'IX)*, Joao Pessoa, Brazil, 7-11 August 2000, 7-11.
7. L. E. Bråten, C. Amaya and D. V. Rogers, "Fade and Inter-Fade Duration at Ka-Band on Satellite-Earth Links: Modeling and System Implications," *Proc. AIAA International Communications Satellite Systems Conference*, Toulouse, France, 17-20 April 2001.
8. L. E. Bråten, C. Amaya and D. V. Rogers, "Fade Durations on Earth-Space Links: Dependence on Path and Climatic Parameters," *Proc. CLIMPARA'2001*, Budapest, Hungary, 28-30 May 2001.
9. L. E. Bråten and W. Åsen, "Prediction of Time Dynamic Rain Attenuation at Millimetre Wavelengths," *Proc. AP2000 Millennium Conference on Antennas & Propagation*, Davos, Switzerland, April 9-14 2000.

Paper 1

"Satellite Visibility in Northern Europe based on Digital Maps"

Published in: *International Journal on Satellite Communications*, vol. 18, issue 1, pp. 47-62, Jan./Feb. 2000.

Paper I is not included due to copyright.

Paper 2

"Prediction of Coverage for a LEO System in Mid- and High-Latitude Urban Areas Using a Photogrammetric Technique"

Published in: *Proc. IEEE Vehicular Technology Conference (VTC'2001),* Rhodes Island, Greece, 6-9 May 2001.

Prediction of Coverage for a LEO System in Mid- and High-Latitude Urban Areas Using a Photogrammetric Technique

Lars Erling Bråten
Telenor Research and Development, Box 83, N-2027 Kjeller, Norway.
Lars.Braten@ties.itu.int

César Amaya
Communications Research Centre Canada, Box 11490, Ottawa, Canada, K2H 8S2.
Cesar.Amaya@crc.ca

David V. Rogers
Communications Research Centre Canada, Box 11490, Ottawa, Canada, K2H 8S2.
Dave.Rogers@crc.ca

Abstract

The performance of a Globalstar-like low-earth-orbit system is predicted based on hemispherical photographs taken in Ottawa, Canada, and Lillestrøm, Norway. The pictures are sorted into three states: vegetation, solid obstacles and clear sky. The simulated satellite look angles are combined with the digital pictures to determine the path state for each satellite, i.e., shadowed, blocked or clear line-of-sight. Cumulative distributions of narrowband fading at L-band are developed for the case when the receiver utilizes one (best or highest) satellite, and up to three-fold diversity with either switching or coherent combining of the received signals. By selecting the best satellite instead of the highest, a significant reduction in fading is obtained. For Lillestrøm, the necessary fade margin to obtain 1% outage is reduced by 13 dB when using 3-fold coherent combining diversity instead of the single best satellite.

1. Introduction

A growing number of land-mobile satellite (LMS) communication systems provide worldwide telecommunication services. These systems suffer from fading due to blockage and shadowing by buildings and vegetation. The fading mechanisms have been investigated and several statistical models have been derived. One method based on the analysis of hemispherical photographs has been developed to derive statistics of whether the path to the satellite is line-of-sight (LOS), shadowed by vegetation, or blocked by solid obstacles [1]. A significant advantage of the method is that it minimizes the need for expensive propagation campaigns to monitor actual signal transmissions, and results may be extrapolated to similar locations and different satellite constellations relatively easily.

This paper reports on the performance prediction of a low-earth-orbit (LEO) system for Ottawa, Canada, and Lillestrøm, Norway. Cumulative distributions of narrowband fading at L-band are developed for the case when the receiver utilizes one (best or highest) satellite, and up to three-fold diversity with either switching or coherent combining of the received signals. The percentage of the sky in each of the three states (LOS, shadowed and blocked) as a function of the elevation angle is derived for both cities.

2. Methodology

Digital pictures of downtown urban environments were taken with a digital camera equipped with a fisheye lens in Lillestrøm and Ottawa.

2.1. Photographs

Lillestrøm is a small city with about 10000 inhabitants situated 28 km northeast of Oslo with latitude of 59.8^{o} North and longitude 11.0^{o} East. The terrain is relatively flat with mainly 2-3 story houses in a mixture of business and residential buildings; the streets have mainly two lanes. Ottawa is a larger city of about a half-million inhabitants, situated at 45.4^{o} North and 75.9^{o} West, with a downtown area dominated by large and high buildings, and wider streets compared to Lillestrøm. Seventy images and about two hundred were acquired to characterize Lillestrøm and Ottawa, respectively. All the pictures were taken at head-height at potential user positions along the sidewalks during late spring when most of the trees had leaves.

An example picture from Ottawa is shown in Figure 1. Following the approach developed in [1], the fisheye picture (top) was unwrapped by transforming the polar coordinate system to a Cartesian one (bottom), with azimuth ranging from 0 to 360 deg along the x-axis and the elevation angle ranging from 0 to 90 deg along the y-axis. The pixels in every image were sorted into one of three groups, representing three different propagation states: LOS (white), shadowing by vegetation (gray), and

Figure 1. Top: Fisheye picture. Bottom: unwrapped picture sorted into clear (white), shadowed (gray) and blocked (black) states

blockage by buildings or terrain (black). The resulting picture matrix was stored with a 0.5^o x 0.5^o resolution and later combined with the satellite constellation look angles.

The percentage of the sky, as a function of the elevation angle, in each of the three states is displayed for Ottawa and Lillestrøm in Figure 2. As expected, the occurrence of the blocked state decreases with elevation angle, and Ottawa experiences a higher degree of blocked events than Lillestrøm.

The combined effects of the terrain and user location on system performance were investigated by reapplying the

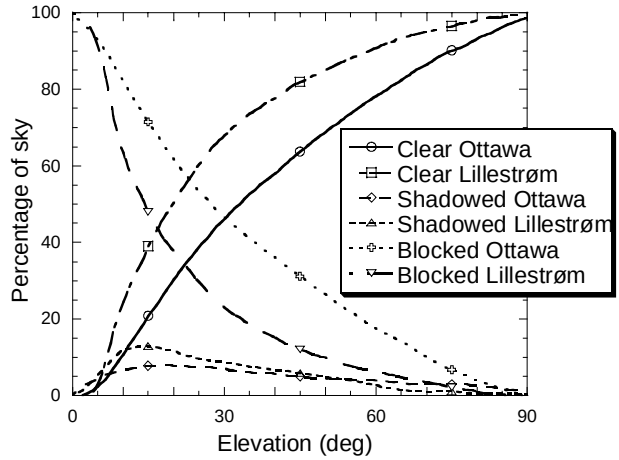

Figure 2. Percentage of sky in clear, shadowed and blocked state as function of elevation angle

images from Ottawa at a higher latitude, i.e., at Oslo (59.9^o North, 10.7^o East), assuming that the urban environment at both cities can be considered similar in a statistical sense.

2.2. Satellite constellation

Satellite elevation and azimuth angles for the Globalstar constellation were simulated and combined with the processed pictures in order to determine the propagation conditions for each satellite as a function of time and user location. The circular orbit LEO constellation consists of 8 planes with 6 satellites each, inclined 52^o with respect to the equatorial plane. The orbit period is 114 min with an orbit height of 1414 km. The satellite positions were calculated over a period of 48 hours with a 5 sec interval. If not otherwise mentioned, all satellites above the local horizon were used in the simulation.

2.3. Three-state L-band channel model

Three statistical channel models corresponding to LOS, shadowing and blockage are combined into a single function by calculating the probability of being in each of the three states (*C, B, S*). The Rice-Nakagami distribution is used to describe the channel envelope *v* when a clear LOS path between the satellite and the user is available. The probability density function (pdf) is:

$$f_{Rice}(v) = 2Kve^{-K\left(v^2+1\right)} I_0\left(2Kv\right) \tag{1}$$

where I_0 is the modified Bessel function of the first kind and the Rice factor *K* is the ratio of direct component to diffuse multipath power.

The distribution developed by Loo [2], which is a sum of a diffuse Rayleigh distributed component with uniformly distributed phase, and a lognormally distributed direct component, is used in both the shadowed and blocked cases, with different parameter values. In blocked situations, the model reduces to a Rayleigh model, while in line-of-sight conditions it reduces to the Rice-Nakagami model. The L-band model parameters used are from [1], taking into account specular reflections and diffracted components in addition to the diffuse component in the blocked urban environment. The Loo pdf may be written as:

$$f_{Loo}(v) = 6.93\frac{Kv}{\sigma}\int_0^\infty \frac{1}{z} e^{-\frac{\left(20\log_{10}(z)-\mu\right)^2}{2\sigma^2} - K\left(v^2+z^2\right)} \cdot I_0\left(2Kvz\right)dz \tag{2}$$

where the parameter μ is the mean value of the normally distributed variable $w = 20\log_{10}(z)$, and σ is the standard deviation of *w*.

Environment	Channel state		
	Clear	Shadowed	Blocked
Urban [1]	K = 7.7 dB	K = 13 dB μ = -10 σ = 3	K = 27 dB μ = -20 σ = 7.3
Urban [4]	K = 8 dB	K = 15 dB μ = -10 σ = 3	K = 20 dB

Table 1. L-band channel model parameters

In this case, the power in the Rayleigh distributed diffuse component is 1/*K*. The parameters for the three states are shown in Table 1, together with the parameters given by Karasawa et al. [4]. Karasawa used the Rayleigh model in the blocked state; otherwise the parameters for the line-of-sight and shadowed cases are quite similar.

Denoting the probability of being in each state as P_C for the open state, P_S for the shadowed state, and P_B for the blocked state, the composite probability density function for the envelope *v* becomes:

$$f_v(v) = P_C \cdot f_{Rice}(v) + P_S \cdot f_{Loo}(v) + P_B \cdot f_{Loo}(v) \qquad (3)$$

The state probabilities P_C, P_S, and P_B are calculated from the combination of the simulated satellite look-angles and the processed three-state pictures. The values for single satellite operation are given for two scenarios in Table 2, the first when the mobile terminal picks one of the best satellites. The best satellite at each time instant is ranked according to if it has a clear, shadowed or blocked path to the user. The second scenario is when the satellite with the highest elevation angle is used.

The probability of being in a clear (LOS) or shadowed state is larger in Lillestrøm than in Ottawa, while the opposite is true for the blocked state. This indicates that the small town characteristics of Lillestrøm outweigh the disadvantage the higher latitude has on the satellite look angles. This latitude effect is observable on the probability values for Oslo, which were obtained by reusing the photographs taken in Ottawa. By inserting the results from Table 2 into Equation 3, the predicted fade cumulative distribution function (CDF) for the three locations are obtained, and displayed in Figure 3.

	Best satellite			Highest satellite		
Location	P_C	P_S	P_B	P_C	P_S	P_B
Ottawa	0.859	0.035	0.106	0.672	0.046	0.282
Ottawa*	0.853	0.035	0.112	0.672	0.046	0.282
Lillestrøm	0.883	0.056	0.062	0.718	0.074	0.209
Oslo	0.766	0.052	0.183	0.605	0.047	0.348

Table 2. Probability of Clear, Shadowed or Blocked channel state for single satellite operation. Ottawa*: minimum elevation angle of 10°

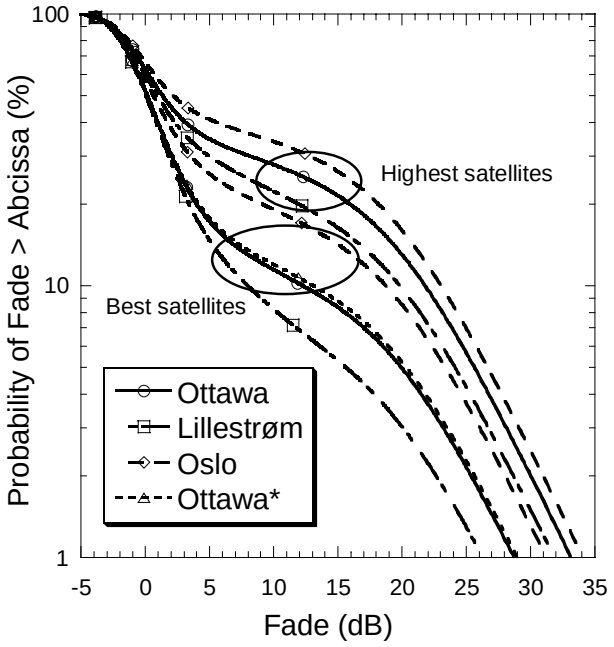

Figure 3. Signal fading for single satellite operation, best and highest satellite

By selecting the best satellite instead of the highest, a significant reduction in fading is obtained for the three sites. Lillestrøm experiences the least severe fading, and Oslo the most. To obtain 5% outage time by using the single best satellite, a margin of 16-23 dB is needed. By increasing the minimum elevation angle from 0° to 10° for Ottawa, the increase in fade margin is negligible.

3. Diversity operation

A method used to mitigate fading caused by shadowing and blockage is satellite diversity. By allowing the user access to more than one satellite at the same time, a diversity gain may be obtained by utilizing switching (handover) diversity between the satellites, or by coherently combining the received signals.

There are a number of different propagation states when using diversity, as opposed to single satellite operation with only three states (*C, B, S*). The minimum number of potentially visible satellites in Ottawa is 4, Lillestrøm and Oslo have at least 3 satellites potentially visible at any time instant. The largest elevation angle to the satellites is 90° in Ottawa, 52° in Lillestrøm and 53° in Oslo.

The N = 6 state-occurrence probabilities, P_n, for two-fold (k = 2) diversity at the three sites are shown in Figure 4. The state probabilities for each location add up to one. Similarly, the N = 10 state-occurrence probabilities for three-fold (k = 3) diversity are displayed in Figure 5.

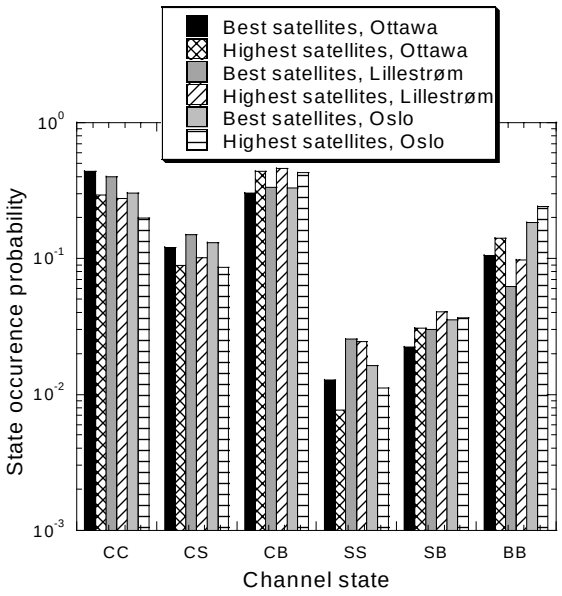

Figure 4. State occurrence probability for two-fold diversity

For *combining diversity* the signal envelopes are added coherently as

$$v = \sum_{l=1}^{k} v_l \tag{4}$$

and the resulting pdf for each path state N is the convolution of the k individual pdf's [3]:

$$f_n(v) = f_{n,1}(v) \otimes ... \otimes f_{n,k}(v), \text{ n = 1,...,N} \tag{5}$$

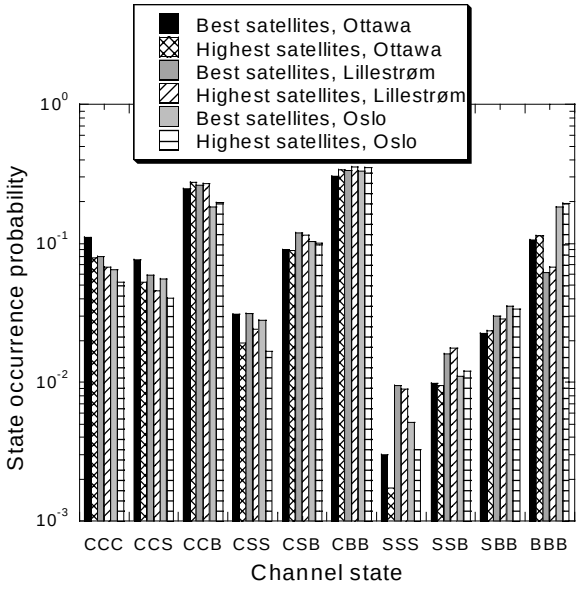

Figure 5. State occurrence probability for three-fold diversity

The combined pdf is then formed by summing the pdfs for each path state, weighted with the state occurrence probability P_n:

$$f_v(v) = \sum_{n=1}^{N} P_n f_n(v) \tag{6}$$

For *switching diversity*, or satellite handover, the user terminal selects the satellite with the strongest signal

$$v = \max(v_1, ..., v_k) \tag{7}$$

The CDF for each path state is the product of the individual CDFs [3]:

$$F_N(v) = \prod_{l=1}^{k} F_{N,l}(v) \tag{8}$$

In the same way as for coherent combining, the combined CDF for switching diversity is the weighted sum of the CDFs for each path state:

$$F_v(v) = \sum_{n=1}^{N} P_n F_n(v) \tag{9}$$

For both coherent combining and switching diversity, the choice of satellites in this study is based on the path states, and not on the instantaneous envelope values.

An example of the predicted fade distributions with and without diversity is shown in Figure 6, where the fade distributions predicted at L-band for coherent combining and switching diversity for the best satellite(s) are displayed for Lillestrøm. Coherent combining of the signals is significantly better than switching, or handover, diversity when seen from a propagation perspective. For Lillestrøm, the necessary fade margin to obtain 1% outage is reduced from about 26 dB for single best satellite operation to about 13 dB when using 3-fold coherent combining diversity.

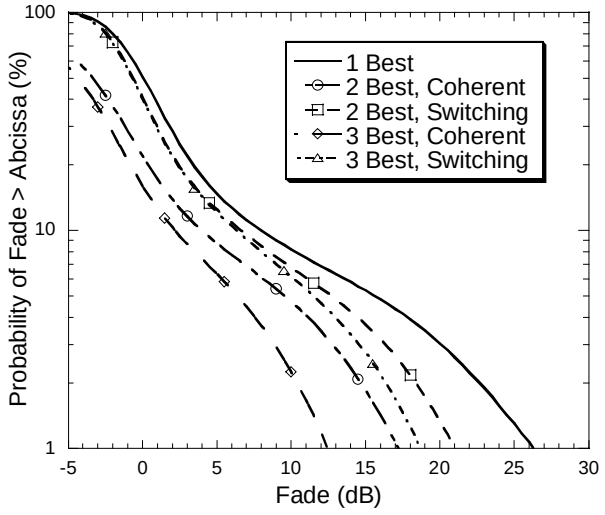

Figure 6. Estimated fade distribution in Lillestrøm for best satellite and up to three-fold diversity

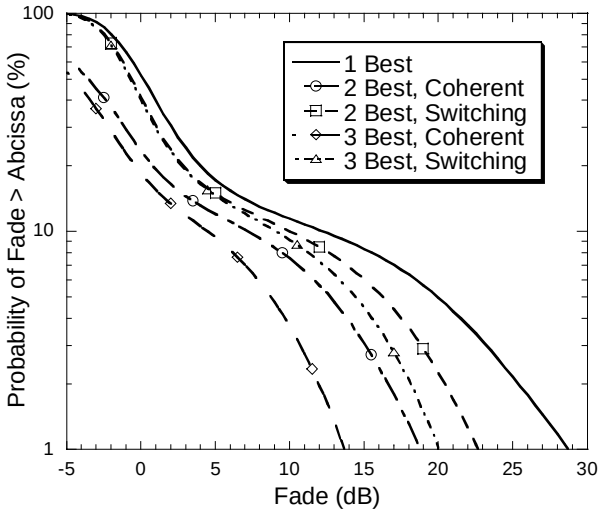

Figure 7. Estimated fade distribution in Ottawa for best satellite and up to three-fold diversity

The fade distribution for the single best satellite worsens significantly when increasing the latitude from 45^o (Ottawa) to 60^o (Oslo), as seen in Figs 7 and 8. However, diversity mitigates this effect to some extent, giving relatively small variations in the necessary fade margin between the three sites.

As seen from Figs 6-8, coherent combining gives better results than switching diversity when seen from a propagation perspective. A disadvantage of coherent combining is the higher use of satellite capacity, as the signals must be transmitted simultaneously over several satellites. It should be noted that no losses due to implementation or time delays associated with handovers are included in the analysis.

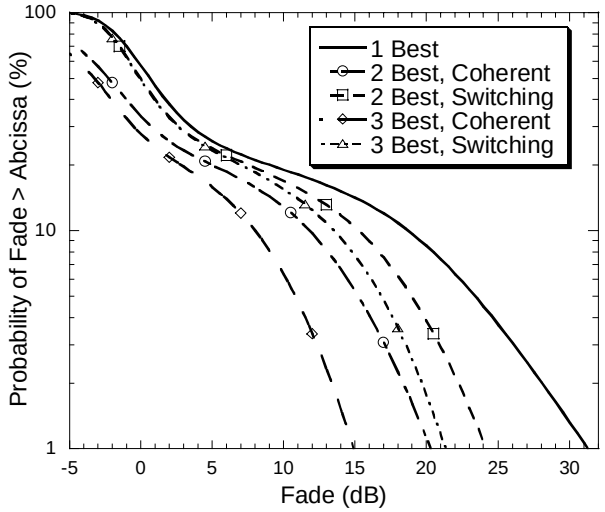

Figure 8. Estimated fade distribution in Oslo for best satellite and up to three-fold diversity

5. Conclusion

In this paper, the fading depth for a single satellite and up to three-fold diversity of a Globalstar-like LEO satellite system in two different cities, Ottawa and Lillestrøm, is obtained using a photogrammetric technique. This technique is particularly useful for the evaluation of diversity system performance in urban areas. It utilizes real scenarios derived from hemispherical pictures of the local environment to produce path states that are then combined for single or multiple satellites in a given constellation in order to predict service availability and quality. It was observed that the necessary fade margin to obtain a given service availability is less in the small, high-latitude city Lillestrøm, than in the mid-latitude city Ottawa. By reapplying the pictures taken in Ottawa to Oslo, the necessary fade margin increased, due to the higher latitude of Oslo and thereby fewer potentially visible satellites. By using the best satellite, instead of the one with highest elevation angle, a significant improvement is achieved. The largest diversity gain is obtained by coherently combining the signals, while the diversity gain obtained by two-fold switching diversity is relatively small.

Acknowledgements

This work is part of an on-going project at the Communications Research Centre Canada, where the first author was a guest researcher and given the opportunity to work on the project. We acknowledge the University of Texas (W. J. Vogel) for sharing the photo processing technology, N. Reed for taking most of the pictures, and T. Nguyen for processing the Ottawa photographs.

References

[1] R. Akturan and W. Vogel, "Path Diversity for LEO Satellite-PCS in the Urban Environment," IEEE *Trans. Ant.Propagat*., vol. 45, pp. 1107-116, 1997.

[2] C. Loo and J. S. Butterworth, "Land Mobile Satellite Channel Measurements and Modelling," *Proc. IEEE,* vol. 86, pp. 1442-1463, July 1998.

[3] A. Papoulis, "*Probability, Random Variables and Stochastic Processes*," Second Edition, pp. 139, McGraw, New York, 1984. ISBN 0-07-048468-6.

[4] Y. Karasawa, K. Kimura and K. Minamisono, "Analysis of Availability Improvement in LMSS by Means of Satellite Diversity Based on Three-State Propagation Channel Model," *IEEE Trans. Vehicular Techn*., vol. 46, no. 4, pp. 1047-1056, 1997.

Paper 3

"Modelling of Mobile Satellite Channels Based on Measurements at 13^{o} and 29^{o} elevation angle"

Published in: *Proc. Tenth International Conference on Antennas and Propagation (ICAP'97)*, Edinburgh, UK, 14-17 April 1997.

MODELLING OF LAND MOBILE SATELLITE CHANNELS BASED ON MEASUREMENTS AT 13° AND 29° ELEVATION ANGLE

L E Bråten (*), N Kawai (**), Y Louahdi (**), and T Tjelta (*)

(*) Telenor Research and Development, Norway
(**) Inmarsat, United Kingdom

Abstract - This paper presents results from land mobile propagation measurements conducted by Inmarsat at 13° and 29° elevation angles in the UK. A number of simultaneous recordings have been made at L-band, using both directive and omni-directional antennas. The measurements took place in the suburbs of London in a variety of propagation environments ranging from open to shadowed areas. Furthermore, the paper presents a new analogue fading channel model for use in simulation of low margin narrow-band systems. The channel model has two states, one representing an open area and the other representing a shadowed area. The model parameters have been fitted to the recorded measurements[1]. The interest has been on models for the open and lightly shadowed states and though some deep fade analyses have been included, the paper mainly focuses on the former one.

I. INTRODUCTION

Land mobile satellite systems provide communication services in a variety of propagation environments. Several systems are planned and scheduled for implementation within a few years to provide personal and data communication. There is also a growing number of systems using high gain directive antennas at the mobile station, especially for higher data rates. Several propagation measurements at L-band using omni-directional antennas have been reported, but only a few considered the effect on the channel dynamics by directive antennas. Inmarsat therefore decided to perform some measurements in typical propagation environments. Measurement data give a first hand understanding of the propagation channel behaviour. They also provide necessary information for simulation studies to be performed. Analogue channel models are required in order to simulate communication systems, e.g. those using forward error control with soft decisions. The time varying channel characteristics are also crucial when designing the synchronisation system, e.g., carrier recovery, symbol timing and framing. The work presented in this paper is an analysis of measurements and a derivation of statistical parameters that in turn may be used in the proposed two-state model for performance simulation.

II. EXPERIMENTAL SET-UP

Three different satellites with elevation angles of 13° and 29° were used as shown in Table 1.

Table 1- Space segment

Satellite	Longitude	Elevation from London
Inmarsat-2 AOR-E	15.5° W	29.3°
Marecs B2	15° W	29.4°
Inmarsat-2 AOR-W	54° W	13.0°

The mobile antennas were mounted on a cruising station wagon. One omni-directional antenna was used to generate a reference signal in addition to the signal from one of two directional antennas with gain of 9 and 11 dBi as shown in Table 2. The received carriers were down converted to base-band, and complex samples together with antenna pointing direction, car heading and speed were recorded. The dynamic range in the measurements is about 20 dB. The analogue tape recordings were digitised and transferred to a work station for statistical analysis.

Table 2- Antenna characteristics

No	Type Omni/ Directional	Peak gain (dBi)	Diameter and Height (cm)	3 dB beam-width az, el (dgr)
1	Directive (D)	9	20, 17.5	70, 40
2	Directive (D)	11	32, 5	36, 52
3	Omni (O)	2	-	360, 180

III. ROUTES DESCRIPTIONS

Four test routes were chosen, representing propagation conditions ranging from line-of-sight to shadowing and blocking. The different environments cover lightly and heavily wooded areas and both rural and urban areas as shown in Table 3.

[1] Parts of this work was supported by Inmarsat.

Table 3- Test runs

Test route	Environment	Classification	Location
R1	Highway, mixture of open and lightly wooded	Highway	Guilford
R2	Heavily wooded road	Heavily wooded	Guilford, Woodford
R3	Suburban road with mixture of open areas, lightly wooded and 2-story houses	Suburban	Woodford
R4	Tall buildings	Urban	Old Street

The roads ranged from motorway, single lane roads, underpasses and roundabouts or a circular route where all possible orientations to the satellite were obtained. The measurements took place during the winter months.

IV. STATISTICAL ANALYSIS

A statistical analysis of the recorded propagation data has been performed, including envelope as well as fade and non-fade duration distributions. The recorded data, sampled at 1000 samples per second, was first low-pass filtered. The cut-off frequency was chosen to 50 Hz in all runs as a compromise between noise and spurious rejection and preserving the Doppler spreading. The power in a initial state, where the vehicle was standing still and no obstacles occurred, was normalised to one before the data was sorted into a shadow area and a open area state with a threshold of 3 and 5 dB for the directional and omni antennas respectively. The envelope threshold values were chosen based on visual inspection of the results of the state sorting algorithm. When sorting the time series into the shadow and the open state using an envelope threshold, a minimum open state duration of 2 m was introduced to avoid change in state due to fast signal fluctuations introduced by multipath scattering. The measurements were sorted and grouped according to propagation environment and antenna type before performing the statistical analysis. The two directive antennas, 1 and 2, were grouped together to obtain better confidence. Each run was carefully inspected and those with repeated equipment failure were not used. Furthermore, the time series with directive antenna mispointing exceeding 5 degrees, were not used. The duration statistics were, due to insufficient speed information for some runs, calculated on the basis of the average vehicle speed in the runs (40 km/h). The two states used in this paper are described in further detail below.

A. Open state model

The open state is represented by a Rice model with a constant line-of-sight signal plus a Rayleigh distributed diffuse component resulting from a number of reflected and diffracted components. The envelope probability density function (PDF) of the total multiplicative fading distortion may be written, Proakis (1)

$$p(r)=\frac{r}{\sigma^2}e^{-\left(r^2+s^2\right)/2\sigma^2}I_0\left(\frac{rs}{\sigma^2}\right) \qquad (1)$$

where the direct component, s, and the diffuse component, σ, may be expressed by the Rice factor K as $\sigma^2=\frac{1}{2(K+1)}$ and $s^2=\frac{K}{K+1}$.

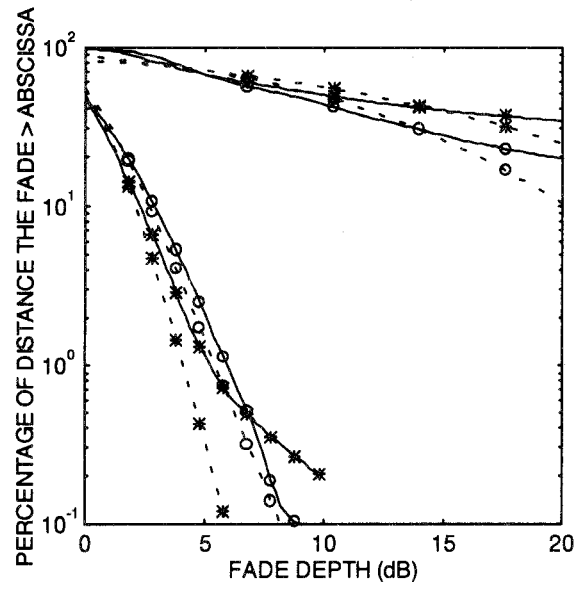

Figure 1: Average CDFs at 29° elevation. Measured (solid), Theoretical (dashed), Directive ant. (*), omni ant. (o)

The average fade depths shown in Figure 1 is the average of all the measured environments at 29°. The open state received power cumulative density functions (CDFs) are the lower family of curves (shallow fades). The low pass filtered signal (see section IV.B for further details) giving the slowly varying direct component are shown in the upper family of curves. Parameters for the average in addition to each test route are shown in Table 4.

B. Shadow state model

The shadow state representing shadowing or blockage is modelled as a linear combination of a slowly varying log-normal distributed line-of-sight signal and a fast varying Rayleigh distributed diffuse component with variance σ_r^2. The extraction of the slowly varying direct component from the total fade signal was done by a Chebyshev type II low-pass filter with cut-off frequency of 5 Hz (free of pass-band ripple). The diffuse component was computed by subtracting the direct component from the total signal.

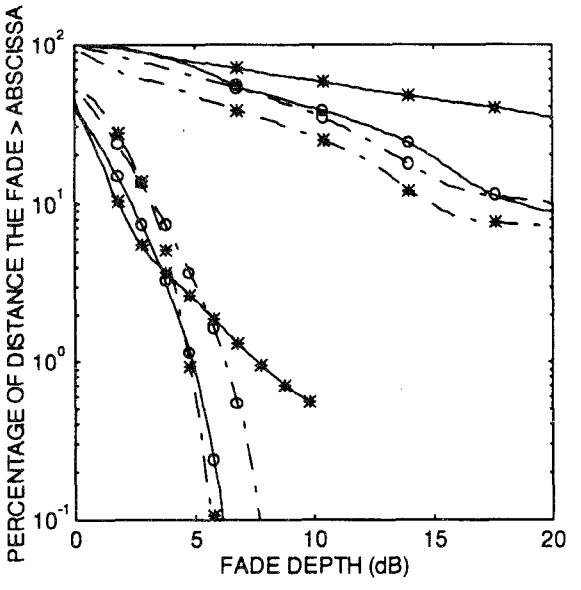

Figure 2: Fade depths at 13° (dashed) and 29° (solid) elevation for R3. Directive ant. (*), omni ant. (o)

The envelope of the direct signal is assumed to have a log-normal PDF, Vucetic and Du (2)

$$p(r) = \frac{1}{r\sigma_1\sqrt{2\pi}} e^{\frac{-(\ln r - \mu_1)^2}{2\sigma_1^2}} \quad (2)$$

with parameters μ_1 and σ_1. The mean value of the direct signal's envelope is

$$\mu_s = e^{\mu_1 + \frac{\sigma_1^2}{2}} \quad (3)$$

and the variance is

$$\sigma_s^2 = e^{2\mu_1 + \sigma_1^2}(e^{\sigma_1^2} - 1) \quad (4)$$

The fade depths in suburban areas for 13° and 29° elevation are shown in Figure 2. The open state received power CDFs are the lower family of curves (shallow fades). The slowly varying direct component are shown in the upper family of curves.

C. Large area model

A multi-state model switching between the states, is often called a Markov process with state probabilities and state-transition probabilities. Here, a two-state model is given using a re-alternating process, i.e. a state always changes to the other state. Unlike a Markov process the model shown in Figure 4 is driven by an environment signal consisting of the open and shadow state duration statistics obtained from measured propagation data.

Table 4- Model Parameters

		Open state			Shadow state						
Environment	Ant	K (dB)	b	c	A (%)	μ_s (dB)	μ_1	σ_1	σ_r	μ_2	σ_2
Average (R1-R4)	D	12.8	1.59	0.79	59	-3.2	-1.33	1.39	0.07	2.08	2.46
29°	O	10.9	1.47	0.75	58	-5.6	-1.1	0.95	0.09	1.74	2.13
Highway (R1)	D	15.4	2.00	0.67	26	-4.3	-0.60	0.45	0.07	1.53	1.53
29°	O	12.7	1.68	0.73	30	-4.1	-0.50	0.25	0.08	1.36	1.57
Heavily wooded (R2)	D	13.4	2.37	1.02	79	-7.2	-1.07	0.69	0.08	2.76	1.58
29°	O	10.4	1.75	0.89	80	-8.5	-1.19	0.71	0.13	2.63	2.15
Suburban (R3)	D	14.8	2.47	0.79	42	-7.0	-1.57	1.24	0.07	1.07	2.24
29°	D	9.1	1.32	0.93	69	-2.2	-0.60	0.84	0.11	3.50	2.10
13°	O	13.1	1.34	0.60	40	-6.5	-1.01	0.73	0.09	1.80	1.90
	O	9.5	1.27	0.68	51	-5.1	-0.89	0.78	0.11	1.71	1.51
Urban (R4)	D	10.6	1.90	1.46	90	-2.1	-3.99	2.74	0.06	3.00	2.55
29°	O	8.9	1.76	1.00	84	-11.0	-2.10	1.29	0.08	1.88	2.23

Recommendation P.681.2 of the International Telecommunication Union (ITU) models shadowing duration by a log-normal distribution function (3). This is the same function as for the fade depth when shadowing is present, see Equation 2. The parameters for the shadowing duration distribution, shown in Table 4, are denoted as μ_2 and σ_2.

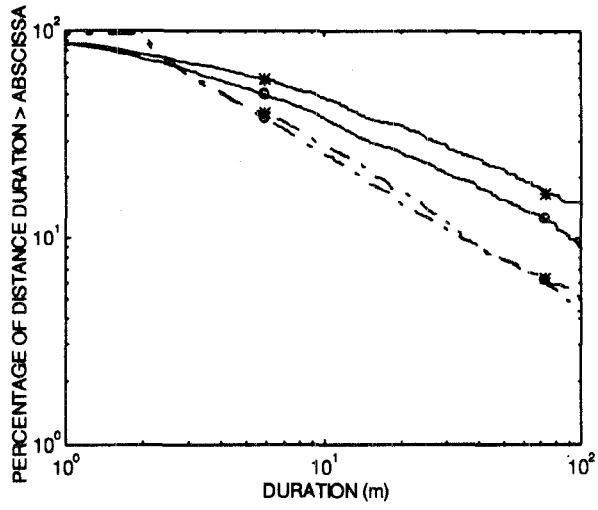

Figure 3: Average shadow (solid) and open (dashed) state duration at 29°. Omni ant (o), Directive ant. (*)

The power law CDF for the open state duration in meters (d) is given by (3)

$$P_x(d \le x) = 1 - \frac{b}{x^c} \qquad (5)$$

where b and c are constants and the minimum non fade duration is limited to $x \le x_{\min} = b^{1/c}$.

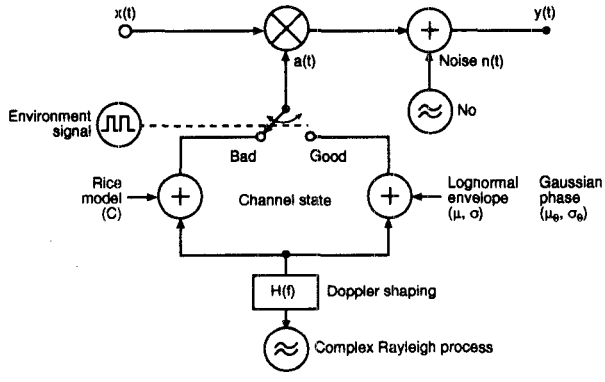

Figure 4: Two state channel model

V. DISCUSSION

A. Occurrence of shadow state

The percentage of distance in the shadow state, A in Table 4, is quite similar for the two antenna types (directive/omni) for most environments, except suburban at 13° elevation (and to some extent urban at 29°) where the directive antenna experiences 18 % more shadowing than the omni-directional antenna. The city measurements conducted by Lutz et al (4) show shadowing coefficients, A, in the range 58 to 72 % at 34°. In 'old city' it was varying between 66 and 79 % at 24°, which is close to the value 79 % found by Robet et al (5). The somewhat larger values shown in this paper for urban environment at 29°, 90 % for the directive antenna and 84 % for the omni-directional antenna, are probably due to a combination of lower elevation and different urban environment. Lutz et al present suburban shadowing coefficients of 45 % at 24° and 71 % at 13°. Corresponding numbers for directive and omni-directional antennas in this paper are 40 and 42 % at 29° and 69 and 51 % at 13°. At 34° elevation, Lutz et al show shadowing coefficients in highway of less than 1 % and, depending on the antenna type, 19 to 25 % at 13°. The numbers found here, 26 % for directive antenna and 30 % for omni-directional antenna, indicating slightly more shadowing.

B. Open area statistics

Shown in Figure 1 is the average open area CDFs for the omni-directional and the directive antennas. While the omni CDF closely follows a Rice distribution, the directive antenna deviates for small percentages of duration. A "Rayleigh" slope of 10 dB per decade seams to fit well, suggesting that a number of reflected and/or diffracted signals are received. In fact, this is also the case for the omni-directional antenna for percentages below 0.1. This results is reasonable due to the sorting of the data, where a minimum open state duration is used. The open state includes short durations of non line-of-sight conditions caused by blocking obstacles less than the duration threshold. Lutz et al present Rice factors of 6 to 10 dB at 34° in city area and 6 to 11.9 dB at 24° in old city, depending on the antenna type. In highway environments the Rice factor varied from about 12 to about 17 dB at both 24° and 34° elevation. The Rice factors shown here correspond well to this, both for the urban and the highway environment. In all environments, except the suburban at 13°, the directive antenna has a higher Rice factor than the omni-directional antenna.

C. Shadow area statistics

Vucetic and Du (2) found mean direct component envelope values (μ_s) of -2.1 dB on a rural road and -3.5 dB for heavy tree shadowing. The environment in Table 4 comparable to the rural road is highway, where the mean is -4.3 for the directive and -4.1 dB for the omni-directional antenna, i.e. about 2 dB more attenuation. The values for heavily wooded areas are -7.2 and -8.2 dB, i.e. about 4 dB increased attenuation. The CDF of the slowly varying direct component envelope in the shadow state is shown in Figure 1. The deviation between the theoretical curve and the measured at low percentages of distance indicates that deep fades can be better modelled by a distribution like the Suzuki. An approximation to the Suzuki distribution is a product of a log-normal distributed variable and a Rayleigh distributed variable, which is used in (4) to model fading.

D. Open and shadow state duration statistics

The open and shadow state durations, shown in Figure 3, are longer than in a previous analysis performed by Hase et al (6). The main reason for this is believed to be the introduction of the minimum open state duration of 2 m before a change to the shadow state is allowed to occur, although using the average speed instead of instantaneous speed in the analysis gives some inaccuracies. By introducing a duration threshold, the open state duration statistics reflect the length between obstacles causing shadowing. Being in the open state, fades due to multipath scattering and small obstacles will not cause state change. It would haven been interesting to introduce a similar minimum length for the shadow state, however, this was not done due to limited computational and time resources. The log-normal distributions for the shadow state duration and the power law distribution for the open state duration, proposed for fade and non fade durations by ITU-R (3), fits well to the measured ones, given that the model parameters obtained from the analyses are used.

VI. CONCLUSIONS

Measurements and statistical analyses of land mobile satellite channel behaviour have been performed. A new two state analog model for simulation of land mobile satellite systems has been developed. The model is a re-alternating state model driven by the statistics of intervening obstacles causing shadowing or blockage of the line-of-sight signal. For each state measured CDFs have been fitted to the theoretical. Future work could be to explore the linear connection found by Conrat and Pajuco (7) between the power in the diffuse component and the power in the shadowed direct component, and also to introduce a 3rd state representing deep fades caused by blocking in addition to open and lightly shadowed areas.

VII. REFERENCES

1 Proakis J. G., 1995, "Digital communications", Third edition, McGraw-Hill, New York

2 Vucetic B. and Du J., 1992, "Channel modelling and simulation in satellite mobile communication systems", IEEE J. on Sel. Areas in Comm., 10, 1209-1217

3 ITU-R Rec. P.681.2, 1995, "Propagation data required for the design of earth-space land mobile telecommunication systems"

4 Lutz E., et al, 1991, "The land mobile satellite communication channel-recording, statistics, and channel model", IEEE Trans. on Veh. Techn., 30, 375-386

5 Robet P. P., et al, 1992, "Land mobile satellite communication channel model for simultaneous transmisson from a land mobile terminal via two satellites", Intern. J. on Satellite Comm., 10, 139-154

6 Hase Y., et al, 1991, "Fade-durations derived from land-mobile-satellite measurements in Australia", IEEE Trans. on Comm., 39, 664-668

7 Conrat J. M. and Pajuco P., 1996, "Fading and shadowing analysis of mobile satellite propagation channel at 1.5 and 2.2 GHz using a helicopter", In Proc. of ACTS Mobile Telecommunications summit, Granada, 2, 624-630

Paper 4

"An Improved Three-State Semi-Markov Model Optimised for Land Mobile Satellite Communication"

Published in: *Proc. AP2000 Millennium Conference on Antennas & Propagation*, Davos, Switzerland, April 9-14 2000.

Correction:
The sentence "Transitions to the blocked state are less likely in wooded areas than in suburban, as expected." on page 3 should be "Transitions to the blocked state are more likely in wooded areas than in suburban." The cumulative distribution function in Eq. 4, with corresponding parameters in Table 1, denotes percentage probability.

AN IMPROVED THREE-STATE SEMI-MARKOV PROPAGATION MODEL OPTIMISED FOR LAND MOBILE SATELLITE COMMUNICATION

Lars E. Bråten[(1)], Terje Tjelta[(2)]

Telenor Research and Development, Instituttveien 23, PoBox 83, N-2027 Kjeller, Norway
E-mail: [(1)]Lars-Erling.Braten@telenor.com, [(2)]Terje.Tjelta@telenor.com

ABSTRACT

A new semi-Markov model for the land mobile satellite channel is developed. The statistical channel model has three states representing open areas, shadowing and blocking of the signal. The duration spent in each state is drawn from ITU-R recommended probability distributions with modified parameters. This is an improvement over the more common Markov model where the duration in each state is forced to follow an exponential distribution. The model enables more accurate prediction and simulation of system performance and availability. The model is applied to measurements conducted by Inmarsat at L-band in the UK.

INTRODUCTION

Land mobile satellite systems provide communication services in a variety of propagation environments. Several systems are planned and scheduled for implementation within a few years to provide personal and data communication. It is therefore important to have realistic dynamic models of the land mobile satellite channel that may be used in system simulations and performance evaluation.

The objective of this study is to improve the statistical channel model used to represent fade and non-fade duration statistics. A commonly used methodology to model the slowly varying environmental effects on the received signal is a Markov chain, see e.g. [1, 2]. The channel properties are assumed quasi-stationary in small time periods, and during these periods represented by stationary stochastic processes. This type of Markov model gives unrealistic values of the duration of fades and non-fades as the state duration must be exponential in Markov models. The time duration statistics are crucial when simulating the synchronisation system, e.g., carrier recovery, symbol timing and framing. We introduce a modification to the Markov model called a semi-Markov process improving the state duration statistics.

STATE MODELLING

The long-term variations in the received signal may be described by a chain of distinct states. The basic idea of hidden chains is shown in Fig. 1a. The position of the switch determines which of the stochastic process $x_i[n]$ that is observed at the output, where each process represents a specific propagation scenario. The shorter-term variations within each state may be modelled by analogue valued channel models. The number of states used to model the propagation channel, often two or three states, are utilised to represent open areas, shadowing and blockage. Commonly used statistical fading distributions of the processes $x_i[n]$ are the Rice-distribution for the open areas ($x_1[n]$), the general Loo-distribution for the shadowed case ($x_2[n]$) and the Rayleigh-distribution for blocked areas ($x_3[n]$) [3]. The random process s[n] represents the switch position, whose state is characterised by a Markov chain with state transition diagram depicted in Fig. 2b.

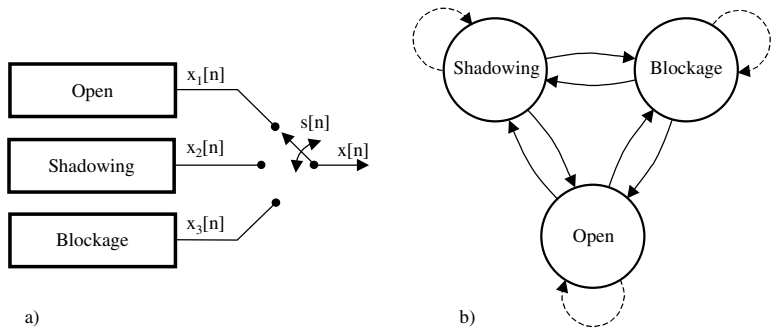

Fig. 1. Generation of the observed sequence (a) and state transition diagram of a Markov chain (b)

The underlying chain s[n] takes on a finite number of values (three here) but these values cannot be observed directly, i.e., the chain is hidden. A Markov chain is a random process taking only on discrete values satisfying the condition in (1) [4]

$$\mathrm{P}\left[s\left[n\right] = s_n \left| s\left[n-1\right] = s_{n-1}, s\left[n-2\right] = s_{n-2}, \ldots \right.\right] = P\left[s[n]=s_n \left| s[n-1]=s_{n-1} \right.\right] \tag{1}$$

Let the possible values s[n] can have be denoted S_1, S_2, ..., S_Q. When s[n]=S_i the Markov chain is said to be in state i and the conditional probabilities $P_{i|j}[n] = \Pr\left[s[n]=S_j \left| s[n-1]=S_i \right.\right]$ are known as the state transition probabilities. If the Markov chain is stationary, the transition probabilities are independent of n.

Duration in each state

Assume that a stationary Markov chain is in state S_i. The probability that any N consecutive samples take on the same value is

$$p_i\left(d = N\right) = \prod_{j=1}^{N} \mathrm{P}_{i|i} = P_{i|i}^{N} \tag{2}$$

The cumulative duration distribution for each state in the Markov chain, becomes therefore

$$P_i\left(d \le N\right) = \sum_{j=1}^{N} p_i\left(d = j\right) = \sum_{j=1}^{N} P_{i|i}^{j} \tag{3}$$

where the duration becomes N times the sampling time or sampling distance.

The physical interpretation is that each state of the Markov chain represents an obstacle, or the lack of one, causing the channel to be in either an open, shadowed or blocked condition. The model stays within a state for a certain time, or equivalently, a distance. This time is directly related to the size of the objects and the spacing between them. Specific types of obstacles are also expected to dominate in a given state. Solid obstacles as houses, bridges etc. will most probable cause a total blockage of the signal while trees would typically lead to a shadowed state. In practice, this also impose a minimum state duration as given by the minimum size of an obstacle being able to cause observable effects on the received signal. Measurement results indicate a minimum state duration of a few meters [2, 5]. This will be the result if short duration deep fades are allowed in the open state and periods with low channel attenuation in the shadowed and blocked states. Deep fades in open areas may be caused by utility poles and multipath propagation.

Semi-Markov Chain

Ideally, we would expect a perfect match between the measured or empirical state duration and the type of duration distribution given in (3). However, previous studies have shown that the open state non-fade duration follows a power law distribution, while the fade-duration distribution is log-normal [6]. The non-fade duration distribution recommended by the ITU-R is [7]

$$P_1\left(d \le N\right) = 1 - \beta N^{-\gamma} \tag{4}$$

where the parameters β and γ depend on the degree of optical shadowing. The ITU-R fade duration model does not separate the degree of attenuation and use only one fading state. A threshold of 5 dB was used to distinguish between non-fade and fade-state; the duration sensitivity to the choice of threshold was relatively low [6]. We would therefore not be surprised if the shadowing and blockage duration statistics exhibit similar empirical distributions. The recommended fade duration distribution is a log-normal model valid for $d \ge 2$ cm

$$P_{2,3}\left(d \le N\right) = \left(1 + erf\left[\left(\ln(d) - \ln(\alpha)\right) / \sqrt{2}\sigma\right]\right) / 2 \tag{5}$$

where σ is the standard deviation of ln(d), ln(α) is the mean value of ln(d) and the error function is defined as $erf\left(x\right) = 2/\sqrt{\pi}\int_0^x e^{-t^2}dt$.

One way to force the duration in each state to follow a defined distribution is obtained if the self-loops in Fig. 2b are removed and the duration in each state is drawn from the required duration distribution function. This type of model for s[n] is called a semi-Markov process [8]. In this model the state transitions do not occur at regular time intervals. The transition between the states are described by the transition probabilities P_{ilj} where i≠j. This is different from a traditional Markov model, where the self loop transitions i=j are allowed.

MEASUREMENT RESULTS

One method to identify the hidden states in the chain is by sorting the timeseries according to a local average power level. We use a local average over five wavelengths and thresholds of five and ten dB's when sorting the time series into the states. The L-band measurements used were conducted by Inmarsat around London and are described in [5] where a similar study was performed, resulting in a two-state re-alternating channel model. In the current study two environmental types are investigated, suburban and a heavily wooded road. The elevation toward the satellite is 29° for the wooded area. Two different satellites with elevation of 13° and 29° respectively have been employed in the suburban measurements. The antenna analysed here is an omni-directional one mounted on a van. The measurements were post-processed by resampling the channel attenuation at every 10 cm and employing a sliding averaging window of 1 m length.

The parameters for the duration distributions (4) and (5) based on measured timeseries are shown in Table 1 together with the recommended values from ITU-R. The main discrepancies between the values extracted from the timeseries and the recommended ones are for β and α. The difference between the extracted parameters and the recommended ones indicate sensitivity to different measurement post-processing methods. In the statistical state models we use the slowly varying local average power to distinguish between the states. The filtering employed to find this local average smoothes the timeseries and seem to decrease the occurrences of short duration events. This smoothing effect and the fact that often more than two states are used lead to a necessary parameter modification in the duration distributions recommended by ITU-R.

The extracted state transition probabilities are given in Table 1. No transitions occurred directly between the open state and the blocked state. Transitions to the blocked state are less likely in wooded areas than in suburban, as expected. The transition probability dependence on elevation angle in the suburban environment is negligible. This indicates that the obstacles causing shadowing and blockage are close to the roadside and they were not avoided by increasing the elevation angle from 13° to 29°.

The empirical state duration statistics for the two environments are depicted in Fig. 2 together with the recommended ITU-R distributions with the modified parameters from Table 1. There is a good agreement between the ITU-R models with the new parameters and the measured state duration statistics for all the three states. The tail of the measured open state duration may be approximated by a straight line on the loglog plot, however, this may exaggerate the occurrence of non-fade events shorter than about 1 m. The open state duration increases with the elevation angle while the blocking duration decreases in the suburban case. The blocking duration is somewhat longer than the shadowing duration. This is expected as the size of the obstacles causing blockage (e.g. houses) would normally be larger than obstacles causing shadowing (e.g. trees). However, the relatively small difference between the duration statistics for these two states is consistent with previous reported results [6]. Along the wooded road the measured shadowing and blockage durations are similar for large percentages of distance.

Table 1. State duration statistics

	State 1		State 2		State 3		Transition probabilities					
	β	γ	α	σ	α	σ	P_{112}	P_{113}	P_{211}	P_{213}	P_{311}	P_{312}
Suburban 29°	88.28	0.61	1.73	1.11	2.62	0.98	1	0	0.65	0.35	0	1
Suburban 13°	83.34	0.66	1.89	0.93	3.28	1.04	1	0	0.65	0.35	0	1
Wooded 29°	59.96	0.84	2.05	1.05	1.55	1.02	1	0	0.42	0.58	0	1
Moderate shad. ITU-R	20.54	0.58	0.22	1.215	-	-	-	-	-	-	-	-
Extreme shad. ITU-R	11.71	0.84	0.22	1.215	-	-	-	-	-	-	-	-

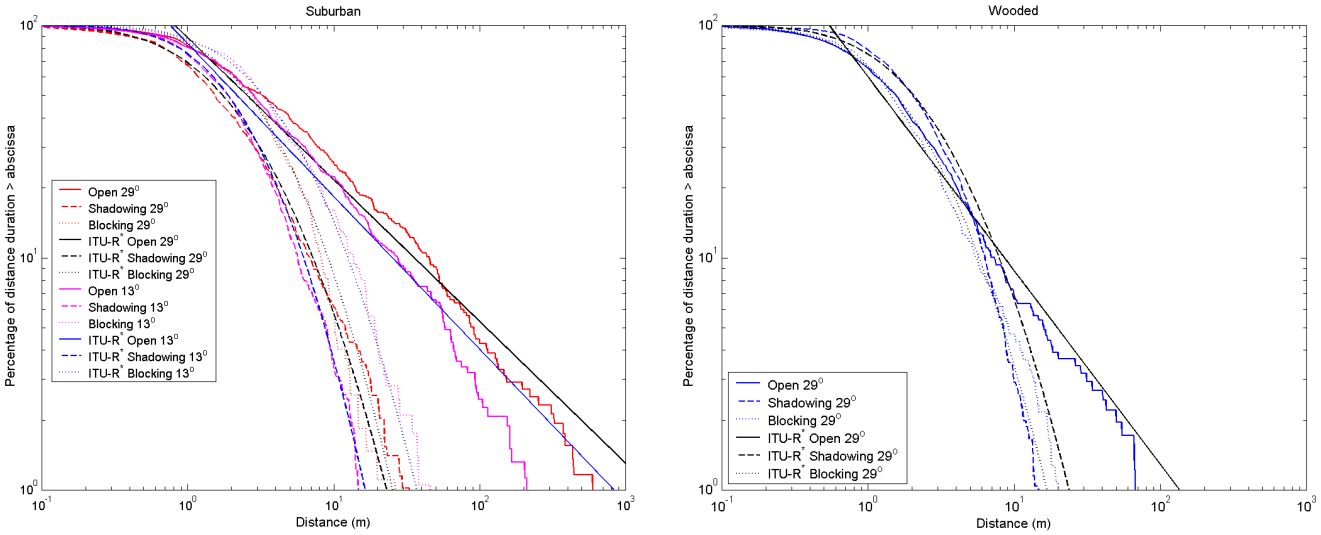

Fig. 2. Duration statistics from wooded and suburban environments. * ITU-R model with modified parameters

For small percentages the duration of blockages somewhat exceed the shadowing duration, probably due to a few solid obstacles along the route.

CONCLUSION

A new three-state semi-Markov land mobile satellite channel model has been developed. The statistical model describes more accurately the duration of states compared to the commonly used Markov model. The semi-Markov model will also improve estimation of system performance and availability. The duration statistics and state transition probabilities have been extracted from measured L-band data in wooded and suburban environments. By modifying the parameters in the duration distributions recommended by ITU-R a good fit is achieved for the three states. This is an improvement over the more common Markov model where the duration in each state is forced to follow an exponential distribution. In the future analysis of more experimental data should be done. A validation could also be derived using building size distributions used for instance in physical-statistical models of the land mobile satellite channel [9].

ACKNOWLEDGEMENT

We will thank INMARSAT for the measurement data.

REFRERENCES

[1] B. Vucetic and J. Du, "Channel modelling and simulation in satellite mobile communication systems", *IEEE J. on Sel. Areas in Comm.*, vol. 10, pp. 1209-1217, 1992.

[2] F. P. Fontan, J. P. Gonzalez, M. J. S. Ferreiro, M. A. V. Castro, S. Buonomo and J. P. Baptista, "Complex Envelope Three-State Markov Model Based Simulator for the Narrow-Band LMS Channel", *Int. J. of Satellite Comm.,* vol. 15, pp. 1-15, 1997.

[3] C. Loo, "A statistical model for land mobile satellite link", *IEEE Trans. on Vehicular Techn.,* vol. 34, no. 3, pp. 122-127, 1985.

[4] C. W. Therrien, *Discrete Random Signals and Statistical Signal Processing*, New York: Prentice Hall, 1992.

[5] L. E. Bråten, N. Kawai, Y. Louahdi og Terje Tjelta, "Modelling of Mobile Satellite Channels Based on Measurements at 13° and 29° elevation angle", *Tenth Int. Conf. on Antennas and Propagation*, ICAP'97, Edinburgh, UK, 14-17 April 1997.

[6] Y. Hase, W. J. Vogel and J. Goldhirch, "Fade-durations derived from land-mobile-satellite measurements in Australia", *IEEE Trans. on Comm.*, vol. 39, pp. 664-668, May 1991.

[7] ITU-R Rec. P.681-4, *Propagation Data Required for the Design of Earth-Space Land Mobile Telecommunication Systems*, International Telecommunication Union, Geneva, 1999.

[8] D. R. Cox, *Renewal Theory,* Methuen, London, 1967. SBN 412 20570 X.

[9] S. R. Saunder and B. G. Evans, "A physical-statistical model for land mobile satellite propagation in built-up areas", In Proc.f of: *Tenth Int. Conference on Antennas and Propagation*, pp. 44-47, April 1997.

Paper 5

"Comparison of Predicted Scintillation with Data Measured from the 50 GHz Italsat Beacon in Norway"

Published in: *Proc. 6th Ka-band Utilization Conference*, Cleveland, USA, May 31-June 2 2000.

one or more of the waves reaches the same order of magnitude as the main wave, deep fade results when the vector components cancel each other [2]. The random enhancement and fading in the received signal power may reach several dB at mm wavelengths.

The purpose of this paper is to present new measurement results of tropospheric scintillation on the 50 GHz beacon from Italsat F1 received at Kjeller, and to compare the monthly empirical cumulative distributions of scintillation intensity with available prediction methods. In the last Section, the diurnal variation in scintillation intensity is presented and some attempt is made to explain the observed peaks during morning and noon.

II. EXPERIMENT DESCRIPTION

The Italian Space Agency planned the Italsat program and the F1 satellite was launched into geostationary orbit in 1991. The satellite was in an increasingly inclined orbit during the measurement campaign. The propagation beacon payload operates at 20, 40 and 50 GHz. Results from the 50 GHz beacon are presented in this paper. This beacon is switched between horizontal and vertical polarization at a frequency of 933 Hz, the same rate as on the Olympus 20 GHz beacon. The beacon signal is transmitted continuously with the exception of the eclipse periods. Beacon measurements started in April 1997 and ended in January 1998. The period analyzed in this study covers April to July 1997.

A. Site description

The Kjeller receive site is located about 20 km northeast of Oslo. Local azimuth towards the Italsat satellite is 178^{o} with an elevation angle of 22^{o}. This region of Norway has mostly an inland climate. During spring, the air may be humid due to unfrozen water in the nearby rivers; when frozen, it is a dry climate. Meteorological data such as precipitation, temperature, pressure, humidity, wind speed and direction are logged at the site.

B. Measurement set-up

The horizontally polarized RF signal is down-converted to IF and demodulated using equipment from a previous Olympus measurement campaign. A PC controls the demodulator and records in phase and quadrature components at a sampling rate of one sample per second. One of the main uncertainties in the link budget shown in Table 1 is the aperture efficiency, which is assumed to be 50 %. The antenna used is an offset parabolic antenna with 1.2 meter diameter. Measurements show that the first side-lobe of the antenna is approximately 10 dB below the main lobe and the main lobe is slightly wider than in theory.

Antenna diameter (m)	1.2
Antenna gain (dBi)	52.9
G/T (dB)	16.8
Satellite EIRP (dB)	26.5
Free space propagation loss (dB)	218.3
Atmospheric attenuation (dB)	2.4
Received C/No within 45 kHz	55.9
Receiver threshold C/No (dBHz)	26.1
Margin (dB)	29.8

Table 1.Link budget for the measurement site.

This indicates some antenna performance degradation translating into a lower gain than in Table 1. In theory, the power margin available to observe the atmospheric influence on the signal attenuation should be about 30 dB. The actual dynamic range used in the analysis is 10 dB due to satellite inclination variations and the use of a non-tracking antenna.

C. Post processing

The fast-varying scintillation component was extracted from the measured signal by subtracting the slowly varying attenuation component, which is caused by precipitation, satellite drift etc. On a decibel scale, the scintillation signal, x is given by

$$x = y - \overline{y} \tag{1}$$

where the slowly varying component $\bar{y}$ is identified with the aid of one-minute averaging of the received signal y. Peak-to-peak scintillation variations as large as 4.6 dB were observed during the first week of May 1997.

In the following Section, the results of four months of measurements are processed, providing a statistical description of scintillation severity. The measured data were separated into "rainy" and "non-rainy" conditions according to a threshold on rain intensity measured by a weighting rain gauge.

III. MEASUREMENT RESULTS

The probability density functions (pdf) for the scintillation fade depth for the months April, May, June and July 1997 are shown in Fig. 1. The curves for April, May and July contain information for both rainy and non-rainy conditions while June was a dry month without rain. The pdf's are quite symmetrical about zero, which is consistent with the Karasawa model where the scintillation fade depth in dB over relatively short time intervals is assumed normally distributed with zero mean [3].

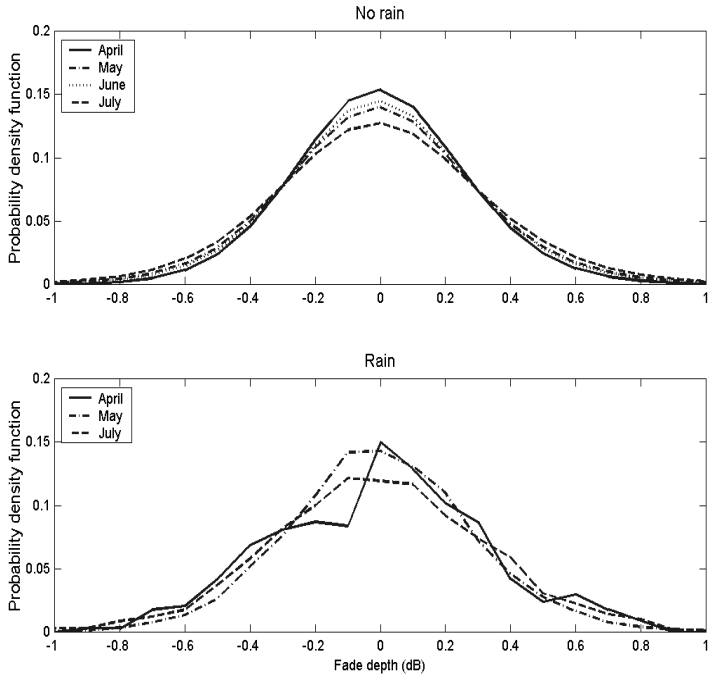

Fig. 1. Scintillation fade depth distribution.

For larger scintillation intensity, deviation from the symmetric shape is expected and a Nakagami-Rice distribution would follow according to the theory developed in [4]. The rain scintillation pdf's are slightly wider than the distributions in non-rainy conditions, implying a somewhat increased variance in scintillation when it is raining. This may be caused by increased atmospheric turbulence in rain as indicated in [5]. The method used in this paper to separate dry and wet conditions was by measuring rain intensity at the receiver site. This does not guarantee a satellite-earth path without rain, but this is expected to be the normal case most of the time.

A. Prediction of scintillation severity

A prediction method for tropospheric scintillation up to 20 GHz is presented in Recommendation ITU-R P.618-6 [1]. The inputs to the model are monthly average humidity and temperature, frequency, antenna diameter and efficiency, and elevation angle towards the satellite. In this model scintillation intensity increases with frequency and decreases with elevation angle.

In the following, the ITU-R prediction method is outlined and applied to the measured scintillation data. The climatic variables used in the model, monthly average temperature and humidity, are shown in Fig. 2, while predicted scintillation and experimental data are presented in Figs. 3 and 4. The saturation water vapor pressure, e_s (hPa), is calculated based on the mean temperature, t (C^o), from

$$e_S = ae^{\frac{bt}{t+c}} \tag{2}$$

with constants a = 6.1121, b = 17.502 and c = 240.97. The reference scintillation standard deviation, σ_{ref}, is given by

$$\sigma_{ref} = 3.6 \cdot 10^{-3} + 10^{-4} \cdot N_{wet} \tag{3}$$

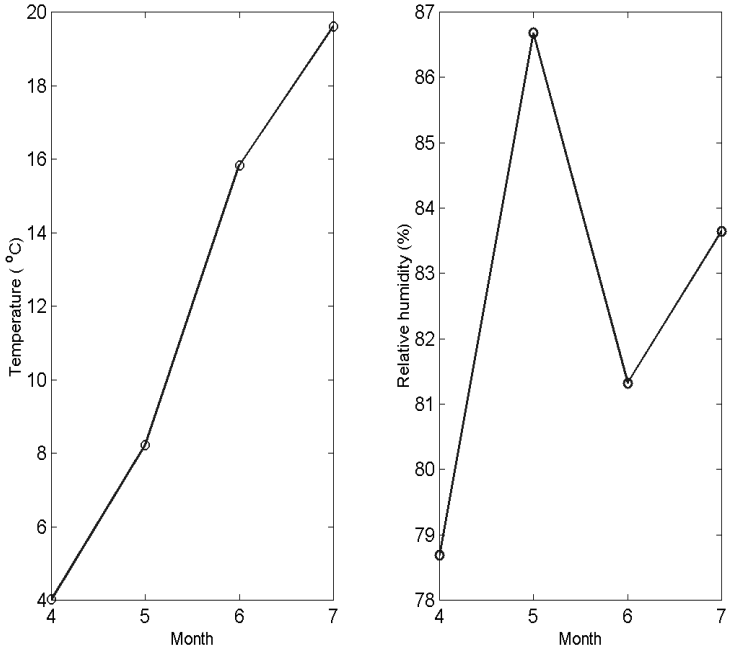

Fig. 2. Monthly average temperature and humidity

The wet component of refractivity, N_{wet}, is based on the mean relative humidity H (%), e_s and t:

$$N_{wet} = \frac{3732 H e_S}{(273+t)^2} \tag{4}$$

The height of the turbulent layer is assumed to be h_L = 1000 (m) and the effective path length through this layer, L, is

$$L = \frac{2h_L}{\sqrt{\sin^2(\theta) + 2.35 \cdot 10^{-4}} + \sin(\theta)} \tag{5}$$

where θ is the elevation angle towards the satellite. The effective antenna diameter, D_{eff}, is estimated from the geometrical diameter, D, and the antenna efficiency, η, as

$$D_{eff} = \sqrt{\eta} \cdot D \tag{6}$$

The antenna efficiency has not been measured, and is conservatively estimated as η = 0.5. There is a weak dependence on antenna size as larger antennas average more spatial fluctuations of the phase of the received waves than smaller antennas. The antenna weighting factor, $g(x)$, is given as

$$g(x) = \sqrt{3.86\left(x^2+1\right)^{11/12} \sin\left(\frac{11}{6}\tan\left(\frac{1}{x}\right)\right) - 7.08x^{5/6}} \tag{7}$$

where

$$x = 1.22 D_{eff}^2 \frac{f}{L} \tag{8}$$

The standard deviation of scintillation, σ, for the considered period and propagation path is

$$\sigma = \sigma_{ref} f^{\alpha} \frac{g(x)}{(\sin(\theta))^{1.2}} \tag{9}$$

where the frequency exponent α is 7/12. Finally, the scintillation fade depth exceeded for time percentage p is

$$x(p) = a(p) \cdot \sigma \tag{10}$$

where

$$a = -0.061(\log_{10}(p))^3 + 0.072(\log_{10}(p))^2 - 1.71 \cdot \log_{10}(p) + 3.0 \tag{11}$$

The scintillation severity in rainy and non-rainy conditions is quite similar during May, June and July as seen in Figs. 3 and 4. For the months April and May there is a relatively good match between the empirical distributions and the current ITU-R prediction method. The predictions somewhat overestimate the fade depth at small percentages of time, especially during rain. During the warmer months of June and July, the difference between results for rainy and non-rainy conditions is small. The ITU-R method overestimates the fade depths at

small percentages of time. As described in [6], the frequency exponent α in Eq. 9 seems to depend on the location. The prediction improves when changing α from 7/12 (ITU-R) to 0.55 for April and May, and to 0.5 for June and July, as shown in Figs. 3 and 4.

These results indicate that the frequency dependence of scintillation may depend on seasonal as well as site-specific climatic conditions. The apparent need for seasonal adjustments of the frequency exponent α suggests that the varying scintillation intensity is not entirely accounted for by the climatic parameters in Eq. 3 to 5 (σ_{ref}, N_{wet} and h_L). The relatively high value of $\alpha \cong$ 0.85 at Spino d'Adda (3.5 m diameter antenna) reported in [6] suggests angle-of-arrival fluctuations may also influence the results.

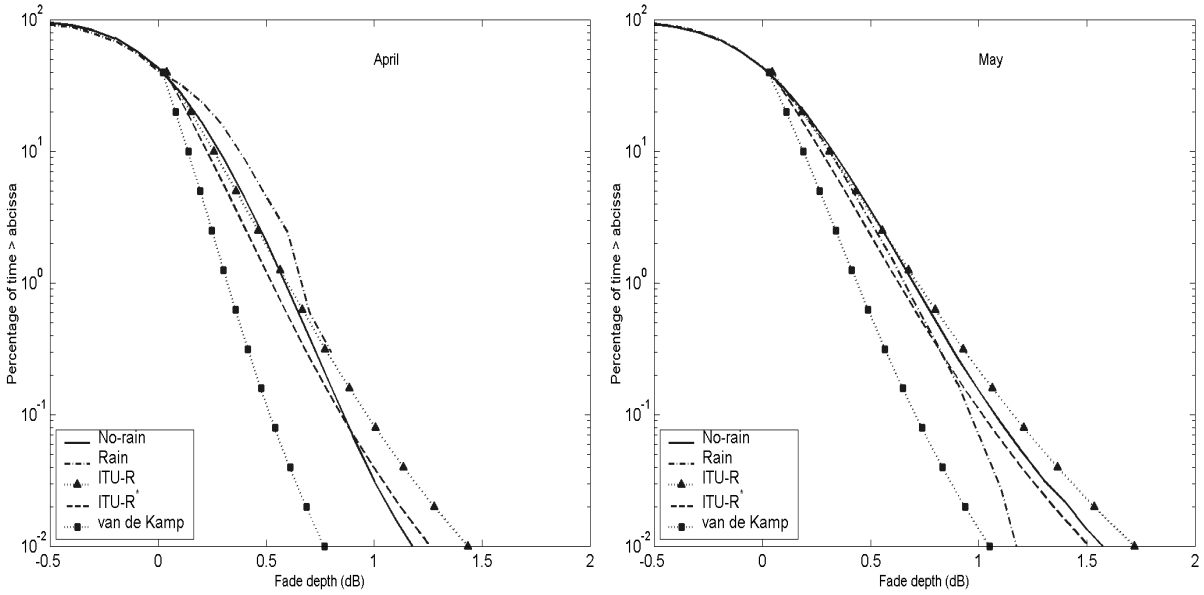

Fig. 3. Cumulative distribution of fade depth for April and May. ITU-R* with $\alpha = 0.55$

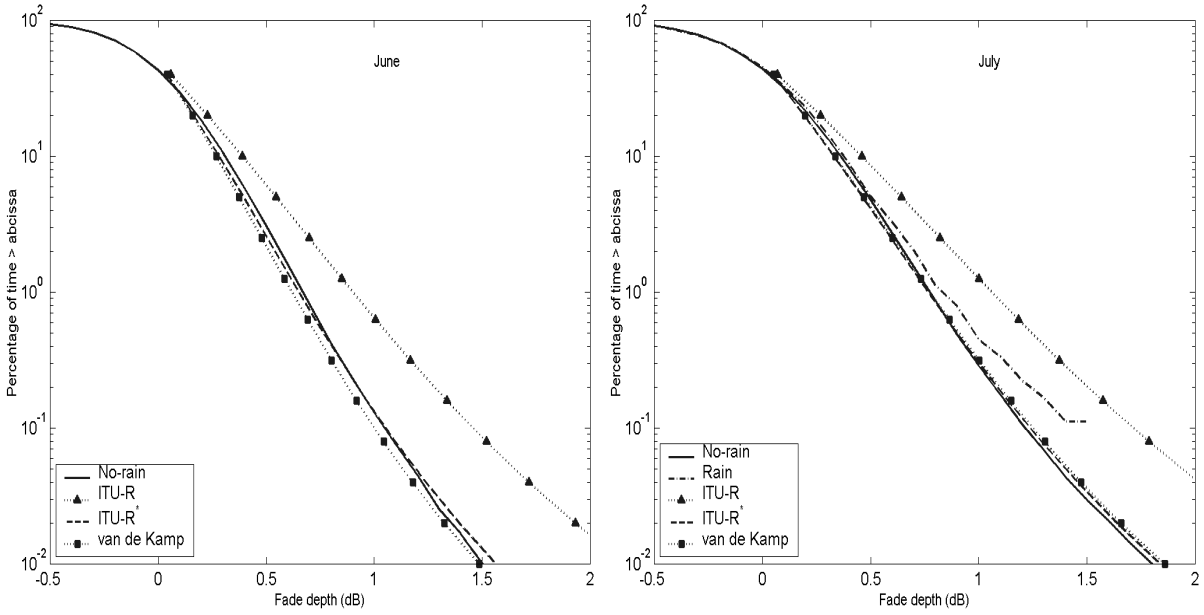

Fig. 4. Cumulative distribution of fade depth for June and July. ITU-R* with $\alpha = 0.5$

An improved method for long-term scintillation prediction including the average water content of heavy clouds is described in [7]. This method takes into account turbulence in clouds and modifies the reference standard deviation according to:

$$\hat{\sigma}_{ref} = 0.98 \cdot 10^{-4} \left(N_{wet} + Q \right) \tag{12}$$

$$Q = -39.2 + 56 \bar{W}_{hc} \tag{13}$$

where $\bar{w}_{hc}$ is the average water content of heavy clouds at the site. This modified reference standard deviation was used in Eq. 9 to 11 to produce the new prediction of monthly average scintillation intensity shown in Figs. 3 and 4 as "van de Kamp". The model gives excellent predictions in June and July; however, during April and May it underestimates the scintillation severity.

B. Diurnal variations

In order to study the diurnal variations in scintillation intensity the monthly averaged one-hour standard deviations were calculated and are shown in Fig. 5. By comparing the daily variation for each month, the indirect influence of the sun (sunrise, sunset and midday) for example can be investigated. The hourly variation in standard deviation shows peaks in the morning (4 - 6 AM) and in the afternoon (14 - 16 PM). This is consistent with the findings reported in [8, 9, 10]. The last two references suggest that the second peak is mostly associated with cumulus clouds.

One possible explanation for the first peak in the morning is increased turbulence during sunrise. The effect of antenna mis-pointing due to satellite position drift and a possible layered atmosphere, as well as angle-of-arrival fluctuations, could also affect the diurnal variation of scintillation.

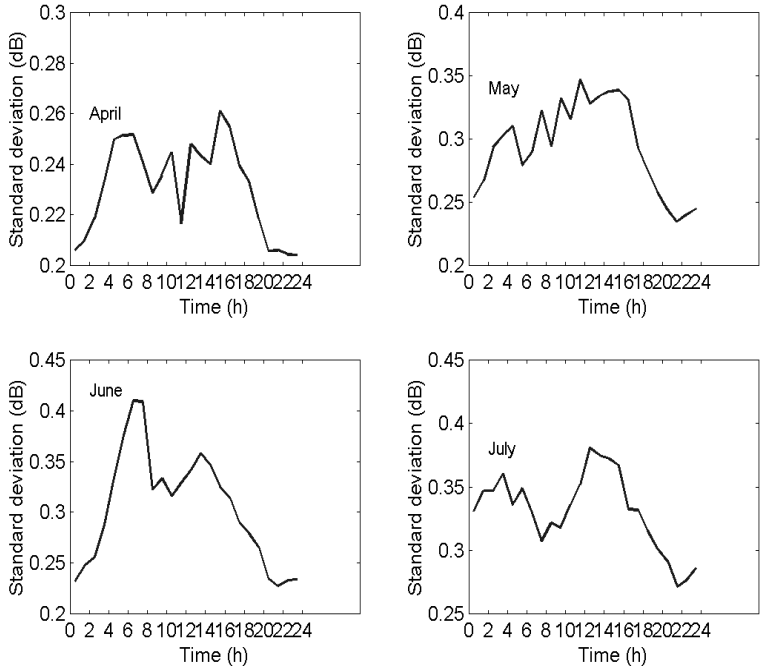

Fig. 5. Daily variation in the one-hour scintillation amplitude standard deviation.

IV. CONCLUSIONS

Four months of new earth-space propagation data for a horizontally polarized signal at 49.5 GHz has been presented and the severity of amplitude scintillation analyzed for both rainy and non-rainy conditions. The measured monthly cumulative density functions of scintillation levels were compared with the ITU-R predictions. A modification of the frequency exponent in the prediction method improves the results, suggesting that this exponent might vary with seasonal as well as site-specific parameters. A modified prediction method developed by van de Kamp et al. was also compared to the measured cumulative distributions. This method gave excellent predictions for the two warm summer months; however, it underestimated the scintillation intensity during spring. The diurnal variation of the scintillation variance was found to have one peak during the morning and one around noon, which is consistent with previously reported findings.

ACKNOWLEDGEMENTS

I would like to acknowledge Per Steinar Hansen for programming the logging software and Oddvar Alsos for building the radio frequency part of the receiver. I would also like to acknowledge helpful discussions and review of the manuscript by R. Olsen and C. Amaya.

V. REFERENCES

[1] Recommendation ITU-R 618-6, "Propagation data and prediction models required for the design of earth-space telecommunication systems," vol. 1999, P Series, International Telecommunication Union, Geneva, Switzerland, 1999.

[2] L. Boithias, "*Radio Wave Propagation*," North Oxford, London, 1987. ISBN 0-946536-06-6.

[3] Y. Karasawa, K. Yasukawa and M. Yamada, "Tropospheric Scintillation in the 14/11-GHz Bands on Earth-Space Paths with Low Elevation Angles," *IEEE Trans. Antennas Propagat.*, vol. 36, pp. 563-569, 1998.

[4] M. M. J. L. van de Kamp, "Asymmetric signal level distribution due to tropospheric scintillation," *Electronic Letters*, vol. 34, pp. 1145-1146, 1998.

[5] B. R. Arbesser-Rastburg and A. Paraboni, "European Research on Ka-Band Slant Path Propagation," *Proc. of the IEEE*, vol. 85, pp. 843-852, 1997.

[6] M. J. L. van de Kamp, C. Riva, J. K. Tervonen and E. T. Salonen, "Frequency dependence of Amplitude Scintillation," *IEEE Trans. Antennas Propagat.*, vol. 47, pp. 77-85, 1999.

[7] M. M. J. L. van de Kamp, J. K. Tervonen, E. T. Salonen and J. P. V. Poiares Baptista, "Improved Models for Long-Term Prediction of Tropospheric Scintillation on Slant Paths," *IEEE Trans. Antennas Propagat.*, vol. 47, pp. 249-260, 1999.

[8] Y. Karasawa, M. Yamada and J. E. Allnutt, "A New Prediction Method for Tropospheric Scintillation on Earth-Space Paths," *IEEE Trans. Antennas Propagat.*, vol. 36, pp. 1608-1614, 1988.

[9] Anon, "Project COST 205: Scintillations in Earth-Space links," *Alta Frequenza*, vol. 54, pp. 209-211, 1985.

[10] J. K. Tervonen, M. J. L. van de Kamp and E. T. Salonen, "Prediction Model for the Diurnal Behaviour of the Tropospheric Scintillation Variance," *IEEE Trans. Antennas Propagat.*, vol. 46, pp. 1372-1378, 1998.

COMPARISON OF PREDICTED SCINTILLATION WITH DATA MEASURED FROM THE 50 GHz ITALSAT BEACON IN NORWAY

Lars E. Bråten

Telenor Research and Development, Instituttveien 23, Po.Box 83, N-2027 Kjeller, Norway.
E-mail: Lars.Braten@ties.itu.int [1]

Abstract - Signal scintillation in the horizontally polarized 49.5 GHz beacon from the Italsat F1 satellite has been measured and analyzed. Four months of scintillation data are sorted into "rainy" and "non-rainy" conditions and long-term probability density functions are extracted on a monthly basis. The empirical monthly cumulative density functions of scintillation levels are compared to the ITU-R predictions and the diurnal fluctuation in variance is described. A seasonal modification of the frequency exponent in the ITU-R prediction method improves the results, suggesting that this parameter might depend on frequency as well as site-specific characteristics. A modified prediction method developed by van de Kamp et al. was also compared with the measured cumulative distributions. This method gave excellent predictions for the two warm summer months; however, it underestimated the scintillation intensity during spring.

I. INTRODUCTION

There is a demand for increased bandwidth in satellite communication, resulting in utilization of frequencies in the Ka-band and even higher. The influence of the atmosphere and precipitation on the propagation conditions typically increases with increasing frequency, and rain attenuation especially may limit the system availability. There have been several experimental campaigns in the past to investigate the fast scintillation in received power caused by multipath propagation in the atmosphere, although the number of experiments at millimeter wavelength is limited. Low margin systems require accurate prediction of propagation impairments to be able to calculate the system availability and service quality. The scope of this study is to investigate the fast varying scintillation in received power and compare the scintillation intensity with the current ITU-R prediction method [1]. The method predicts the cumulative distribution of tropospheric scintillation at elevation angles greater that 4^o and is recommended for applications up to at least 20 GHz.

The atmosphere is characterized by its radio refractive index n, depending on meteorological conditions and varying in both time and space. Atmospheric scintillation is characterized by rapid variations in angle-of-arrival, amplitude and phase of a received radio signal. The signal scintillation is caused by rapid variation in radio refractivity, $N = (n\text{-}1) \cdot 10^6 = N_{dry} + N_{wet}$, along the path. As altitude increases, the refractivity decreases with pressure and tends toward zero as the atmospheric radio refractive index n tends toward one. The overall decrease with altitude is normally subject to large variations in the lower part of the atmosphere due to fluctuations in temperature and pressure. In the atmosphere, there are small-scale rough and irregular surfaces with locally equal refractive index. There are several possible paths for the radio waves between the satellite and the receiver due to the non-homogenous refractivity. The various paths existing at the same time create multiple secondary waves with path length differences interfering with the main wave. Most often, the secondary waves are of small magnitude compared to the main wave, resulting in scintillation in the received power level. If

[1] The author is presently a guest researcher at the Communications Research Centre Canada, PO Box 11490, Station H, 3701 Carling Avenue, Ottawa, K2H 8S2, Canada. Tel +1 613 998 2772, Fax +1 613 998 4077

Paper 6

"Fade Duration at Ka-band on a Satellite-Earth Link in Vancouver: Modeling and Comparison with Measurements"

Published in: *Proc. IX Simpósio Brasileiro de Microondas e Optoeletrônica (SBMO'IX)*, Joao Pessoa, Brazil, 7-11 August 2000, 7-11.

Corrections:

Equation 3, " $P_{D|A}\left(d > D\middle|a \quad A\right) = \sum_{i=1}^{N} a_i e^{b_i t}$ " should be

" $P_{D|A}\left(D > d\middle|A \quad a\right) = \sum_{i=1}^{N} a_i e^{b_i d}$ "

Equation 6, " $P_{D|A}\left(d > D\middle|a \quad A\right) = gb d^{b\ 1} e^{g d^{b}}, 0 < d < \quad, g > 0, b > 0$ " should be

" $P_{D|A}\left(D > d\middle|A \quad a\right) = e^{g d^{b}}, 0 < d < \quad, g > 0, b > 0$ "

Fade Duration at Ka-Band on a Satellite-Earth Link in Vancouver: Modeling and Comparison with Measurements

Lars E. Bråten and César Amaya

Abstract —Fade duration statistics derived from five years of beacon measurements with the Advanced Communications Technology Satellite (ACTS) in Vancouver, Canada, at 20.2 and 27.5 GHz are compared with models for fade duration. It is found that the Weibull distribution gives the overall best agreement, closely followed by the Paraboni-Riva model and the lognormal distribution. Parameters for the Weibull distribution are given for both frequencies and at the attenuation threshold values. A relation between fade duration and fade duration interval distributions is derived and used to generate fade duration interval statistics.

Index Terms - Satellite communications, fade duration, availability

I. INTRODUCTION

There is a demand for higher capacity in satellite systems resulting in commercial utilization of Ka-band and even higher frequencies. These frequency bands are susceptible to hydrometeor-induced fades causing a reduction in system availability. Fade duration statistics are important for evaluating fade mitigation techniques required to obtain a given system availability. Most important are fades exceeding 2-4 dB, generally associated with attenuation due to hydrometeors (rain, snow, clouds etc.). The most common way to present fade duration statistics is the cumulative conditional probability of a fade event lasting longer than a specified time given an exceeded attenuation threshold value (see, e.g., [1-5]). This measure gives an indication of the number of communication outages that last for a period equal to or exceeding a given threshold. An alternative way of presenting fade duration statistics is by describing the occurrence of fades within different time intervals. This information may be useful when designing systems employing fade mitigation techniques as adaptive data rate control [6].

Previously reported models for fade duration have shown that rain fade durations exceeding about one minute are lognormally distributed while shorter durations follow a power-law distribution [2, 3]. The shortest fade durations are mainly related to tropospheric scintillation, while longer durations are related to time and space variations of precipitation along the path. The lognormal assumption for fade duration is also supported for fades exceeding 5 dB in [5]. These findings have resulted in the modeling of two separate regimes (lognormal and power-law), although models describing both regimes have also been reported [1, 7].

The authors are with Communications Research Centre Canada, 3701 Carling Avenue, Ottawa, Ontario, Canada K2H 8S2. L. Bråten is presently a Guest Researcher at CRC on leave from Telenor R&D, Norway, Tel. +1 613 998 2772, Lars.Braten@ties.itu.int. C. Amaya: Tel +1 613 998 2197, Cesar.Amaya@crc.ca. Fax +1 613 998 4077.

In Canada, the Communications Research Centre (CRC) have promoted and coordinated efforts to carry out long-term measurements of the ACTS signal at 20.2 and 27.5 GHz at two sites: one on the campus of the University of British Columbia (UBC) in Vancouver, and the second on the premises of CRC in Ottawa [8]. This paper deals with data collected over the period 1994-1998 at the Vancouver site. Several candidate fade duration models are compared with the 5-year fade duration distributions at both frequencies derived from measurements of the ACTS beacons. The receive site has co-ordinates 49.25°N, 123.22°W, giving a path elevation angle of 29.3° with an azimuth direction of 150.5°. The station, with a height of 165 m above sea level, is within the ITU-R rain zone D. The terminal antenna is 1.2 m in diameter and the beacon signal level acquisition rate is 1 Hz. Vancouver experiences a Pacific maritime climate with mainly widespread rain events introducing low attenuation levels of long duration. The number of days with thunderstorms averages only 7 per year. The summer months (June to August) are dry, with only 10 % of the annual total precipitation falling during this season. October to April is the rainy season. Pacific air streams ensure mild winters, mild but not hot summers, and small seasonal temperature differences, making it a moderate climate. The presence of western mountains aligned parallel to the coast and the prevailing westerly airflow from the Pacific generates a particular orographic rain pattern in Vancouver strongly influencing the maritime weather characteristics. Measured data presented in the paper include the year 1997, where the accumulated amount of rain was about 20 % larger than normal due to the occurrence of the El Niño phenomenon [9].

II. MEASUREMENT RESULTS

The Vancouver receiver station was one of seven ACTS Propagation Terminals (APTs) provided for the measurement campaign by NASA; the other six were installed at sites representing different geographical and climatic regions in the continental U.S. Several problems affected attenuation measurements with the APTs. It was found that the terminals are sensitive to water on both the antenna reflector surface and the feed window [10]. Peak attenuations of 6 and 8 dB at

20.2 and 27.5 GHz, respectively, due to the wetting of the antenna surfaces (both reflector and radome of the feed horn) were observed during a water sprayer test at Vancouver [11].

Several physical models were developed by ACTS experimenters to estimate the additional attenuation due to antenna wetting. The attenuation thresholds used in the fade duration distributions presented here were adjusted to compensate for the wetting effect according to the site dependent values given in [12]. This correction is thought to be reasonably accurate, although probably not all wetting effects are accounted for (e. g. the drying-up time of the antenna after a rainfall). An additional problem affects the 27.5 GHz beacon: water on the feed window produces a mismatch between the antenna and the low-noise amplifier, resulting in up to 2 dB of additional loss at high rain rates [10].

TABLE I
Annual average number of fades

Fade depth (dB) at 20.2 GHz	1.3	2.8	4.4	6.9
Number of fades	34048	2829	397	96
Fade depth (dB) at 27.5 GHz	1.3	2.7	4.3	6.4
Number of fades	59373	15422	3970	850

The fade duration distributions were extracted from beacon signals sampled at 1 Hz, implying that signal scintillation is present in the data. This results in an increased number of short duration events especially for lower attenuation thresholds. In addition, the slowly varying attenuation due to gaseous absorption is present.

The conditional fade duration distributions at 20.2 and 27.5 GHz from the 5-year measurements at Vancouver are shown in Fig. 1. The curves have been normalized to the total number of fades over the whole period. The annual average number of fades at each fade threshold is shown in Table I.

The fade duration generally increases with the fade threshold levels at both frequencies in a very similar way. This suggests that a common linear relationship (on a log-log scale) could exist between the different fade-depths, as mentioned in [2]. This scaling would, however, only hold for short fade durations, where the cumulative distribution functions (CDFs) can be approximated by a power-law distribution. Previous reports on the frequency dependence of the number of fade events at the same attenuation thresholds showed an increase with frequency [4]; the same behavior is reflected in the ACTS measurements shown in Table I. This is expected as the probability of occurrence of fading at a given level increase with frequency. The distributions at 20.2 and 27.5 GHz are quite similar, especially at the lowest threshold (1.3 dB) where the corresponding curves closely follow each other up to a duration of about 3 minutes.

III. FADE DURATION MODELS

Fade duration distributions are often presented as the percentage of time that the duration *d* exceeds a given value *D*, given that the attenuation *a* exceeds a threshold *A*. A method proposed in [2] for separating regional climatology from the inherent effects of hydrometeors is to represent the fade duration using conditional probabilities. Thus, the joint probability of observing a fade duration exceeding *D* at a fade level exceeding *A* is expressed as:

$$P_{D,A}\left(d \geq D, a \geq A\right) = P_{D|A}\left(d \geq D \middle| a \geq A\right) \cdot P_A\left(a \geq A\right) \quad (1)$$

where the conditional probability, $P_{D|A}(d \geq D \,|a \geq A)$, represents the hydrometer effects common to all regions. The regional dependence might be represented by the probability of observing a fade level exceeding *A*, $P_A(a \geq A)$; this probability could be extracted from local measurements or using attenuation prediction models like that recommended by the ITU [13].

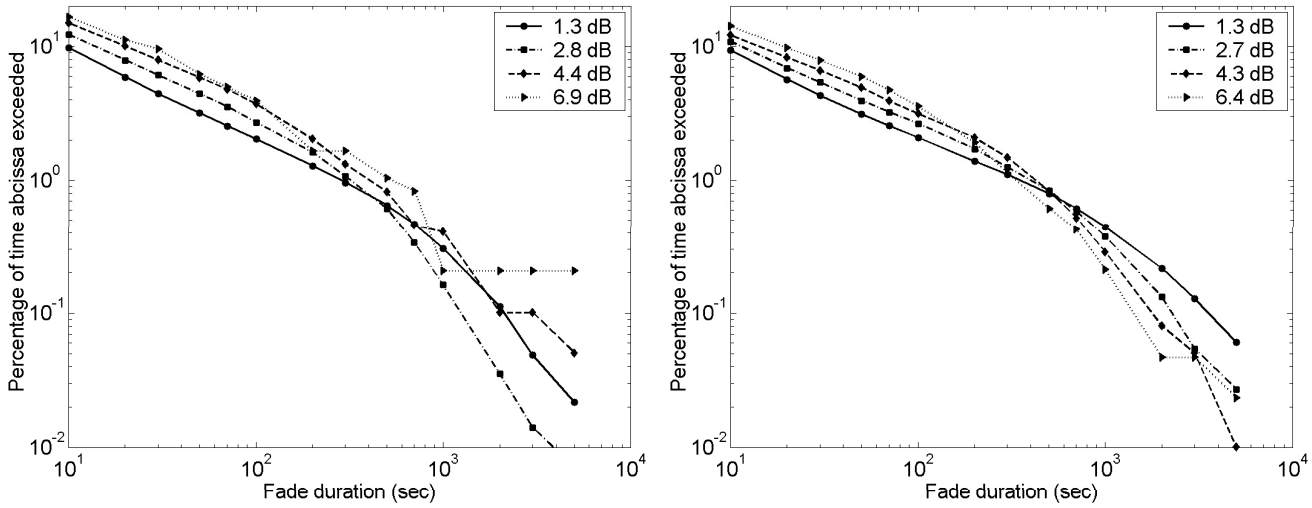

a) 20.2 GHz

b) 27.5 GHz

Fig. 1. Fade duration distributions from data measured at Vancouver

An alternative way of presenting conditional fade duration distributions is to sort the fade events into duration intervals in order to obtain fade interval statistics [6]:

$$P_{D|A}\left(D_1 \le d < D_2 \,|\, a \ge A\right) = P_{D|A}\left(d > D_1 \,|\, a \ge A\right) - P_{D|A}\left(d \ge D_2 \,|\, a \ge A\right) \quad (2)$$

where D_1 and D_2, ($D_2 \ge D_1$), are the fade duration times given a fade level, a, greater than or equal to the threshold, A. The linkage between the two statistical measures of fade duration is shown in (2). Once the conditional fade duration distribution is known, the fade interval distribution may be calculated. In the following Sections, different models for the conditional fade duration distribution are compared with measurement results.

A) Fade duration characteristics

The visual inspection of fade duration data at Vancouver shows that short events approximate straight lines on a log-log plot while the tails approximate straight lines on a semi-logarithmic plot. Two functions satisfying the required short-term linearity on the log-log scale and the long-term linearity on the semi-logarithmic scale are the power-law and the exponential function, respectively. Single distributions following both these two linear characteristics are the gamma and Weibull distributions; the latter have previously been used to model fade duration on terrestrial links [7]. However, the most commonly used for long durations is the lognormal distribution. A description of these statistical distributions may be found in [14].

Paraboni and Riva [3] developed a model that is a combination of a power-law distribution for short events and a lognormal distribution for durations exceeding one minute. An alternative model, previously used to model fade duration statistics derived from radiometer measurements, is a cascaded exponential model [1]:

$$P_{D|A}\left(d > D \,|\, a \ge A\right) = \sum_{i=1}^{N} \alpha_i e^{-\beta_i t} \quad (3)$$

where $P(d > D \mid a \ge A)$ is the conditional cumulative distribution of fade duration given that the fade exceeds the threshold. To ensure that the CDF equals one for zero fade duration the constrain, sum of α_i = 1, is imposed on the coefficients of (3). The decay constants $1/\beta_i$ have units of seconds and are called *characteristic durations*. It can be speculated that the components in (3) take into account, in order of decreasing decay times, atmospheric gases and clouds, and stratiform and convective rain [1]. The effect of antenna wetting might also be included using a shorter decay time.

B) Extraction of model parameters

The models investigated were fitted to five years of measured data by minimizing a mean square logarithmic error function. An attempt to model each year was also performed, resulting in a relatively large yearly variation in the parameters. Constraints are added to this function in the case of the cascaded exponential and the Paraboni-Riva model to ensure that the sum of coefficients equals one and to obtain a continuous transition between the two model regimes, respectively. A visual inspection of the results indicated that the most suitable models are the Weibull, Paraboni-Riva and lognormal models.

C) Comparison of models and error analysis

The model performance criterion chosen is similar to the function used in the parameter-fitting process: the error at fade duration bin number i, ε_i, is:

$$\varepsilon_i = \log_{10}\left(\frac{P_{Measured}\left(d > D \,|\, a \ge A\right)}{P_{Model}\left(d > D \,|\, a \ge A\right)}\right) \quad (4)$$

The mean, μ_ε, and standard deviation, σ_ε, of ε_i is calculated for all the threshold values. A weighting function, combining the mean and standard deviation of ε_i, is used to rank model performance:

$$\rho_\varepsilon = \sqrt{\mu_\varepsilon^2 + \sigma_\varepsilon^2} \quad (5)$$

The results of the error analysis are summarized in Table II. The overall best distribution, when averaging over the four thresholds, is the Weibull distribution closely followed by the Paraboni-Riva and lognormal model.

TABLE II
Overall model performance, 5-year measurement period

	20.2 GHz			27.5 GHz		
	μ_ε	σ_ε	ρ_ε	μ_ε	σ_ε	ρ_ε
Weibull	-0.0013483	0.060361	0.060376	-0.0028297	0.060055	0.060121
Paraboni-Riva (3 min)	-0.0060547	0.076585	0.076824	-0.011746	0.093316	0.094052
Lognormal	-0.0034756	0.09627	0.096332	-0.0042116	0.10543	0.10552
Paraboni-Riva (1 min)	0.0028614	0.096685	0.096728	0.0044352	0.11047	0.11056
Gamma	0.0011502	0.16757	0.16757	0.0010235	0.13928	0.13928
Power-law	0.025816	0.20445	0.20608	0.019237	0.20581	0.20671
Cas. Exp. (N = 2)	-0.016053	0.23256	0.23312	-0.018926	0.24382	0.24456
Cas. Exp. (N = 3)	-0.019549	0.23197	0.23279	-0.066537	0.24901	0.25775

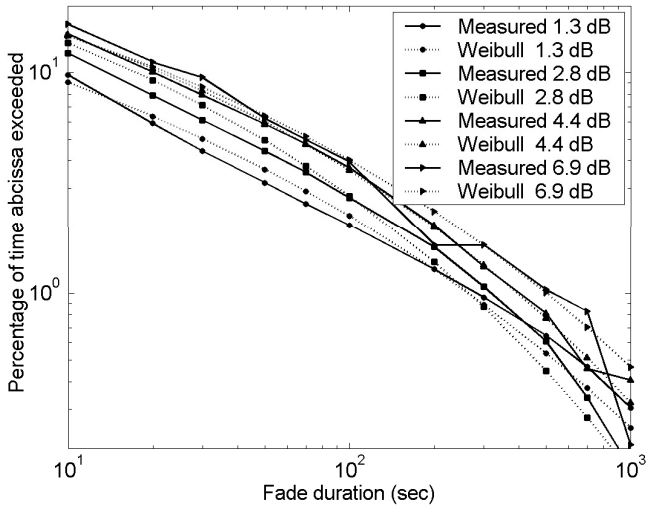

Fig. 2. Weibull model and measured fade duration distributions at 20.2 GHz

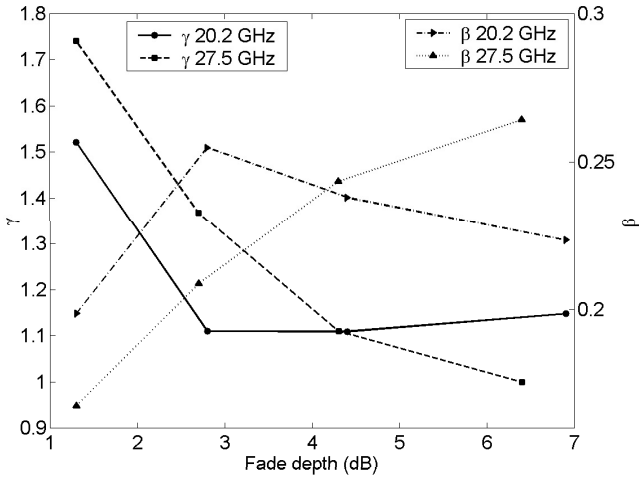

Fig. 3. Weibull parameters γ and β as a function of fade depth and frequency

The performance of the Paraboni-Riva model showed an improvement when the duration threshold separating the power-law and lognormal regimes was shifted from one to three minutes. The Weibull distribution performed better than the Paraboni-Riva model for both frequencies and at all the fade thresholds, except at 6.9 dB, 20.2 GHz, where the lognormal model was slightly better.

A method to empirically check the Weibull distribution consists of plotting *ln(d)* versus $ln(-ln(P_{D|A}(d>D|a\geq A)))$, which should give an approximate straight line [14]. It turns out that the fade duration distribution for all the threshold values and for both frequencies do indeed approximate straight lines, increasing the confidence in the model. Fig. 2 shows the comparison of fade duration distributions for various fade thresholds, covering the 5-year data at 20.2 GHz, with curves obtained using the Weibull distribution.

The cascaded exponential distribution deviates from measurements for the short-duration events. The best fit was obtained using $N = 3$ terms in (3) at 20.2 GHz, and $N = 2$ at 27.5 GHz. Previously reported results showed, however, an excellent fit between a double-exponential distribution and fade duration derived from radiometric measurements at 12 GHz [1, 15]. The deviation occurring with the beacon-based fade duration distributions reported here is probably due to the inclusion of short duration amplitude scintillation, which is not present in radiometer data, and possible remaining residual wet antenna effects. Comparisons between the candidate models, including the Weibull distribution, and fade duration data extracted from 12.5 GHz radiometric measurements at Ottawa in 1997 showed that the double-exponential model produced the best fit.

C) Weibull distribution parameters

The Weibull distribution has two parameters, γ and β:

$$P_{D|A}(d > D \,|\, a \geq A) = \gamma\beta d^{\beta-1} e^{-\gamma d^{\beta}}, 0 < d < \infty, \gamma > 0, \beta > 0 \quad (6)$$

The exponential distribution is a special case of the Weibull distribution with $\beta = 1$. The parameters extracted for the Weibull fade duration model are shown in Fig. 3.

The Weibull parameters for 27.5 GHz vary monotonically with the attenuation threshold level while the parameters for 20.2 GHz show a non-monotonic behavior with a clear knee for both curves in the region around 3 dB of fade depth. This suggests that two different effects could be present; however, the limited amount of data analyzed as well as residual antenna wetting effects not removed in the correction impede the finding of a conclusive reason for this behavior.

D) Fade duration interval statistics

An alternative way of presenting fade duration statistics is by describing the occurrence of fades within different time intervals. This information might be useful when designing systems employing fade mitigation techniques as adaptive data rate control [6].

The fade duration interval distribution in (2) can be modeled as a linear combination of two Weibull distributions, each pair using the same fade thresholds but two different fade duration values. By applying the Weibull model with parameters for 20.2 GHz shown in the previous section the fade duration interval statistics shown in Fig. 4 were obtained. As observed, approximately 90 % of the fades are between 0 and 10 s, while about 1 % are between 300 and 600 s. This implies that only about 10 % of the fades would potentially lead to an Integrated Services Digital Network (ISDN) system outage where a limit of 10 s defines the system availability [16].

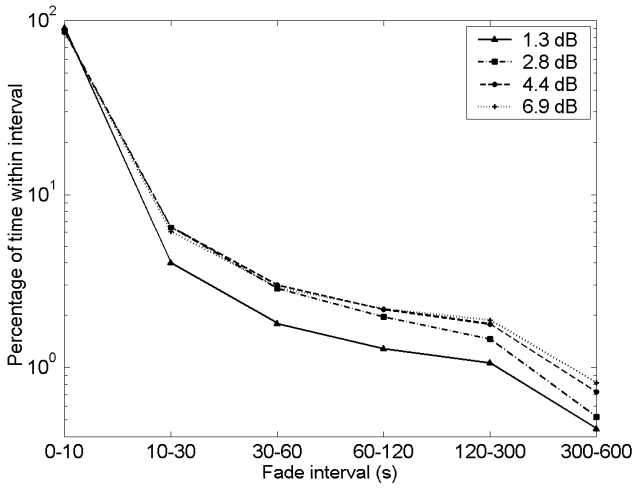

Fig. 4. Cumulative distribution of fade duration intervals at 20.2 GHz

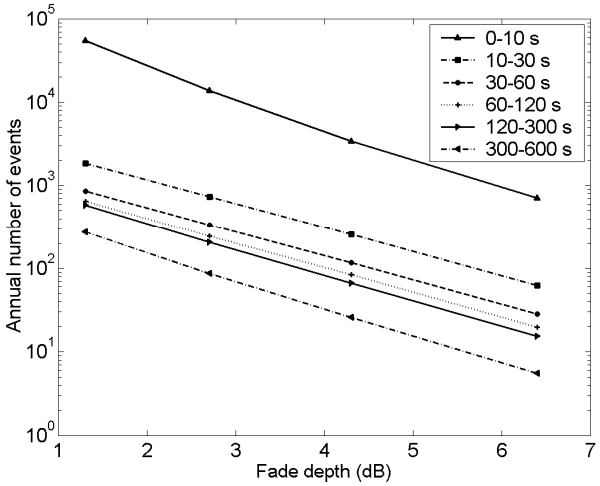

Fig. 5. Annual average distribution of fade duration intervals at 27.5 GHz

An alternative way of presenting fade duration interval statistics is by combining the average annual number of fades, given in Table I, with parameters from the previous Section inserted in (2). The annual average fade duration interval distribution for 27.5 GHz is shown in Fig. 5.

.

IV. CONCLUSION

Models for fade duration distributions have been compared with results derived from 5 years of ACTS beacon data recorded in Vancouver at 20.2 and 27.5 GHz. The data presented were corrected to compensate for the antenna wetting effects affecting the APTs terminals, although some residual errors are believed still to be present. The ability of various cumulative distribution functions to fit fade duration data was evaluated in order to find the best fade duration model. With the present dataset, the Weibull model gives the best results, followed by the Paraboni-Riva and lognormal models. At 20.2 GHz, the parameters of the Weibull model showed a non-monotonic behavior when represented as a function of the fade depth. The fade duration interval distribution is shown to be a linear sum of fade duration distributions. A combination of Weibull fade duration models was used to generate fade duration interval statistics.

Data from the ACTS beacon measurements at the CRC site at Ottawa will be analyzed in the future. The advantage of using these data is that they are not influenced by antenna wetting and other problems affecting recordings with the APT's terminals. Moreover, it will be possible to compare results at Vancouver and Ottawa, two sites located in regions where the characteristics of precipitation are very different.

REFERENCES

[1] R, Lekkla, K. S. McCormick and D. V. Rogers, "12-GHz Fade Duration Statistics on Earth-Space Paths in South-East Asia," *Proc. URSI CLIMPARA '98*, pp. 167-170, Ottawa, Canada, 27-29 April 1998.

[2] H. Helmken, R. E. Henning, J. Feil, L. J. Ippolito and C. E. Mayer, "A Three-site Comparison of Fade-Distribution Measurements," *Proc. IEEE*, vol. 85, no. 6, pp. 917-925, 1997.

[3] A. Paraboni and C. Riva, "A New Method for the Prediction of Fade Duration Statistics in Satellite Links Above 10 GHz," *Int. J. Satellite Comm.*, vol. 12, pp. 387-394, 1994.

[4] W. L. Stutzman, T. Pratt, A. Safaai-Jazi, P. W. Remaklus, J. Laster, B. Nelson and H. Ajaz, "Results from the Virginia Tech Propagation Experiment Using the Olympus Satellite 12, 20 and 30 GHz Beacons," *IEEE Trans. Ant. Propagat.*, vol. 43, no. 1, pp. 54-62, 1995.

[5] W. J. Vogel, G. W. Torrence and J. E. Allnutt, "Rain Fades on Low Elevation Angle Earth-Satellite Paths: Comparative Assessment of the Austin, Texas, 11.2 GHz Experiment," *Proc. IEEE*, vol. 81, no. 6, pp. 885-896, 1993.

[6] A. Safaai-Jazi, H. Ajaz and L. Stutzman, "Empirical Models for Rain Fade Time on Ku- and Ka-Band Satellite Links," *IEEE Trans. Ant. Propagat.*, vol. 43, no. 12, pp. 1411-1415, 1995.

[7] E. Couto de Miranda, R. S. L. Sousa, E. Costa and L. A. R. da Silva Mello, "Dynamic Analysis of Attenuation on Five Converging Links at 15 GHz Located in the Great São Paulo Area, Brazil," *Proc. ICAP'97*, vol. 2, pp. 367-373, Edinburgh, UK, 14-17 April, 1997.

[8] C. Amaya, D.V. Rogers, K. S. McCormick, "Ka-band Propagation Measurements in Canada with the Advanced Communications Technology Satellite," *Proc. URSI CLIMPARA '98*, pp. 171-174, Ottawa, Canada, 27-29 April 1998.

[9] C. Amaya and D. Rogers, "Characteristics of Rain Fading on Ka-Band Satellite-Earth Links in a Pacific Climate," *Proc. International Microwave and Optoelectronics Conf.*, Rio de Janeiro, Brazil, 9-12 August 1999.

[10] R. K. Crane and D. V. Rogers, "Review of the Advanced Communication Technology Satellite (ACTS) Propagation Campaign in North America," *IEEE Ant. Propagat. Magazine*, vol. 40, no. 6, pp. 23-28, 1998.

[11] M. M. Z. Kharadly and R. Ross "Analysis and Modeling of Corrupt Data due to Antenna Surface Wetting During Rain Events," *Proc. First International Workshop on Radiowave Propagation Modelling for SatCom Services at Ku-band and above*, ESTEC, Noordwijk, The Netherlands, 28-29 October 1998.

[12] "The ACTS Propagation Experiment Page", Internet www page, at URL: *http://weather.ou.edu/~actsrain/* (version current at 7. March 2000).

[13] Recommendation ITU-R P.618-6, "Propagation data and prediction methods required for the design of earth-space telecommunication systems," vol. 1999, P Series, International Telecommunication Union, Geneva, Switzerland, 1999.

[14] J. D. Kalbfleisch and R. L. Prentice, "*The Statistical Analysis of Failure Time Data*," Wiley, New York, 1980, ISBN 0471055190.

[15] C. Amaya, D. V. Rogers and K. S. McCormick, "30/20/12-GHz Slant-Path Attenuation Measurements at Ottawa, Canada," *Proc. URSI Comm. F. Triennial Open Symp. on Wave Propagation and Remote Sensing*, pp. 308-311, Aveiro, Portugal, 22-25 Sept. 1998.

[16] Recommendation ITU-T G.821, " Error performance of an international digital connection operating at a bit rate below the primary rate and forming part of an integrated services digital network," G Series, International Telecommunication Union, Geneva, Switzerland, 1996.

Paper 7

"Fade and Inter-fade Duration at Ka-Band on Satellite-Earth Links: Modeling and System Implications"

Published in: *Proc. AIAA International Communications Satellite Systems Conference,* Toulouse, France, 17-20 April 2001.

Correction:

The left legend in Fig. 3b should read "Time percentage < abcissa"

FADE AND INTER-FADE DURATION AT KA-BAND ON SATELLITE-EARTH LINKS: MODELING AND SYSTEM IMPLICATIONS

Lars E. Bråten[(1)], César Amaya[(2)], and David V. Rogers[(2)]

(1) Telenor Research and Development, P.O. Box 83, N-2027 Kjeller, Norway
Tel. +47 63 84 87 15, E-mail: Lars-Erling.Braten@telenor.com
(2) Communications Research Centre Canada, 3710 Carling Avenue,
Box 11490, Station H, Ottawa, Ontario, Canada, K2H 8S2
E-mails: Cesar.Amaya@crc.ca, Dave.Rogers@crc.ca

Abstract *- Fade duration statistics derived from beacon measurements at four North American locations: Vancouver, Ottawa, Norman and Reston, with the Advanced Communications Technology Satellite (ACTS) at 20.2 and 27.5 GHz are compared with models for fade duration. It is observed that at three of the four sites, a three-term cascaded exponential distribution function gave the best results. At the Vancouver site, the Weibull distribution performed slightly better. An algorithm that estimates service availability by combining fade and inter-fade durations is developed and applied to data collected at Ottawa. The difference between the attenuation and availability statistics was found to be negligible.*

I INTRODUCTION

There is a demand for higher capacity in satellite systems resulting in commercial utilization of Ka-band and even higher frequencies. These frequency bands are susceptible to hydrometeor-induced fading which can cause a reduction in system availability. Fade and inter-fade duration statistics are important for evaluating fade mitigation techniques required to obtain a given system availability. Most important are fades exceeding 2-4 dB, generally associated with attenuation due to hydrometeors. Fade duration is defined as the time interval between threshold crossings at a given level of attenuation. The most common way to present fade duration statistics is the conditional cumulative probability function (CDF) of a fade event lasting longer than a specified time, given an exceeded attenuation threshold value. For communication systems designed to operate with a given fade margin, fade and inter-fade duration statistics indicate the number as well as duration of outages. The fade duration statistics can also be used to dimension memory systems able to store data while the communication link is unavailable.

Previously reported models for fade duration have shown that rain fade durations exceeding about one minute are lognormally distributed while shorter durations follow a power-law distribution [1], [2]. The shortest fade durations are mainly related to tropospheric scintillation, while longer durations are related to time and space variations of precipitation along the path. These findings have resulted in the modeling of two separate regimes (lognormal and power-law), although models including both regimes have also been reported, i.e., the cascaded exponential model [3]-[6] and the Weibull distribution [7], [8].

This paper reports on the analysis of fade duration data collected during the propagation campaign with the ACTS satellite at four different locations, Vancouver and Ottawa in Canada, and Reston (Virginia) and Norman (Oklahoma) in the U.S. Several different fade duration models are compared with measurements at both frequencies and their performance evaluated. A model to estimate service availability based on fade and inter-fade duration is described, and its application illustrated using data recorded at Ottawa.

II MEASUREMENTS

Seven identical ACTS Propagation Terminals (APTs) were provided by NASA for the measurement campaign at 20.2 and 27.5 GHz. One was located in Vancouver while the other six were installed at sites representing different geographical and climatic regions in the continental U.S. The data analyzed in this study were measured by the APTs located in Vancouver, Norman and Reston. The terminal antenna diameter was 1.2 m. At the site located at the Communications Research Centre Canada in Ottawa, the ACTS beacons were measured using independent terminals at each frequency with 2.4 m diameter antennas.

The data acquisition rate at all sites was 1 Hz, implying that signal scintillation was present in the unfiltered data, resulting in an increased number of short duration events. The Ottawa data were also filtered by a 30 sec running average to investigate the effect of fast fluctuations on the fade duration distributions. The empirical fade and inter-fade duration distributions were based on five years of measurements at the sites with APTs and one year in Ottawa. Some characteristics of the measurement locations are given in Table 1.

	Vancouver	Ottawa	Norman	Reston
Coordinates	49.3° N	45.6° N	35.2° N	39.0° N
	123.2° W	75.6° W	97.4° W	77.3° W
Elev. angle	29.3°	32.2°	49.1 °	39.2 °
Height (m)	110	70	420	80
Time period	1994-1998	97/09-98/08	1994-1998	1994-1998
ITU-R rain zone	B/D	K	M	K

Table 1. Receive locations and their path/climate characteristics

Antenna wetting was a problem affecting measurements with the APTs. The terminals were sensitive to water on both the antenna reflector surface and the feed window. Physical models were developed by ACTS experimenters to estimate the additional attenuation due to this effect [9]. The attenuation thresholds used in the fade duration distributions presented here were adjusted to compensate for antenna wetting according to the site-dependent values given in [10]. This correction is thought to be reasonably accurate, although probably not all wetting effects are accounted for. The receiver system in Ottawa is negligibly affected by this problem.

The conditional fade duration distributions from the 5-year unfiltered measurements at Vancouver, Norman and Reston, and the one-year of unfiltered measurements from Ottawa are shown in Figs. 1-2. The curves have been normalized to the annual average number of fades at each fade threshold, shown in Table 2. By filtering the beacon data by a 30 sec running average to suppress scintillation, a significant reduction in the annual average number of fades is observable. It should be cautioned that some of the shorter fades may possibly be caused by equipment effects.

	Increasing attenuation levels			
Ottawa, unfiltered, 20.2 GHz	5894	1583	887	365
Ottawa, unfiltered, 27.5 GHz	11021	4197	2310	1174
Ottawa, filtered, 20.2 GHz	259	125	82	39
Ottawa, filtered, 27.5 GHz	505	280	189	109
Vancouver, 20.2 GHz	34048	2829	397	96
Vancouver, 27.5 GHz	59373	15422	3970	850
Norman, 20.2 GHz	46639	14791	6328	2949
Norman, 27.5 GHz	69136	28434	14893	8115
Reston, 20.2 GHz	83314	18928	6782	2900
Reston, 27.5 GHz	113567	34182	16004	7162

Table 2. Annual average number of fades corresponding to the fade threshold levels in Figs 1-2.

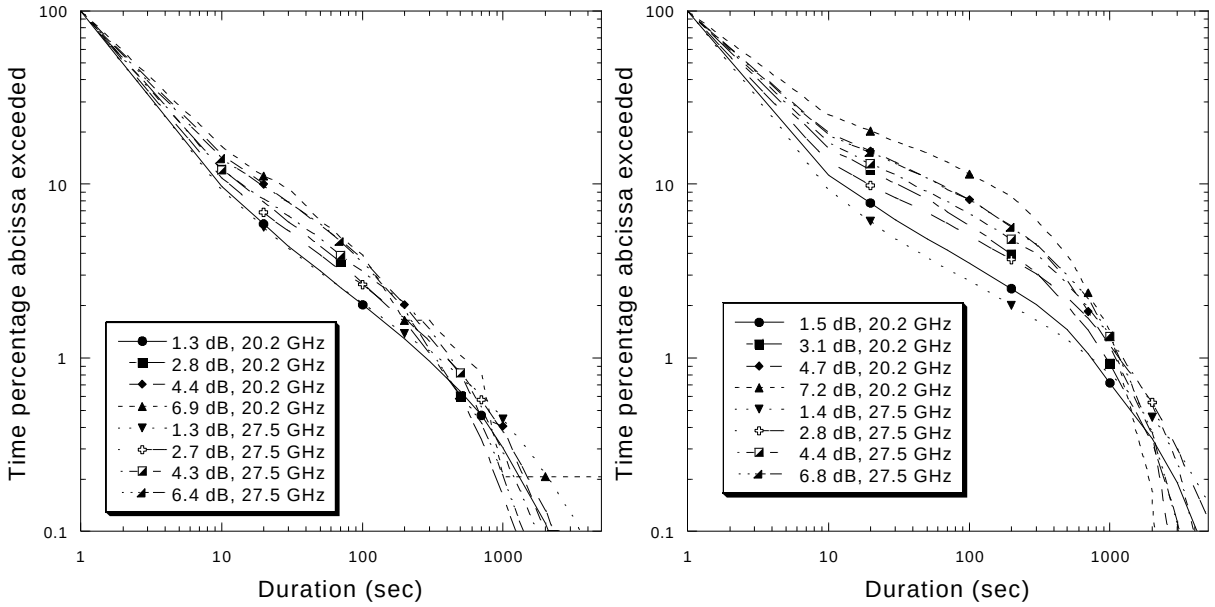

a) Vancouver b) Norman

Figure 1. Conditional cumulative distribution of fade duration

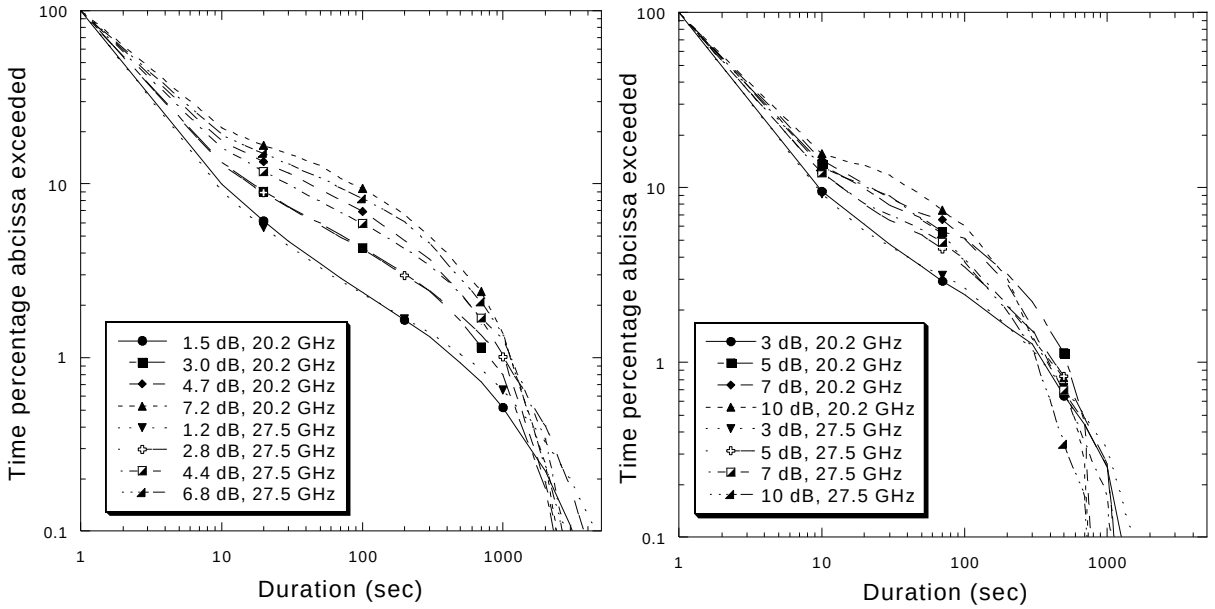

a) Reston b) Ottawa (unfiltered)

Figure 2. Conditional cumulative distribution of fade duration

The quantity measured at the NASA sites was total attenuation, including attenuation due both to hydrometeors and gases. The slowly varying attenuation due to gaseous absorption may lead to more frequent occurrence of long duration fades especially at the low attenuation thresholds. In Ottawa, the gaseous attenuation was removed to produce attenuation with respect to clear sky.

III MODELING OF FADE DURATION

Fade duration distributions are often presented as the percentage of time that the duration D exceeds a given value d, given that the attenuation A exceeds a threshold a.

Paraboni and Riva developed a model for fade duration that is a combination of a power-law distribution for short events and a lognormal distribution for durations exceeding one minute [1]. The shortest fade durations are mainly related to tropospheric scintillation, while longer durations are mostly related to time and space variations of precipitation along the path. Alternative models reported in the literature are the cascaded exponential and the Weibull distribution. The ability of these models, as well as the lognormal and gamma distributions, to fit the measured data was tested.

The *cascaded exponential* model has previously been used to model fade duration statistics in South East Asia, North America, and France [3]-[6]:

$$P_{D|A}\left(D > d \,\middle|\, A \quad a\right) = \sum_{i=1}^{N} a_i e^{\,b_i d} \tag{1}$$

The decay constants $1/b_i$ have units of seconds and are called *characteristic durations* [3]. To ensure that the CDF equals one for zero fade duration the constraint, sum of a_i = 1, is imposed on the coefficients of Eq. 1. The fade duration distribution based on stochastic rain attenuation models reported in [11], [12] correspond to Eq. 1 with only one term, N = 1. Previous studies have shown that a double exponential function (N = 2) can successfully model fade duration distributions at 12, 20, and 30 GHz, retrieved from radiometric measurements (which do not detect scintillations) [3]-[5]. To take into account fast fluctuations in the beacon signals caused by scintillation, up to N = 3 terms were used in the present study.

Analyses of satellite-earth links in Brazil and of the ACTS satellite link measured in Vancouver identified a third fade duration model as appropriate, the *Weibull* distribution [7], [8]. This distribution has two positive parameters, g and b:

$$P_{D|A}\left(D > d \,\middle|\, A \quad a\right) = e^{\,g\,d^{\,b}}, 0 \quad d < \tag{2}$$

The exponential distribution is a special case of the Weibull distribution with b = 1. The duration, d, used in the theoretical models was modified by subtracting the minimum measured fade duration of 1 sec to ensure that the CDFs intersect the ordinate with a value of one.

The models were fitted to the measured data by minimizing a mean square logarithmic error function. The error, e_i, at fade duration bin number i, is:

$$e_i = \log_{10} \frac{P_{Measured}\left(D > d_i \,\middle|\, A \quad a\right)}{P_{Model}\left(D > d_i \,\middle|\, A \quad a\right)} \div \tag{3}$$

The mean, m_e, and standard deviation, s_e, of e_i were calculated for all the threshold values. A weighting function, combining the mean and standard deviation of e_i, was used to rank model performance as displayed in Table 3:

$$r_e = \sqrt{m_e^2 + s_e^{\,2}} \tag{4}$$

Location	Freq. (GHz)	Gamma	Weibull	Parab.-Riva	Log-normal	Exp. (N = 1)	Cas. Exp. (N = 2)	Cas. Exp. (N = 3)	Best model
Ottawa	20.2	0.052163	0.12517	0.15335	0.15651	0.8447	0.084932	0.032642	Cas. Exp. N = 3
(unfiltered)	27.5	0.038627	0.090333	0.12597	0.12085	0.91589	0.098175	0.022227	Cas. Exp. N = 3
Ottawa	20.2	0.046873	0.04112	0.058518	0.055585	0.098162	0.032942	0.033579	Cas. Exp. N = 2
(filtered)	27.5	0.055255	0.039512	0.041669	0.0332	0.12438	0.021204	0.020798	Cas. Exp. N = 3
Vancouver	20.2	0.16583	0.061266	0.1026	0.099385	1.1785	0.23734	0.069936	Weibull
	27.5	0.13741	0.062061	0.11711	0.10881	1.2335	0.22236	0.064449	Weibull
Norman	20.2	0.062045	0.14164	0.18439	0.19209	0.91783	0.13511	0.038634	Cas. Exp. N = 3
	27.5	0.058773	0.12259	0.17486	0.1733	1.0247	0.1514	0.044855	Cas. Exp. N = 3
Reston	20.2	0.088511	0.16177	0.21378	0.22528	1.0287	0.16895	0.063009	Cas. Exp. N = 3
	27.5	0.082242	0.14296	0.19501	0.19748	1.0625	0.16683	0.054164	Cas. Exp. N = 3

Table 3. Overall fade duration model performance, r_e

At three of four sites, a three-term cascaded exponential fade duration model gave the best results. The single outlier site is Vancouver, where the Weibull distribution performed slightly better. Similar results for radiometer data were reported in [5], where the maritime rain climate in Vancouver was identified as a possible reason. After filtering the Ottawa data by a 30 sec running average, the performance of the double and triple cascaded exponential are almost identical. Unfiltered, or smoothed by a shorter filter of 10 sec, resulted in a three component model at Ottawa. This indicates that the third term in the cascaded exponential takes into account fast signal level variations due to scintillation. This third exponential term might not be necessary if fast fluctuations in the beacons are filtered out, or if the underlying duration data are extracted from radiometer measurements. Limited tests of 12 GHz radiometer data at Ottawa in this study, as well as the good performance of the double cascaded exponential model reported in [5], support this hypothesis.

IV SERVICE AVAILABILITY

An algorithm based on fade and inter-fade duration measurements was developed to calculate the percentage of time a system is available. The algorithm utilizes a hysteresis with two duration thresholds, one describing the number of seconds a fade must last before service unavailability is declared, and one to decide if the duration of an inter-fade event is long enough to bring the system back to the available state. The definition of available and unavailable time selected is that of ITU-T Recommendation G.821, based on a 10 second criterion [13]. The start of an unavailable time-period is defined as the beginning of a period in which the attenuation is continuously greater than a threshold level for more than 10 sec. The end of the unavailable time-period is defined as the beginning of the period in which the attenuation is continuously below the threshold level for more than 10 sec. The algorithm may be applied if either measured time series or simulated time series based on measured cumulative distributions of fade and inter-fade durations are available.

Measured unfiltered time series of fade and inter-fade duration from Ottawa, with CDFs shown in Figs. 2b and 3a respectively, were used to compare the annual available time as a function of fade margin and the CDF of rain attenuation. An example of system availability prediction is given in Fig. 3b, with time limits of 10 sec, 1 min and 5 min applied. The difference between the annual rain attenuation CDF and the availability is small for the lowest time limit of 10 sec. A similar study in Japan at 19.5 GHz [14] found a much larger difference between the available time and the rain attenuation distributions. The negligible difference between the two distributions found in the current study is consistent with previous findings reported in [15].

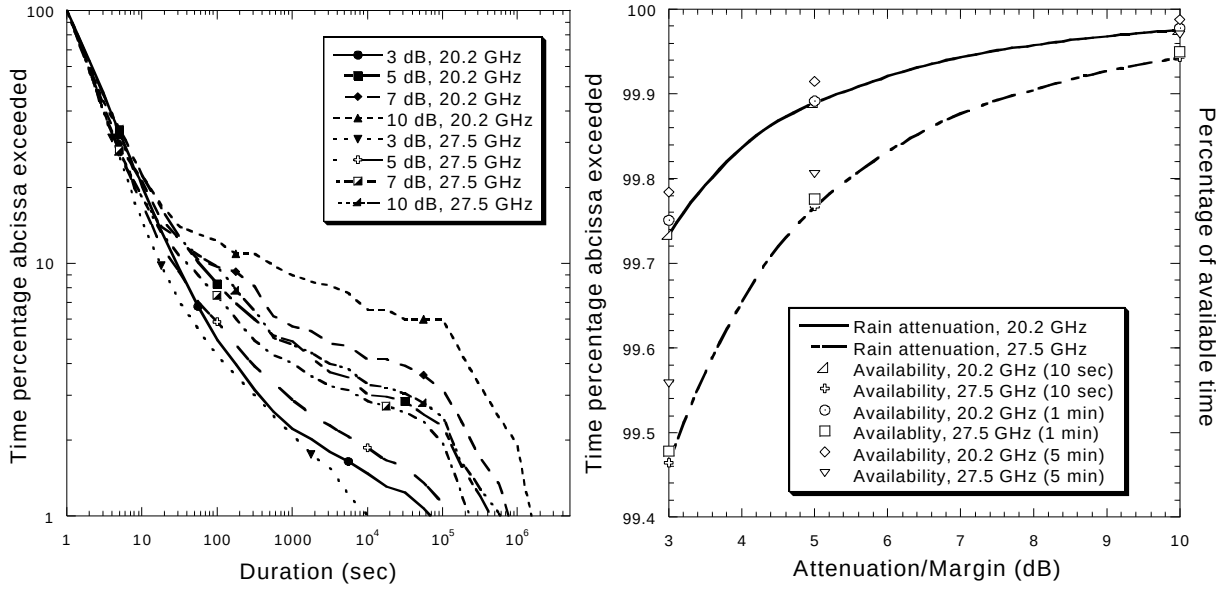

a) Inter-fade duration, Ottawa (unfiltered) b) Rain attenuation and availability, Ottawa

Figure 3. Conditional inter-fade CDF (a) and annual rain attenuation CDF and availability (b)

The availability increases for longer time limits, resulting in system availability above the annual rain attenuation. This characteristic might be useful for non-real time systems able to store information during the unavailable time before transmission during the available time.

V CONCLUSIONS

Models for fade duration distributions were compared with results derived from ACTS beacon data recorded in Vancouver, Ottawa, Reston and Norman at 20.2 and 27.5 GHz. The data presented were corrected to compensate for antenna wetting effects affecting the APT terminals. The ability of various cumulative distribution functions to fit fade duration data was evaluated in order to find the best fade duration model. With the present dataset from Vancouver, the Weibull distribution gives the best results. However, for the three other sites a triple cascaded exponential model seems to capture well the nature of fade duration statistics.

An algorithm estimating service availability, based on fade and inter-fade duration results was derived. Its application was illustrated using data measured at the Ottawa site, showing negligible differences between attenuation and availability statistics.

ACKNOWLEDGEMENTS

This work was done while the first author was a guest researcher at the Communications Research Centre Canada and given the opportunity to work on the ACTS data.

REFERENCES

[1] A. Paraboni and C. Riva, "A New Method for the Prediction of Fade Duration Statistics in Satellite Links Above 10 GHz," *Int. J. Satellite Comm.,* vol. 12, pp. 387-394, 1994.

[2] H. Helmken, R. E. Henning, J. Feil, L. J. Ippolito and C. E. Mayer, "A Three-site Comparison of Fade Distribution Measurements," *Proc. IEEE,* vol. 85, no. 6, pp. 917-925, 1997.

[3] R, Lekkla, K. S. McCormick and D. V. Rogers, "12-GHz Fade Duration Statistics on Earth-Space Paths in South-East Asia," *Proc. URSI CLIMPARA'98*, pp. 167-170, Ottawa, Canada, 27-29 April 1998.

[4] C. Amaya, D. V. Rogers and K. S. McCormick, "30/20/12-GHz Slant-Path Attenuation Measurements at Ottawa, Canada," *Proc. URSI Comm. F. Triennial Open Symp. on Wave Propagation and Remote Sensing,* pp. 308-311, Aveiro, Portugal, 22-25 Sept. 1998.

[5] K. S. McCormick and D. V. Rogers, "Fade Duration Distributions Derived from the ACTS Radiometer Data," *Proc. Twenty-Third NASA Propagation Experimenters Meeting (NAPEX XXIII) and the Advanced Communications Technology Satellite (ACTS) Propagation Studies Workshop,* Falls Church, Virginia, U.S., 2-4 June 1999.

[6] O. Veyrunes, P. Le Clerc and H. Sizun, "Results of Millimetre Wave Propagation Analysis," *Proc. Millennium Conf. on Antennas and Propagation,* vol. 2, Davos, Switzerland, 9-14 April 2000.

[7] E. de Miranda, M. S. Pontes, L. A. R. da Silva and R. S. L. Souza "A Comprehensive Study of Slant-Path Attenuation in Brazil, Second Part: Dynamic Statistics," *Proc. AP2000 Millennium Conference on Antennas & Propagation*, Davos, Switzerland, April 9-14 2000.

[8] L. E. Bråten and César Amaya, "Fade Duration at Ka-band on a Satellite-Earth Link in Vancouver: Modeling and Comparison with Measurements," *Proc. IX Simpósio Brasileiro de Microondas e Optoeletrônica*, SBMO, Joao Pessoa, Brazil, 7-11 August 2000..

[9] D. V. Rogers and R. K. Crane, "Propagation Results from the Advanced Communications Technology Satellite (ACTS) and Related Studies," *Proc. 2000 International Symposium on Antennas and Propagation,* vol. 4, pp. 1439-1447, Fukuoka, Japan, 21-25 August 2000.

[10] "NASA's ACTS Propagation Experiment, Ka Band Propagation Data CDs 5 years, May 1999," ACTS Data Center, Westenhaver Wizard Works, Inc. Stone Mountain, GA 30087, U.S.

[11] T. Maseng and P. M. Bakken, "A Stochastic Dynamic Model of Rain Attenuation," *IEEE Trans. Comm,,* vol. 29, no. 5, pp. 660-669, 1981.

[12] R. M. Manning, "A Unified Statistical Rain-Attenuation Model for Communication Link Fade Predictions and Optimal Stochastic Fade Control using a Location Dependent Rain-Statistics Database," *Int. J. Satellite Comm.,* vol. 8, pp. 11-30, 1990.
[13] Recommendation ITU-T G.821, "Error Performance of an International Digital Connection Operating at a Bit Rate Below the Primary Rate and Forming Part of an Integrated Services Digital Network," G Series, International Telecommunication Union, Geneva, Switzerland, 1996.
[14] H. Fukuchi, Y. Otsu, "Available Time Statistics of Rain Attenuation on Earth-Space Path," *Proc. IEE*, vol. 135, no. 6, pp. 387-390, December 1988.
[15] D. C. Rabone, D. G. Charlton, P. T. Thompson and D. K. McCarthy, "Statistics of Available/Unavailable Time due to Attenuation on Satellite Paths," *Proc. Sixth International Conference on Antennas and Propagation*, ICAP89, pp. 14-18, Coventry, U.K., 4-7 April 1989.

Paper 8

"Fade Durations on Earth-Space Links: Dependence on Path and Climatic Parameters"

Published in: *Proc. CLIMPARA'2001*, Budapest, Hungary, 28-30 May 2001.

FADE DURATIONS ON EARTH-SPACE LINKS: DEPENDENCE ON PATH AND CLIMATIC PARAMETERS

Lars E. Bråten[1], César Amaya[2] and David V. Rogers[2]

[1] Telenor Research and Development, P.O. Box 83, N-2027 Kjeller, Norway
Tel: +47 63848715, Fax: +47 63819810, E-mail: Lars-Erling.Braten@telenor.com
[2] Communications Research Centre Canada, Box 11490, Station H, Ottawa, Ontario, Canada, K2H 8S2
Tel: +1 613 998 2197/5174, Fax: +1 613 9984077, E-mails: Cesar.Amaya@crc.ca, Dave.Rogers@crc.ca

Abstract

A prediction model for fade durations is derived from satellite beacon measurements at five North American locations: Vancouver, Ottawa, Norman, Reston and Tampa, with the Advanced Communications Technology Satellite (ACTS) at 20.2 and 27.5 GHz. The analysis explores the relationship between fade duration and both link specific parameters and local climatic conditions, enabling the model to be applied to other sites and frequencies as well. The model predicts both the conditional fade duration distribution, and the annual average number of fades. The prediction errors, obtained applying the new model on the same set of data, are compared with those produced by previously reported models for fade duration. The new model has a lower average, root mean square (r.m.s.) and standard deviation of the logarithmic error.

Keywords: Fade duration, Climatic parameters, Satellite communication

Introduction

Fade duration statistics are important for evaluating fade mitigation techniques intended to improve telecommunication system availability. Fade duration is defined as the time interval between threshold crossings at a given level of attenuation. For communication systems designed to operate with a given fade margin, fade duration statistics indicate the number as well as duration of outages.

It was concluded from analyses of fade durations measured at several ACTS locations in Canada and the U.S. that a cascaded exponential model captures well the nature of fade durations derived from both beacon and radiometer data [1]. Recent investigations have suggested a possible connection of fade duration to a parameter describing the relative fraction of convective and stratiform rain, such as the convectivity component in the Rice-Holmberg model [2]. McCormick and Rogers found a clear dependence of fade durations measured at Ka-band on attenuation and to some extent on rain convectivity for their cascaded exponential model [3]. This paper deals with the development of a new three-term exponential prediction model for fade durations and its connection to climatic and path specific features. The performance of the model is compared to previously reported fade duration models for satellite-earth paths.

Measurements

Seven identical ACTS Propagation Terminals (APTs) were provided by NASA for the measurement campaign at 20.2 and 27.5 GHz. The data analyzed in this study were measured by the APTs located in Vancouver, Canada, and Norman, Reston and Tampa in the U.S. The terminal antenna diameter was 1.2 m. At the *Communications Research Centre Canada* in Ottawa, the ACTS beacons were measured using independent terminals at each frequency with 2.4 m diameter antennas. The data acquisition rate at all sites was 1 Hz, implying that signal scintillation was present in the unfiltered data, resulting in an increased number of short duration events. Some characteristics of the measurement locations are given in Table 1; the Rice-Holmberg parameters M (annual total rainfall) and b (thunderstorm ratio) are taken from [4].

The APTs were sensitive to water on both the antenna reflector surface and the feed window. The attenuation thresholds used in the fade duration distributions presented here were adjusted to compensate for antenna wetting according to the site dependent values given in [5]. The receiver system in Ottawa is negligibly affected by this problem.

Fade duration models

The first prediction model for fade durations on satellite-earth paths was developed by Paraboni and Riva (P-R) [6]. The model assumes that long fade durations are lognormally distributed while shorter durations follow a power-law distribution.

	Vancouver	Ottawa	Norman	Reston	Tampa
Coordinates	49.3° N, 123.2° W	45.6° N, 75.6° W	35.2° N, 97.4° W	39.0° N, 77.3° W	28.1°N, 82.4°W
Elev. Angle	29.3°	32.2°	49.1 °	39.2 °	52 °
Tilt angle, CW from vertical	-19°	22°	4°	26°	30°
Height (m)	110	70	420	80	50
Measurement period	1994-1998	97/09-98/08	1994-1998	1994-1998	1994-1998
Measured attenuation	Total	w.r.t. Clear sky	Total	Total	Total
Rain rate 0.01% ($R_{0.01\%}$ mm/h)	13	37	71	59	83
ITU-R rain zone	B/D	K	M	K	N
Annual total rainfall M (mm)	1181	800	831	916	1277
Thunderstorm ratio b	0.09	0.15	0.35	0.28	0.73

Table 1. Receive locations and their path/climate characteristic

The path specific inputs to the prediction model are frequency and elevation angle, producing an estimated fade duration cumulative distribution (CDF) for a given attenuation threshold. An improvement of this model was presented in [7]. A prediction model based on terrestrial measurements is given in [8].

Previous studies of fade duration distributions based on the ACTS beacon data identified the three-term *cascaded exponential model* as the overall best model for unfiltered data at Ottawa, Norman and Reston [1]. A similar test performed in this study on the data from Tampa gave the same result. For the Vancouver data, the Weibull distribution performed slightly better. Fade duration distributions are often presented as the percentage of time that the duration D exceeds a given value d, given that the attenuation A exceeds a threshold a. The conditional cascaded exponential distribution is given as:

$$P_{D|A}\left(D > d \,|\, A \quad a\right) = \sum_{i=1}^{N} a_i \times e^{-\frac{d}{b_i}} \qquad (1)$$

The positive decay variables b_i have units of seconds, they are called *characteristic durations* and represent average durations of fades [2]. Typical contributors to short and long rain induced fade events are convective and stratiform rain, respectively, in addition to very short scintillation events for unfiltered data. These different types of events might be represented with individual terms in the cascaded exponential model, with characteristic durations corresponding to the average event durations. Scintillation contributes to fast fading of very short duration, and is represented in this analysis by the first term in Eq. 1, b_1. Convective rain produces fades of short duration, represented by b_2, while the assumed slowly varying attenuation due to stratiform rain is represented by the long-duration term, b_3. Using this notation, the positive variables a_i describe the *conditional occurrence probability* of the distinct types of events in the conditional distribution. To ensure that the CDF equals one for zero fade duration the boundary condition, sum of $a_i = 1$, is imposed on the variables in Eq. 1.

Results from previous studies indicated that a double exponential model ($N = 2$) is adequate to model attenuation derived from radiometric measurements. To take into account fast fluctuations in the beacons, caused by scintillation, a $N = 3$ term model is tested in this study [1]. Fast fluctuations will be present not only for low attenuation thresholds, but also for deeper fading, as tropospheric scintillation may be superimposed on the rain-induced attenuation.

Parameter identification and linear regression

The objective of the regression analysis is to seek a pattern with respect to local climatic and path specific parameters, permitting the development of a prediction procedure for fade duration distributions. The triple term cascaded exponential models was fitted to the measured data by minimizing a mean square logarithmic error function, e_i:

$$e_i = \log_{10} \frac{P_{Measured}\left(D > d_i \,|\, A \quad a\right)}{P_{Model}\left(D > d_i \,|\, A \quad a\right)} \qquad (2)$$

where i is the fade duration bin number. The numerical fitting procedure of the measured and model conditional CDFs produced six variables (a_1, ..., b_3) for each duration distribution. The parameter selection procedure, described in [9], is used to identify the minimum number of parameters giving a satisfactory regression model for each of these variables. Examples of parameters tested are functions of attenuation, elevation angle, rainfall rate and the Rice-Holmberg parameters. The procedure consists of several steps, where at each step the parameters are correlated with the reference variable, identifying the most significant parameter. The contribution from this parameter is subtracted from the reference by constructing an intermediate regression model, before identifying the next significant parameter. The coefficients accompanying the most significant parameters are adapted to the reference data (a and b) by minimizing the least mean square distance between the reference and the regression model using a standard linear regression tool. The succession of the models developed for the six variables is based on decreasing R^2 statistics. The quantity R^2 is called the coefficient of determination and is given by the correlation between the regression model output and the reference variables. The closer R^2 approaches 1, the more statistically significant is the regression. Care is taken to ensure that the coefficients 95 % confidence interval does not cross zero. After a model is developed for one of the variables a_1, ..., b_3, it is used when recalculating the remaining variables before the next model is identified, and so on.

Conditional occurrence probabilities, a:

A correlation analysis between the candidate parameters and the reference variables a_1, ..., b_3 is carried out, and the best model is obtained for the conditional occurrence probability for short duration fades, a_2. The most significant parameters are identified, and the regression model for a_2 becomes:

$$a_2 = a \quad b \times 10^{L_s/20} \quad c \times M^3 \qquad (3)$$

where M is the annual total rainfall (mm) parameter in the Rice-Holmberg model. The frequency scaled attenuation threshold, L_s (dB), denotes the attenuation thresholds for a beacon with a frequency of 27.5 GHz. The attenuation thresholds used to extract the fade duration statistics at 20.2 GHz is modified by moving the frequency to 27.5 GHz, followed by a scaling the attenuation thresholds according to Recommendation ITU-R P.618-6 [10]. The scaling is performed to include the frequency dependence of rain attenuation in the model. The model coefficients and statistics are shown in Table 2, where *ANF* is the annual number of fades

Variable	Model coefficients a	b	c	d	Statistics R^2
a_1	$9.44 \cdot 10^{-1}$	$8.64 \cdot 10^{-3}$	$1.38 \cdot 10^{-11}$		0.82
a_2	$1.39 \cdot 10^{-1}$	$1.12 \cdot 10^{-1}$	$7.84 \cdot 10^{-12}$		0.78
b_1	3.52	$2.08 \cdot 10^{-2}$			0.37
b_2	$2.99 \cdot 10^{2}$	$8.46 \cdot 10^{1}$			0.15
b_3	$-2.52 \cdot 10^{1}$	$1.53 \cdot 10^{3}$	$2.85 \cdot 10^{3}$	$1.53 \cdot 10^{8}$	0.75
ANF	$1.31 \cdot 10^{1}$	$1.88 \cdot 10^{-1}$	2.15		0.79

Table 2. Regression coefficients used in the model for a and b and *ANF*

exceeding 1 second duration. The conditional probability of occurrence for short duration fades decreases with decreasing attenuation threshold and increasing total annual rainfall.

After re-optimization of the parameters by using Eq. 3 for a_2, the best regression model is obtained for the conditional occurrence probability for very short fades, a_1:

$$a_1 = a \quad b \times R + c \times M^{3} \tag{4}$$

where R is the equivalent rainfall rate corresponding to the attenuation threshold for the path obtained by inverting the expression for the attenuation in Recommendation ITU-R P.618-6 [10]. Rainfall rate as a fade duration model parameter was first used by Gibbins and Paulson for predicting fade duration on terrestrial links [8]. The conditional occurrence probability for very short duration fades decreases with increasing rain rate and increasing total annual rainfall. As an alternative to a regression model for a_3, we use the relation $a_3 = 1 - a_1 - a_2$. This ensures that the boundary condition for the cascaded exponential model is fulfilled.

Characteristic times, b:

The long fades, produced mainly by stratiform rain and to some extent gaseous absorption, are represented by the third term in Eq. 1, b_3. At the Ottawa location, the shallow long fades due to gas attenuation are removed. This results in shorter average duration for b_3 compared to the other sites, especially for fades smaller than about 5 dB. This difference is ignored, and a common regression model developed for the characteristic time b_3:

$$b_3 = a + b \times 10^{L_s/20} + c \times e^{b^{-1}} \quad d \times e^{R_{0.01\%}} \tag{5}$$

where b is the thunderstorm ratio in the Rice-Holmberg model. The point rainfall rate at 0.01% of the time, $R_{0.01\%}$, is given in Table 1. The characteristic time for long duration fades decreases with increasing attenuation, decreasing thunderstorm ratio and decreasing rainfall rate, $R_{0.01\%}$.

It turned out to be difficult to find a good regression model for the two last variables, b_1 and b_2. The best modeling result with respect to the R^2 statistics is obtained for b_1, representing the dynamics of very short fades:

$$b_1 = a \quad b \times (L_s \quad 7)^{2} \tag{6}$$

The characteristic duration for very short fades has a maximum for a frequency scaled attenuation of about 7 dB. It should be cautioned that some of the shorter fades may possibly be caused by equipment effects.

The short duration fades, produced by, for example convective rain, is represented by the characteristic duration b_2:

$$b_2 = a \quad b \times \ln(b^{-1}) \tag{7}$$

The mean duration for convective fades increases as b increases. As seen from the R^2 statistics given in Table 2, the models for four of the six variables is satisfactorily represented by the regression models. The problems finding a good model for b_1 and b_2 may be due to errors originating from the previously found regression models and possible also due to correlation between the variables a_1, ..., b_3.

Annual number of fades, ANF:

The annual number of fades, *ANF*, as a function of fade depth in dB, approximate straight lines on a log-log plot for all of the measurement sites very well. Similar findings for a terrestrial link were reported in [11]. A model for *ANF*, based on linear regression on *ln(ANF)*, is:

$$ANF = e^{a \quad b \times b^{-1}} \times L_s^{c} \tag{8}$$

where the coefficients are given in Table 2. The annual number of fades decreases as b decreases and as fade threshold increases. The prediction method given in [8] does not include fades as short as one second, and underestimates the annual number of fades. An example of predicted and measured conditional fade duration with the new model is shown for Vancouver in Fig. 1.

Discussion

The variables found in the fitting process did not always follow consistent variations at both frequencies, or with the attenuation threshold. This indicates that the three-term cascaded exponential model might be too complex, and that a fewer number of variables is sufficient to characterize the fade duration process. However, the separation of the duration distribution function into separate cascaded terms allows a useful physical interpretation of the results. Investigations of fade duration distributions obtained from radiometers may be one way of reducing the distribution complexity, as a two-term model should be sufficient

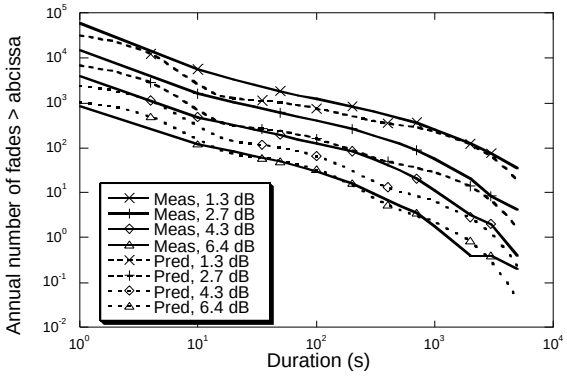

Figure 1. Measured and predicted fade duration at Vancouver, 27.5 GHz

Model	Duration	5 s	10 s	60 s	180 s	300 s	600 s	Overall
Paraboni - Riva	m_p	123.3	174.0	124.2	77.3	56.6	38.3	98.9
	r.m.s	127.3	178.9	131.8	89.8	74.1	65.2	117.9
	s_p	32.0	42.4	44.7	46.3	48.3	53.5	64.2
Regression	m_p	25.4	9.6	33.3	30.1	16.3	8.3	20.5
	r.m.s	30.0	24.1	80.4	51.0	40.2	37.6	47.6
	s_p	16.2	22.4	74.1	41.6	37.3	37.1	43.0

Location	Paraboni -Riva		Regression	
	m_p	s_p	m_p	s_p
Ottawa	137.9	42.9	43.5	27.5
Vancouver	132.7	39.3	1.5	27.9
Norman	58.7	58.5	18.9	40.0
Virginia	78.8	60.9	13.6	49.7
Tampa	86.7	74.3	25.0	53.1

Table 3. Prediction models error e_p

to capture the shape of the CDF. Similarly, the short fades caused by scintillation may be filtered out from the original time series to simplify the fade duration modeling.

Comparison of the conditional prediction models

The performance of the new model is compared to the P-R fade duration model for satellite-earth paths, [6], and to the modified version reported in [7]. A logarithmic error function is used to compare predicted ($D_{p,i}$) and measured ($D_{m,i}$) durations at bin *i* for the conditional fade duration distributions:

$$e_{p,i} = 100 \times \ln \left(\frac{D_{p,i}}{D_{m,i}} \right) \quad (8)$$

The error is calculated for a range of different fade durations, and the mean, m_p, standard deviation, s_p, and r.m.s. value are displayed in Table 3. The interpolations performed to compare the predicted and measured fade duration are performed in the logarithmic domain, as the fade duration CDFs in a double logarithmic scale are nearly linear.

Inspection of the average errors for the P-R model, displayed in Table 3, reveals that this model overestimates the occurrence probability of fades, especially for short durations. For the ACTS data, predictions obtained by the modified P-R model were less accurate than those obtained from the original one. Averaged over the 5 locations, 2 frequencies and the 6 tested durations, the new regression model performed better with respect to both the average, r.m.s. and standard deviation of the error for the current set of data, not unexpected for a model fit to these same data. A simplified regression model based on the attenuation alone, as reported in [2] and [3], had a performance between the two models displayed in Table 3.

Conclusion

A three-term cascaded exponential prediction model for fade duration distributions was developed. The model is derived from, and tested on, ACTS beacon data recorded in Vancouver, Ottawa, Reston, Norman and Tampa at 20.2 and 27.5 GHz. The main purpose of the analysis was to explore the links between fade durations and both meteorological and path specific parameters. The proposed model predicts both the annual number of fades, and the conditional fade duration distribution. The new prediction method performed well compared to previously reported fade duration models for the data sets considered in this paper. Future work includes verifying the findings with other independent measurements.

Acknowledgement

We thank Dr. C. Riva for kindly providing the programs implementing the Paraboni-Riva model.

References

1. L. E. Bråten, C. Amaya and D. V. Rogers, Fade and Inter-Fade Duration at Ka-Band on Satellite-Earth Links: Modeling and System Implications, Proc. AIAA Int. Comm. Sat. Sys. Conf., Toulouse, Apr. 2001.
2. R. Lekkla, K. S. McCormick and D. V. Rogers, 12-GHz Fade Duration Statistics on Earth-Space Paths in South-East Asia, Proc. URSI CLIMPARA'98, pp. 167-170, Ottawa, Apr.1998.
3. K. S. McCormick and D. V. Rogers, Fade Duration Distributions Derived from the ACTS Radiometer Data, Proc. NAPEX XXIII and ACTS Propagat. Studies Workshop, pp. 195-205, Falls Church, Virginia, June 1999.
4. R. K. Crane and A. W. Dissanayake, ACTS Propagation Experiment: Attenuation Distribution Observations and Prediction Model Comparison, Proc. IEEE, Vol. 85, N. 6, pp. 879-892, June 1997.
5. NASA's ACTS Propagation Experiment, Ka Band Propagation Data CDs 5 years, May 1999, ACTS Data Center, Westenhaver Wizard Works, Inc. Stone Mountain, GA 30087, U.S.
6. A. Paraboni and C. Riva, A New Method for the Prediction of Fade Duration Statistics in Satellite Links Above 10 GHz, Int. J. Satellite Comm., Vol. 12, pp. 387-394, 1994.
7. F. C. Barbaliscia, et al., Propagation modelling at 40/50 GHz, Final Report to Intelsat Contract N. Intel-1998, 1999.
8. C. J. Gibbins and K. S. Paulson, Duration of Rain Events and Rain Attenuations at Millimetric Wavelengths, Proc. Millennium Conf. on Antennas and Propagat., Davos, Apr. 2000.
9. T. Tjelta, R. L. Olsen and L. Martin, Systematic Development of New Multivariable Techniques for Predicting the Distribution of Multipath Fading on Terrestrial Links, IEEE Trans. Antennas Propagat., Vol. 38, N. 10, pp. 1650-1665, Oct. 1990.
10. Recommendation ITU-R P.618-6, Propagation data and prediction methods required for the design of Earth-space telecommunication systems, P Series, International Telecommunication Union, Geneva, 1997.
11. Contribution to ITU-R, WG 3M, from Telia, Doc. 88-E, Measured Relationship Between Rain Attenuation, Number of Events and Mean Duration of Events, International Telecommunication Union, Geneva, 1999.

Paper 9

"Prediction of Time Dynamic Rain Attenuation at Millimetre Wavelengths"

Published in: *Proc. AP2000 Millennium Conference on Antennas & Propagation*, Davos, Switzerland, April 9-14 2000.

Correction:

The operating frequency of the link was 60 GHz, not 38 GHz as stated in the paper.

PREDICTION OF TIME DYNAMIC RAIN ATTENUATION AT MILLIMETRE WAVELENGTHS

Lars E. Bråten[(1)], Walther Åsen[(2)]

[(1)]Telenor Research and Development, Instituttveien 23, PoBox 83, N-2027 Kjeller, Norway
Email: Lars-Erling.Braten@telenor.com

[(2)]Norwegian Post and Telecommunications Authority, PoBox 447, N-0104 Oslo, Norway
Email: Walther.Asen@npt.no

ABSTRACT

This paper presents forecasting and modelling of rain attenuation based on measurements of a 38 GHz terrestrial link. Parameters for the Maseng-Bakken dynamic rain attenuation model have been extracted from measurements. Linear auto-regressive moving average and dynamic Bayesian methods for rain attenuation prediction have been compared over a time span ranging from 10 to 100 seconds. The most suitable prediction method based on the prediction standard deviation is a logarithmic auto-regressive estimator of first order.

INTRODUCTION

Knowledge of attenuation due to precipitation is increasingly important at millimetre wavelengths and below. Communication systems where propagation effects due to precipitation have an effect on the signal transmission could adapt the transmission methodology that maximises the throughput of information and optimises the delivery time. Examples of fade mitigation techniques are given in [1, 2]. The required forecast horizon for adaptive systems is typically in the order of a few seconds. An example requiring longer forecasts is a broadband cellular system delivering information on demand. This could for instance be pay per view or file transfer. Prior knowledge of the foreseen propagation impairments may be used by the service provider to optimise system performance. The required quality of service (QoS) for such a system depend on the service offered. For a TV program the customer may consider it important that no interruptions occur during the program. However, they may tolerate a small amount of delivery delay. By combining for instance variable information transfer rate and buffering of information on the user side, short interruptions due to heavy rainfall could be avoided.

The objective of this study is to develop a prediction methodology forecasting the rain attenuation as far as possible into the future. This predictor may be used to optimise specific QoS parameters considered important for both the service provider and the customer. We have used two approaches when developing the forecasting methodology; auto regressive moving average (ARMA) and a Bayesian dynamic linear model (DLM). In the classical approach to statistical estimation the parameter to be estimated is assumed to be a deterministic, but unknown constant [3]. In the Bayesian case, we assume the parameter of interest is a random variable whose particular realisation we must estimate [4]. Classical estimation methods find it difficult to make any use of prior knowledge of the unknown parameter, while the Bayesian approach incorporate prior knowledge, and may thus improve the prediction. The parameters for a dynamic rain attenuation model developed by Maseng and Bakken is also extracted from measurements to better understand the underlying statistical process of rain attenuation [5].

RAIN FADING, DYNAMICS AND STATISTICS

The Maseng-Bakken statistical dynamic model of rain attenuation is adopted, enabling system simulation and providing insight to the fading process [5, 6]. The received signal attenuation α (in dB) is modelled as a log-normally distributed variable. By utilising a memoryless nonlinearity the attenuation is transformed into a stationary Gaussian process with zero mean and unit variance

$$x(t) = \ln\left(\alpha(t)/\alpha_m\right)/\sigma_a \tag{1}$$

where α_m is the median attenuation and σ_a the standard deviation of $\ln(\alpha)$. The log-normality seems to be a relatively good assumption, except perhaps for the larger attenuation values where the model exaggerates the occurrence of deep

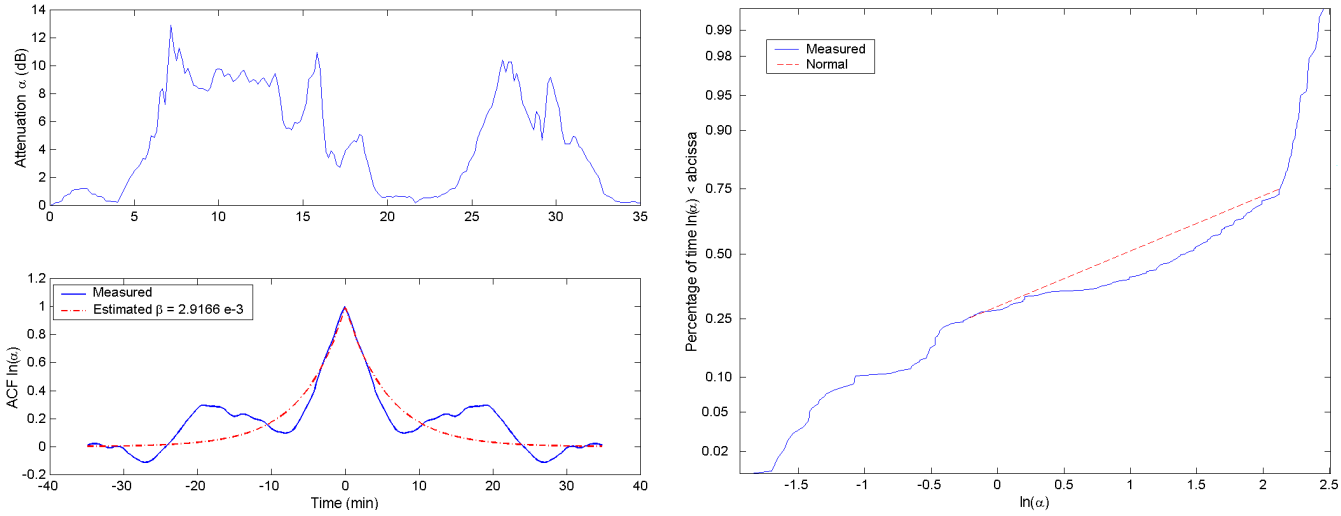

Fig. 1. Rain event 11, August 1994

fades, see the normal plot in Fig. 1. The mean-reverting process x is known as an Ornstein-Uhlenbeck process. We have used terrestrial propagation measurements for 12 rain events to extract the parameters displayed in Table 1. The measurement site is located 20 km north-east of Oslo, where the attenuation in a 600 m terrestrial link at 38 GHz is monitored [7].

The time dependence is described by the parameter β, which is used in a first order infinite impulse response filter to shape the auto correlation function (ACF). This ACF is assumed to have a relatively simple shape of a decaying exponential function corresponding to an auto regressive process of first order (AR(1))

$$R_{XX}(\tau) = e^{(-\beta \cdot |\tau|)} \tag{2}$$

The ACF in (2) reasonable well represents the measured ACF although the non-monotonic nature of some of the measured ACF is not included in this simple function, see Fig. 1. Previously reported values for β are 1.7 10^{-3} [5] and 1.8 10^{-3} [6]. This is somewhat lower than the values found in the current study. A small value of β corresponds to slowly varying rain attenuation dynamics. To model rain rate instead of attenuation is straightforward, assuming the commonly used power law relationship between attenuation and rain rate.

Table 1. Rain events and extracted parameters for x(t)

Event	Median α_m	Standard dev. σ_a	β (10^{-3})/s	Date
1	2.47	1.11	9.22	Oct. 95
2	0.84	1.37	6.45	Sept. 95
3	1.82	1.31	8.50	July 95
4	5.04	0.99	2.37	July 95
5	4.35	1.21	3.41	July 95
6	4.33	1.32	3.57	July 95
7	2.45	1.20	14.04	June 95
8	3.22	1.00	1.95	June 95
9	3.17	0.88	1.63	June 95
10	2.07	1.23	18.45	Sept. 94
11	4.10	1.26	2.92	Aug. 94
12	4.65	1.20	1.46	Aug 94
Mean	2.96	1.08	5.69	

MEDIUM TERM PREDICTION OF TIME VARYING RAIN ATTENUATION

In this study the focus is on medium term forecasting of the rain attenuation. The main reason for looking at medium term prediction is to focus on system parameters rather than transmission parameters.

Application of Bayesian Forecasting Principles

Dynamic Bayesian Forecasting is based on very general formulations of the dynamics of a system as a whole [5]. In addition we have used the DLM framework to establishment specific formulations and additional assumptions. Variance learning is used for the system variance, we have assumed that the forecast errors have a Normal distribution, and we are predicting ln(α). Recurrence relations are found by assuming that the à posteriori distribution of the observable quantity and all the explaining underlying parameters are proportional to their à priori distributions, and then applying Bayes' theorem.

A simple k-step ahead DLM forecast function is formulated: $f(k,\delta(k)) = m$, where m is the estimated level at time t, and $\delta(k)$ is the optimised discount factor for the k seconds forecast. This means that the future is estimated to stay at the same value as the current discounted estimate of the past. The values for $\delta(k)$, k=10, 20 ¨ 100 seconds used in Fig. 2 are 0.01, 0.01, 0.01, 0.01, 0.79, 0.87, 0.92, 0.94, 0.95 and 0.96. General polynomials of higher degrees (functions of the forecasting steps) could also be suggested as forecast functions, but since there is very little correlation between successive attenuation changes in attenuation time series [8], such models are not likely to be successful.

Auto Regressive Moving Average Prediction

Previous investigations of short-term predictors for the attenuation α identified an auto regressive moving average model, ARMA(3,3), minimising the prediction error variance [9]. We will investigate whether prediction of the logarithmic version of the attenuation, ln(α), improve the predictions compared to linear prediction of the attenuation α directly. The rain attenuation model suggest an AR(1) model for ln(α). By using state- space software, ARMA (including AR and MA) models with order up to four have been fitted to measured rain attenuation, and the prediction error variance has been calculated. Models for the attenuation α (in dB) was derived in addition to the logarithmic ones. The mean prediction errors for the most promising predictors are given in Table 2 and the prediction error standard deviation as function of k depicted in Fig. 2.

Results for an Example Attenuation Time Series

The attenuation time series used for validation of the predictor performance is a concatenated series of measured attenuation events (nr. 2, 8, 9 and 11). The concatenation was done to increase the confidence when estimating the prediction error standard deviation. It should be noted that the predictions are for the case it is raining. A two-state semi-Markov model could be used to divide between non-rain and rainy conditions. As reference estimators we use a predictor containing the attenuation value k-steps behind, i.e. "the future values will equal the last observed value". The mean of the standard deviation of the prediction errors for the best estimators are given in Table 2.

The mean performance of the logarithmic AR(1) and ARMA(3,4) models are about the same, somewhat better than the DLM and reference estimator. The ARMA(3,3) estimator give the largest mean standard deviation. The performance of the estimators as a function of how far into the future one is predicting is displayed in Fig 2.

As anticipated the forecast based on a logaritmic AR(1) estimator, corresponding to the channel simulator model, perform well. When forecasting further into the future the value of the ARMA predictors go toward zero, giving a prediction error standard deviation equal to the observed attenuation standard deviation. For the DLM predictor it is found for the example event that there is no point in using a high order polynomial for predictions. The advantage of using the DLM instead of the simple predictor is evident for prediction times larger than about 40 seconds.

Table 2. Mean prediction error standard deviation

	Reference	ARMA(3,3)	DLM	Log. AR(1)	Log. ARMA(3,4)
$\bar{\sigma}$ (dB)	4.54	6.13	4.46	3.98	4.05

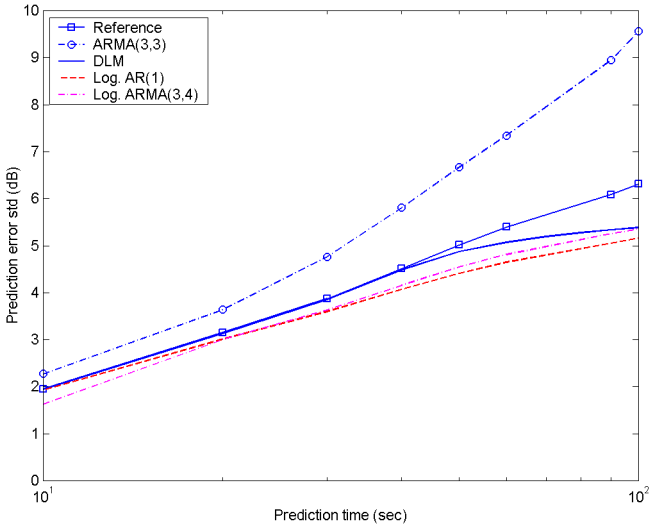

Fig. 2. Prediction error standard deviation as function of prediction time for rain events 2, 8, 9 and 11

It should be noted that the value of the prediction error standard deviation is for a specific link (38 GHz, 600 m). Different link lengths and or frequencies would change the observed attenuation values and thereby the prediction errors. The performance ranking of the algorithms is, however, not expected to change significantly. The overall prediction capability of any of the methods may seem poor, especially when comparing with our reference model. This may be due to rapid variations in the time series, as indicated by the high β values displayed in Table 1.

CONCLUSION

Predictions of rain attenuation have been performed and new parameters for the Maseng-Bakken dynamic rain attenuation model have been extracted from measurements. ARMA and DLM forecasting methods for rain attenuation have been applied to measured attenuation time series. Standard deviations of prediction errors have been calculated for forecasts between 10 and 100 s, and the best predictor found was a logarithmic auto regressive model of order one. Suggested future work is to apply the predictors in a system simulation study to access the potential improvement in quality of service parameters as availability and delivery delay. The Maseng-Bakken rain attenuation model could also be modified to improve the cumulative distribution for large attenuation values.

REFERENCES

[1] C. B. Cox and T. A. Coney, "Advanced Communications Technology Satellite (ACTS) Fade Compensation Protocol Impact on Very Small-Aperture Terminal Bit Error Rate Performance", *IEEE J. on Sel. Areas in Comm.*, vol.17, no. 2, pp 173-179, Feb. 1999.

[2] G. Fairhurst, S. L. Pang, P.S. Wan, "Smart codec: an adaptive packet data link", *Communications, IEE Proceedings*, June 1998, pp. 180-185, vol. 145, Issue 3.

[3] G. E. P. Box and G. M. Jenkins, *Time Series Analysis, Forecasting and Control*, Holden-Day, San Francisco, 1970.

[4] M. West and J. Harrison, *Bayesian Forecasting and Dynamic Models*, Second Edition, Springer, 1997.

[5] T. Maseng and P. M. Bakken, "A Stochastic Dynamic Model of Rain Attenuation", *IEEE Trans. on Comm*, vol. 29, pp. 660-669, May 1981.

[6] A. Burgueno, E. Vilar and M. Puigcerver, "Spectral Analysis of 49 Years of Rainfall Rate and Relation to Fade Dynamics", *IEEE Trans. on Comm.*, vol. 38, pp. 1359-1366, Sept. 1990.

[7] T. Tjelta, A. Nordbotten and J. Kårstad, "Effects of precipitation and reflections from a snow covered ground measured at 40 and 60 GHz on a 600 m experimental link in Norway", ICAP'97, Edinburgh, 14-17 April 1997

[8] L. Dossi, "Real-time prediction of attenuation for applications to fade countermeasures in satellite communications", *Electronic Letters*, vol. 26, issue 4, pp. 250-251, Feb. 1990.

[9] B. Gremont, M. Filip, P. Gallois and S. Bate, "Comparative Analysis and Performance of Two Predictive Fade Detection Schemes for Ka-Band Fade Countermeasures", *IEEE J. on Sel. Areas in Comm.*, vol. 17, pp. 180-192, Feb. 1999.